

Florida State University Libraries

Electronic Theses, Treatises and Dissertations

The Graduate School

2010

Entanglement and Bond Fluctuations in Random Singlet Phases

Huan Doan Tran



THE FLORIDA STATE UNIVERSITY

COLLEGE OF ARTS AND SCIENCES

ENTANGLEMENT AND BOND FLUCTUATIONS IN RANDOM SINGLET PHASES

By

HUAN DOAN TRAN

A Dissertation submitted to the
Department of Physics
in partial fulfillment of the
requirements for the degree of
Doctor of Philosophy

Degree Awarded:
Summer Semester, 2010

The members of the committee approve the dissertation of Huan Doan Tran defended on June 23, 2010.

Nicholas E. Bonesteel
Professor Directing Dissertation

Sanford Safron
University Representative

Vladimir Dobrosavljevic
Committee Member

Jorge Piekarewicz
Committee Member

Lloyd Engel
Committee Member

Approved:

Mark Riley, Chair, Department of Physics

Joseph Travis, Dean, College of Arts and Sciences

The Graduate School has verified and approved the above-named committee members.

To my family

ACKNOWLEDGEMENTS

First and foremost, I sincerely thank my major professor and advisor, Dr. Nicholas Bonesteel for being a patient, motivating, fair, honest, challenging, and involved mentor. His endless effort to support me is absolutely crucial for me to complete this beautiful project. I am lucky enough to work with him for the last several years and the lessons I have learned from him will definitely be with me for my future career in science.

I am in debt of my whole family. Without their supports, it is simply impossible for me to overcome so many difficulties, many more than I had expected before. The completion of my study at Florida State University is definitely an achievement of them, my wife Nguyen Thi Nguyet, my children Tran Nguyet Minh and Tran Thuy Dan, my parents, Dr. Tran Doan Bien and Mrs. Mai Thi Yen, and my brother, Tran Doan Huyen.

The results presented in this dissertation have been completed with contributions from discussions with Professor Kun Yang and Dr. Georgios Zikos. I thank Professors Dobrosavljevic, Piekarewicz, Safron and Dr. Engel for serving in my committee and giving me many valuable comments.

During my stay at Florida State University, I received valuable encouragements and helps from many colleagues and friends. I sincerely thank Professors Doan Nhat Quang, Nguyen Huyen Tung, Vu Ngoc Tuoc, and Pho Thi Nguyet Hang for what they did for me in the last some years. Many thanks also go to friends from “Talamese”, the Community of Vietnamese in Tallahassee, for their generous hospitalities and friendships. Kind encouragements and helps have come with me from many other friends, some of them have significant impacts on my life. Although I will not name them here, I will never forget what they did for me. Let me call them *my “hidden variables”* and tell them that I am in debt of them!

I appreciate so many helps from Dr. Simon Capstick, Sherry Tointigh, Alice Hobbs, Arshad Javed, Katie Crow, and Melissa Adams. At Florida State University, I have some friends with whom I enjoyed their friendships and discussions. They are Robert J. Cipri,

Yafis Barlas, Tesfaye A. Gebre, Yohanes Hamann Roni Pramudya, Eden Steven, Hanna Terletska, Daniel Zeuch, and others.

Last but not least, I acknowledge supports and encouragements from Dr. Doan Lien Phung during the time I made the first steps to Florida State University. I also acknowledge supports from Institute for Complex Adaptive Matter (UC Davis), Materials Computation Center (UIUC), and the Congress of Graduate Students (FSU) for the travel grants with which I made many scientific visits both inside and outside the United States.

TABLE OF CONTENTS

List of Tables	viii
List of Figures	ix
Abstract	xvii
1. INTRODUCTION	1
1.1 Models	1
1.2 Valence-bond basis	5
1.3 Random singlet phase	13
1.4 Generalized models	18
1.5 Goals and outline	24
2. VALENCE-BOND MONTE CARLO	27
2.1 Ground state projection	27
2.2 Valence-bond Monte Carlo	28
2.3 Method benchmarks	33
2.4 Concluding remarks	39
3. VALENCE-BOND ENTANGLEMENT ENTROPY	43
3.1 von Neumann entanglement entropy	44
3.2 Valence-bond entanglement entropy	50
3.3 Valence-bond Monte Carlo results	53
3.4 Concluding remarks	61
4. VALENCE-BOND FLUCTUATION	76
4.1 Valence bonds in random singlet phases	76
4.2 Valence-bond fluctuation	78
4.3 Fluctuation length scales in random singlet phases	87
4.4 Concluding remarks	96
A. PROOFS OF SOME RESULTS	102
A.1 Spin singlet projection operator	102
A.2 von Neumann entropy	103
REFERENCES	106

BIOGRAPHICAL SKETCH 112

LIST OF TABLES

2.1	Triplet state energy per bond $E_1(N)/N$ of the uniform spin-1/2 AFM Heisenberg chain for various chain size N . Results from the Lanczos technique were calculated up to $N = 20$ spins while those for $N > 20$ were extrapolated and marked by asterisks. Calculations from a conventional Monte Carlo simulation was done for chains of up to $N = 48$ spins. For comparison, the triplet state energy $E_1(N)$ for the uniform chains of up to $N = 128$ sites was calculated using valence-bond Monte Carlo. Results are given here in unit of $J_i = J$. . .	38
2.2	Finite-size gap $\Delta E(N)$ of the uniform spin-1/2 AFM Heisenberg chain for various chain size N . Results from the Lanczos technique were calculated up to $N = 20$ sites while those for $N > 20$ were extrapolated and marked by asterisks. Calculations from two Monte Carlo simulations were done for chains of up to $N = 48$ sites. For comparison, the finite-size gap $\Delta E(N)$ for chains of up to $N = 128$ sites was calculated using valence-bond Monte Carlo. Results are given here in unit of $J_i = J$	39

LIST OF FIGURES

1.1	Bratteli diagrammatic representation of the Hilbert space of a chain of N spin-1/2 particles. The horizontal axis is the number N of spins in the chain while the vertical axis is the total spin $S^{(\text{tot})}$ of the chain. The number attached to a vertex shows the number of states represented by this vertex, which is, by definition, the number of paths going from the origin to the vertex. Blue path is an example of such states where the chain size is $N = 8$ spins and the total spin $S^{(\text{tot})} = 1$. The red numbers along the horizontal axis are the dimensionality of the singlet sector $\mathcal{H}_N^{(0)}$ of the total Hilbert space corresponding to given values of N	4
1.2	The singlet state of two spins localizing at site i and j (two solid blue circles) is represented by a red curve connecting them. The arrow pointing from site i to site j implies that this bond represents the singlet state $ s_{ij}\rangle$, which differs from $ s_{ji}\rangle$ by a minus sign: $ s_{ij}\rangle = - s_{ji}\rangle$	6
1.3	A typical valence-bond state used for describing chains of anyons and chains of spins. Blue circles are the anyons/spins while red curves are valence bonds. Letters “A” and “B” label the sublattices of the chain. Any valence bond of this state connect sites from <i>different</i> sublattices. Arrows are not necessary because they are always assumed to point from a site belonging to the sublattice \mathcal{A} and a site belonging to the sublattice \mathcal{B}	7
1.4	A one-to-one correspondence between a state path with total spin zero on the Bratteli diagram and a non-crossing valence-bond state of 10 spins.	9
1.5	(a) Two non-crossing valence-bond states $ \alpha\rangle$, $ \beta\rangle$ with $N = 12$ sites. (b) To determine the overlap of these states one simply overlays the two bond configurations and counts the number of closed loops, N_{loops} , which is equal 4 on this figure. The overlap $\langle\beta \alpha\rangle$ of the two states is then determined by $d^{N_{\text{loops}}-N/2}$ where d is the quantum dimension, which equal 2 for spins. For the states $ \alpha\rangle$ and $ \beta\rangle$ shown on this figure, the overlap is $\langle\beta \alpha\rangle = d^{4-6} = d^{-2}$	11

1.6	A diagrammatic representation of a singlet projection operator Π_i^0 . Operating on a given valence-bond state, Π_i^0 creates a singlet bond connecting two spins at sites i and $i+1$ and introduces an additional factor of $1/d$ (for spins, $d = 2$). Time direction goes from the bottom to the top of the diagram. For more interpretations of this diagrammatic representation of Π_i^0 , see Figure 1.7 for the actions of Π_i^0 on two given valence-bond states.	12
1.7	Actions of two projection operators Π_1^0 and Π_2^0 on a given valence-bond state. The spins are numbered for easily describing the actions of Π_i^0 , which directly operates on sites i and $i+1$. The actions of Π_1^0 make one closed loop (see the (a) panel), which introduces a factor of d so the overall factor raised by Π_1^0 is $\frac{1}{d} \times d = 1$. On the other hand, the actions of Π_2^0 makes no closed loop (see the (b) panel), so in this case, the overall factor $\frac{1}{d}$. For spins, the quantum dimension $d = 2$	12
1.8	An illustration for the decimation procedure. J_2 is assumed to be the strongest coupling of the chain, so J_2 is much larger than the two adjacent coupling $J_2 \gg J_1$ and $J_2 \gg J_3$ (see the sub-figure of J_i vs i). Two spins 2 and 3 are frozen into a singlet state, and can be crossed out from the Hamiltonian. The effective interaction between spins 1 and 4 is then given by $\tilde{J}_{14} = \frac{2}{d^2} \frac{J_1 J_3}{J_2}$. The “quantum dimension” d of spin-1/2 particles, which is used extensively in this dissertation, is equal 2, thus $\tilde{J}_{14} = \frac{1}{2} \frac{J_1 J_3}{J_2}$	15
1.9	An ideal random singlet ground state which is represented by a single valence-bond state. The two spins of a singlet pair can be arbitrary remote and the effective interaction between them is rapidly decreasing with the distance.	16
1.10	An illustration of the renormalization group flow under which an arbitrary distribution of coupling strength $P(\beta)$ (left panel) is driven to a fixed point distribution $P_\Gamma(\beta) = \frac{1}{\Gamma} e^{-\beta/\Gamma}$ (right panel).	17
1.11	Two non-Abelian anyons (solid blue circles) can fuse into a state with total topological charge 0 or 1, corresponding to the anyonic singlet or triplet states, respectively. It is assumed that there is an energy cost J for the anyons to be in the triplet state instead of the singlet state.	20
1.12	A Bratteli diagram for the Hilbert space of a chain of N non-Abelian anyons with $k = 3$ — a chain of Fibonacci anyons. The horizontal axis shows the number of anyons N of the chain while the vertical axis shows the total topological charge of the chain. The dotted lines form a “prohibited area” where state paths can not enter due to the limit at $k/2$ of the total topological charge shown by the red line. The number attached to a given vertex shows the number of states represented by this vertex, which is, again, the number of state paths going from the origin to the vertex. For example, the blue path represents a state of a chain of 8 anyons with total topological charge 0. The red numbers along the horizontal axis show the dimensionality of $\mathcal{H}_N^{(0)}$	22

2.1	(Top) a diagrammatic representation of the action of a sequences of singlet projection operators on a given starting valence-bond state. The singlet projection operators act on the initial valence-bond state in a sequence. The resulting state $ \alpha_1\rangle$ and the weight factor $w(\alpha_1)$ are determined using the rules described in section 1.2.5. (Bottom) resulting state $ \alpha_2\rangle$ and the weight factor $w(\alpha_2)$ when the third operator in the sequence on the top panel of this figure, which is Π_4^0 , is updated by Π_9^0 (see the red arrows and circles). This update is accepted or rejected according to the usual Metropolis-Hastings algorithm.	30
2.2	Ground state energy per site $E_0(N)/N$ (in unit of J) as functions of N , the size of the uniform chains of anyons with $d = \sqrt{2}$, $\frac{1}{2}(\sqrt{5} + 1)$ and 2 which correspond to $k = 2$, $k = 3$ and $k \rightarrow \infty$. Error bars are smaller than the symbol size. The specific values of chain size taken are $N = 6, 8, 10, 12, 14, 16, 20, 24, 32, 40, 48, 64, 96, 128$. Dashed lines represent the exact results using Bethe ansatz (2.15).	41
2.3	Ground state energy per bond $E_0(N)/N$ (in unit of J) of a uniform chain of interacting non-Abelian anyons as a function of quantum dimension d . Solid red line is the exact results using Bethe ansatz (2.15) while blue squares are the results from valence-bond Monte Carlo calculations for the values of d corresponding to $k = 2, 3, 4, 5, 6, 8, 10, 15$ and ∞ . Numerical results are estimated at the chain size $N = 128$. Error bars are smaller than the symbol size.	42
3.1	A system of two spin-1/2 particles forming a singlet state which can be decomposed into two regions A and B and then the von Neumann entanglement entropy can be determined.	45
3.2	A state $ \alpha\rangle$ of $2\mathcal{N}$ anyons which pair up to \mathcal{N} singlets. The subsystem A is taken to include \mathcal{N} ends of the \mathcal{N} singlet bonds.	46
3.3	An illustration for a block A of $L = 5$ contiguous spins embedded in a spin chain. The complement of the block (subsystem) A is defined as the subsystem B for calculating the block entanglement entropy.	47
3.4	The random singlet ground state of a random chain. Given a block A of $L = 7$ sites, the number of bonds n_L leaving the block is determined to be $n_L = 3$ so in this state, the block entanglement entropy is $S_L = n_L \log_2 d = 2 \log_d \dots$	48
3.5	Conformal distance L_C , the concept which is introduced to minimize finite-size effect. For a chain of N sites and the periodic boundary condition, the conformal distance of a block of L sites in the chain is given by $L_C = N/\pi \sin(\pi L/N)$.	55
3.12	Definition of disorder strength u , the parameter which specifies the distribution $P(J)$ of the couplings J_i in such a way in which J_i are uniformly distributed on $[1 - u, 1 + u]$.	58

3.6	Semi-log plot of the valence-bond entanglement entropy S_L^{VB} of the uniform model with $d = 2$ as a function of block conformal length L_C defined as $L_C = N/\pi \sin(\pi L/N)$. System parameters are $N = 1024$, $n = 20N$ with periodic boundary conditions. Data is averaged over 50 independent simulations. The exact asymptotic scaling of S_L^{VB} by Jacobsen and Saleur is sketched by the solid line. Error bars are smaller than the symbol size. . . .	63
3.7	Semi-log plot of the valence-bond entanglement entropy S_L^{VB} of the uniform model with $d = \frac{1}{2}(\sqrt{5} + 1)$ as a function of block conformal length L_C defined as $L_C = N/\pi \sin(\pi L/N)$. System parameters are $N = 1024$, $n = 20N$ with periodic boundary conditions. Data is averaged over 50 independent simulations. The exact asymptotic scaling of S_L^{VB} by Jacobsen and Saleur is sketched by the solid line. Error bars are smaller than the symbol size. . . .	64
3.8	Semi-log plot of the valence-bond entanglement entropy S_L^{VB} of the uniform model with $d = \sqrt{2}$ as a function of block conformal length L_C defined as $L_C = N/\pi \sin(\pi L/N)$. System parameters are $N = 1024$, $n = 20N$ with periodic boundary conditions. Data is averaged over 50 independent simulations. The exact asymptotic scaling of S_L^{VB} by Jacobsen and Saleur is sketched by the solid line. Error bars are smaller than the symbol size. . . .	65
3.9	Log-log plot of the bond length distribution $P(l)$ of the uniform model with $d = 2$ as a function of bond conformal length l_C . System parameters are $N = 1024$, $n = 20N$. Data is averaged over 50 independent simulations. Periodic boundary condition is employed. The exact asymptotic scaling is sketched by the solid line. Error bars are smaller than the symbol size. . . .	66
3.10	Log-log plot of the bond length distribution $P(l)$ of the uniform model with $d = \frac{1}{2}(\sqrt{5} + 1)$ as a function of bond conformal length l_C . System parameters are $N = 1024$, $n = 20N$. Data is averaged over 50 independent simulations. Periodic boundary condition is employed. The exact asymptotic scaling is sketched by the solid line. Error bars are smaller than the symbol size. . . .	67
3.11	Log-log plot of the bond length distribution $P(l)$ of the uniform model with $d = \sqrt{2}$ as a function of bond conformal length l_C . System parameters are $N = 1024$, $n = 20N$. Data is averaged over 50 independent simulations. Periodic boundary condition is employed. The exact asymptotic scaling is sketched by the solid line. Error bars are smaller than the symbol size. . . .	68
3.13	Semi-log plots of the valence-bond entanglement entropy S_L^{VB} of a random chain with $d = 2$ as a function of block conformal length L_C . System parameters are $N = 1024$, $n = 20N$, and $u = 1.0$. Results are averaged over 2000 disorders. Periodic boundary condition is employed. RG scaling is sketched by the solid line. Error bars are smaller than the symbol size. . . .	69

3.14	Semi-log plots of the valence-bond entanglement entropy S_L^{VB} of a random chain with $d = \frac{1}{2}(\sqrt{5} + 1)$ as a function of block conformal length L_C . System parameters are $N = 1024$, $n = 20N$, and $u = 1.0$. Results are averaged over 2000 disorders. Periodic boundary condition is employed. RG scaling is sketched by the solid line. Error bars are smaller than the symbol size. . . .	70
3.15	Semi-log plots of the valence-bond entanglement entropy S_L^{VB} of a random chain with $d = \sqrt{2}$ as a function of block conformal length L_C . System parameters are $N = 1024$, $n = 20N$, and $u = 1.0$. Results are averaged over 2000 disorders. Periodic boundary condition is employed. RG scaling is sketched by the solid line. Error bars are smaller than the symbol size. . . .	71
3.16	Log-log plots of the bond length distribution $P(l)$ of a random chain with $d = 2$ as a function of bond conformal length l_C . System parameters are $N = 1024$, $n = 20N$, and $u = 1.0$. Results are averaged over 2000 disorders. Periodic boundary condition is employed. RG scaling is sketched by the solid line. Error bars are smaller than the symbol size.	72
3.17	Log-log plots of the bond length distribution $P(l)$ of a random chain with $d = \frac{1}{2}(\sqrt{5} + 1)$ as a function of bond conformal length l_C . System parameters are $N = 1024$, $n = 20N$, and $u = 1.0$. Results are averaged over 2000 disorders. Periodic boundary condition is employed. RG scaling is sketched by the solid line. Error bars are smaller than the symbol size.	73
3.18	Log-log plots of the bond length distribution $P(l)$ of a random chain with $d = \sqrt{2}$ as a function of bond conformal length l_C . System parameters are $N = 1024$, $n = 20N$, and $u = 1.0$. Results are averaged over 2000 disorders. Periodic boundary condition is employed. RG scaling is sketched by the solid line. Error bars are smaller than the symbol size.	74
3.19	d dependence of the valence-bond central charge, c_d^{VB} , for uniform (higher part) and random chains (lower part), along with the true central charges for the conformally invariant uniform models with $d = 2 \cos \frac{\pi}{k+2}$, in units of $\log_2 d$. The solid red line is the exact result in Eq. (3.41), the black squares are the central charges of the uniform chain of interacting non-Abelian anyons for different values of k (the dashed line is a guide to the eye), the green line is the real-space RG result $\tilde{c}/\log_2 d = \ln 2$ for the random models, and the blue circles and triangles are our valence-bond Monte Carlo results for uniform and random models, respectively. The inset shows the finite size extrapolation used to find c^{VB} for the uniform models with $k \rightarrow \infty$ and $k = 2$	75

4.1	A geometry of the definition of valence-bond fluctuation σ_L^2 , which is defined as the variance of n_L , the number of bond crossing one of two ends of the block of length L . Two dashed regions with size of $\sim \xi$ from two ends of the block are called “active regions” in the sense that only the fluctuations of the bonds which have one end in the regions contribute to σ_L^2 . The union of the active regions is called a “total active region” with the size of either equal or smaller than L	80
4.2	Valence-bond fluctuation σ_L^2 for the uniform chain described by Eq. (1.36) with $d = 2$ as function of block conformal length $L_C = N/\pi \sin(\pi L/N)$ for minimizing finite-size effects. The solid line depict the exact asymptotic scaling (4.6) with the coefficient c_2 determined by (4.7). Parameters for the calculation is $N = 1024$, $n = 60N$. Error bars are smaller than the symbol size.	82
4.3	Valence-bond fluctuation σ_L^2 for the uniform chain described by Eq. (1.36) with $d = \frac{1}{2}(\sqrt{5}+1)$ as function of block conformal length $L_C = N/\pi \sin(\pi L/N)$ for minimizing finite-size effects. The solid line depict the exact asymptotic scaling (4.6) with the coefficient c_2 determined by (4.7). Parameters for the calculation is $N = 1024$, $n = 60N$. Error bars are smaller than the symbol size.	83
4.4	Valence-bond fluctuation σ_L^2 for the uniform chain described by Eq. (1.36) with $d = \sqrt{2}$ as function of block conformal length $L_C = N/\pi \sin(\pi L/N)$ for minimizing finite-size effects. The solid line depict the exact asymptotic scaling (4.6) with the coefficient c_2 determined by (4.7). Parameters for the calculation is $N = 1024$, $n = 60N$. Error bars are smaller than the symbol size.	84
4.5	Valence-bond fluctuation σ_L^2 for random chains described by Eq. (1.36) with $d = 2$ as functions of block conformal length $L_C = N/\pi \sin(\pi L/N)$ for minimizing finite-size effects. Various values of u , the parameter which specifies the disorder strength are chosen as $u = 1.0, 0.75, 0.5, 0.25, 0.10$. σ_L^2 for the uniform chain ($u = 0.0$) is also shown for a comparison. Parameters for the calculation is $N = 1024$, $n = 60N$. Error bars are smaller than the symbol size.	88
4.6	Valence-bond fluctuation σ_L^2 random chains described by Eq. (1.36) with $d = \frac{1}{2}(\sqrt{5} + 1)$ as functions of block conformal length $L_C = N/\pi \sin(\pi L/N)$ for minimizing finite-size effects. Various values of u , the parameter which specifies the disorder strength are chosen as $u = 1.0, 0.75, 0.5, 0.25, 0.10$. σ_L^2 for the uniform chain ($u = 0.0$) is also shown for a comparison. Parameters for the calculation is $N = 1024$, $n = 60N$. Error bars are smaller than the symbol size.	89

4.7	Valence-bond fluctuation σ_L^2 random chains described by Eq. (1.36) with $d = \sqrt{2}$ as functions of block conformal length $L_C = N/\pi \sin(\pi L/N)$ for minimizing finite-size effects. Various values of u , the parameter which specifies the disorder strength are chosen as $u = 1.0, 0.75, 0.5, 0.25, 0.10$. σ_L^2 for the uniform chain ($u = 0.0$) is also shown for a comparison. Parameters for the calculation is $N = 1024$, $n = 60N$. Error bars are smaller than the symbol size.	90
4.8	Scaling plot according to Eq. (4.9) for the data of σ_L^2 shown on figure 4.5 (random chains with $d = 2$). On the scaling plot, only data with L odd are kept. Corresponding to disorder strength $u = 0.1, 0.25, 0.50, 0.75$, and 1.0 , the fluctuation length scale is found to be $\xi = 140, 70, 37, 21$, and 11 . Two lines illustrate the scaling (4.6) in the resonating regime and the saturation scaling in the locking regime. Explanation for symbols are shown on the figure. . . .	92
4.9	Scaling plot according to Eq. (4.9) for the data of σ_L^2 shown on figure 4.6 (random chains with $d = \frac{1}{2}(\sqrt{5}+1)$). On the scaling plot, only data with L odd are kept. Corresponding to disorder strength $u = 0.1, 0.25, 0.375, 0.50, 0.625, 0.75$, and 1.0 , the fluctuation length scale is found to be $\xi = 575, 215, 145, 87, 65, 48$, and 24 . Lines illustrate the scaling (4.6) in the resonating regime and the saturation scaling in the locking regime. Explanation for symbols are shown on the figure. The arrow points to the data points which can not be completely scaled because σ_L^2 does not saturates for $u = 0.1$ (see figure 4.6 for plots of σ_L^2). . . .	93
4.10	Scaling plot according to Eq. (4.9) for the data of σ_L^2 shown on figure 4.7 (random chains with $d = \sqrt{2}$). On the scaling plot, only data with L odd are kept. Corresponding to disorder strength $u = 0.1, 0.25, 0.375, 0.50, 0.625, 0.75$, and 1.0 , the fluctuation length scale is found to be $\xi = 720, 390, 195, 140, 102, 66$, and 32 . Lines illustrate the scaling (4.6) in the resonating regime and the saturation scaling in the locking regime. Explanation for symbols are shown on the figure. The arrows point to the data points which can not be completely scaled because σ_L^2 does not saturates for $u = 0.1$ and $u = 0.25$ (see figure 4.7 for plots of σ_L^2).	94
4.11	Fluctuation length scale ξ for $d = 2$ and crossover length scale ξ_0 for random spin-1/2 XXX chains as functions of u	98
4.12	Fluctuation length scale ξ for $d = \sqrt{2}$ and crossover length scale ξ_0 for random spin-1/2 XX chains as functions of u	99
4.13	Log-log plot of fluctuation length scale ξ as a function of disorder strength u of random chains described by Eq. (1.36) with $d = 2$, $d = \frac{1}{2}(\sqrt{5}+1)$ and $d = \sqrt{2}$. Three straight lines depict the attempted power laws $u^{-\gamma}$ with $\gamma = 1.0$ for $d = 2$, $\gamma = 1.4$ for $d = \frac{1}{2}(\sqrt{5} + 1)$, and $\gamma = 1.65$ for $d = \sqrt{2}$	100

4.14 Log-log plot of fluctuation length scale ξ as a function of disorder strength δ of random chains described by Eq. (1.36) with $d = 2$, $d = \frac{1}{2}(\sqrt{5} + 1)$ and $d = \sqrt{2}$. Three straight lines depict the attempted power laws $\delta^{-\gamma}$ with $\gamma = 1.0$ for $d = 2$, $\gamma = 1.4$ for $d = \frac{1}{2}(\sqrt{5} + 1)$, and $\gamma = 1.65$ for $d = \sqrt{2}$ 101

ABSTRACT

The set of valence-bond states — states in which localized spin-1/2 particles are correlated in singlet pairs said to be connected by valence bonds — provides a useful basis for visualizing singlet ground states of quantum spin systems. For example, the ground state of the uniform one-dimensional nearest-neighbor spin-1/2 antiferromagnetic (AFM) Heisenberg model (the prototypical spin-liquid state) can be viewed as a strongly fluctuating liquid of valence bonds with a power-law length distribution. This intuitive picture directly reflects the long-range spin correlations in this state, as well as the existence of gapless excitations created by breaking long bonds.

Valence-bond states also play a key role in describing the physics of random spin-1/2 AFM Heisenberg chains. For these systems, it was shown by Fisher, using a real space renormalization group analysis, that on long-length scales the ground state is described by a single valence-bond state known as a random singlet state. This single valence-bond state should be viewed as a caricature of the true ground state, which will certainly exhibit bond fluctuations on short-length scales.

In valence-bond Monte Carlo (VBMC) simulations valence-bond states are used to stochastically sample singlet ground states of quantum spin systems. One of the appealing features of VBMC is that if one imagines viewing the sampled valence-bond states over many Monte Carlo time steps the resulting “movie” would correspond closely to the intuitive resonating valence bond picture described above. For random Heisenberg chains (and related models) VBMC should therefore provide a useful method for directly studying the phenomenon of random singlet formation on long-length scales, while at the same time capturing the short-range fluctuations which will always be present.

In this dissertation I present results of VBMC studies for a class of models which include the uniform and random spin-1/2 AFM Heisenberg chains, as well as models describing chains of interacting non-Abelian quasiparticles — exotic quasiparticles conjectured to exist in certain fractional quantum Hall states. In addition to numerically computing and analyzing the so-called valence-bond entanglement scaling in these models, I introduce a new quantity which I refer to as the valence-bond fluctuation (the central new result and the main contribution of this dissertation). It is shown that this quantity, which is easy to compute in valence-bond Monte Carlo, provides a direct signature of random singlet phase formation by essentially allowing one to directly “see” the “locking” of the ground state into a particular valence-bond state on long-length scales. A detailed scaling analysis of this new quantity is then used to extract the dependence of the fluctuation length scale on disorder strength. Where possible, the results are compared to previous numerical and analytic work on the relevant models.

CHAPTER 1

INTRODUCTION

In this introductory chapter I give some of the essential background needed to understand the results presented in this dissertation. The chapter begins with an introduction to the spin-1/2 antiferromagnetic (AFM) Heisenberg chain — one of the best studied models in physics. Some properties of the Hilbert space of a collection of spin-1/2 particles are then reviewed, and the valence-band basis, a useful basis for visualizing the total spin 0 sector of this Hilbert space, which plays a key role throughout this dissertation, is described. The chapter then focuses on the so-called random singlet phase, a phase which appears when disorder (even weak disorder) is present in the spin-1/2 AFM Heisenberg chain. This is followed by a description of how the spin-1/2 AFM Heisenberg chain can be modified to yield a class of related models characterized by a single parameter d . For special values of d , these models can be thought of physically describing chains of interacting non-Abelian anyons — exotic quasiparticles which can exist in certain fractional quantum Hall states. With this background, the chapter concludes by giving some of the motivation for studying these models and presenting an outline of the rest of the dissertation.

1.1 Models

1.1.1 Quantum spin chains

Quantum spin chains, in which localized quantum spins interact via the exchange interaction, are of great interest from both theoretical and experimental points of view. The exchange interaction, a purely quantum mechanical effect caused by the Coulomb repulsion and the Pauli exclusion principle, has been understood since the very early years of quantum mechanics as the key to the microscopic theory of quantum magnetism and other cooperative phenomena involving electron spins [1].

Although real materials are essentially three-dimensional, low-dimensional quantum spin models, such as quantum spin chains, are scientifically valuable for many reasons. First, three-dimensional models are generally difficult to solve analytically, while in lower dimensions analytic solutions can often be obtained for clean (no disorder) models. Examples include Onsager's solution [2] for the two-dimensional Ising model or Bethe's ansatz solution [3, 4, 5] for the one-dimensional spin-1/2 AFM Heisenberg model with exchange interaction between nearest neighbor spins. Second, many real interesting materials which have well-localized spins and different exchange interactions along different orientations can be well described by low-dimensional quantum spin systems. Cuprate insulators, the materials which can be doped to produce high temperature superconductors, are excellent examples of systems well described by a two-dimensional Heisenberg model [6]. Some examples include an organic ion-radical salt which consists of 3,3'-dimethyl-2,2'-Thiazolinocyanine⁺ and TCNQ⁻ [7] and the crystalline Sr₂Cu(PO₄)₂ [8], can be modeled as a perfect spin-1/2 AFM Heisenberg chain.

The great interest given to quantum spin chains also comes from the many fascinating quantum phenomena in their ground states and low-lying excitations. Among these phenomena, quenched disorder gives rise to various exotic phases, which are realized neither in regular quantum systems nor classical random systems [9, 10]. The interplay of disorder and quantum fluctuations in the disordered models plays an essential role in these phases.

One of the models studied in detail in this dissertation is one of the fundamental quantum spin chains, the isotropic critical spin-1/2 AFM Heisenberg chain with nearest neighbor exchange interactions. The Hamiltonian describing this model is

$$H = \sum_{i=1}^N J_i \vec{S}_i \cdot \vec{S}_{i+1}, \quad (1.1)$$

where the $J_i > 0$ are the antiferromagnetic exchange couplings, while $\vec{S}_i = (S_i^x, S_i^y, S_i^z)$ is the spin-1/2 operator at site i in the vector form. We will refer to the model with constant J_i , i.e., $J_i = J_0$, as the *uniform chain*. This model is exactly solvable by Bethe ansatz [3, 4, 5] and is known to possess gapless excitations and power-law spin correlations. It is the main goal of this dissertation to study the critical *random chains* with random J_i , focusing on the random singlet phase which is relevant to the model with any finite strength of disorders [10].

1.1.2 Hilbert space

For a more detailed discussion on the model, I will describe here the relevant Hilbert space. The Hilbert space of a spin-1/2 Heisenberg chain can be examined using the rule of angular momentum coupling applied for the spins. The combination of two spins S_1 and S_2 results in a state with the possible total spin $S^{(\text{tot})}$ determined by the familiar rule for addition of angular momentum (referred to as a “fusion rule” in what follows),

$$S_1 \otimes S_2 = \bigoplus_{j=|S_1-S_2|}^{|S_1+S_2|} j. \quad (1.2)$$

As an example, the Hilbert space of the states of two spin-1/2 particles (or simply “spins” in what follows) is formed by two subspaces, one with total spin 0 and the other with total spin 1

$$\frac{1}{2} \otimes \frac{1}{2} = 0 \oplus 1. \quad (1.3)$$

The decomposition (1.2) can be used to diagrammatically express the Hilbert space of a chain of spins by means of the Bratteli diagram [11] which is shown on the Figure (1.1). On this diagram, the horizontal axis shows the number N of spins while the vertical axis shows the total spin $S^{(\text{tot})}$. Starting from $N = 0$ (corresponding to the origin of the diagram), spins are added to the chain one by one, and the fusion rule (1.2) is used to determine the possible total spins of the resulting state. A vertex at the coordinates $(N, S^{(\text{tot})})$ corresponds to the state with the chain size N and the total spin $S^{(\text{tot})}$. As an example, the vertex indicated by an arrow on the figure has coordinates $(N = 8, S^{(\text{tot})} = 1)$, implying that it corresponds to the state with total spin 1 of the chain of 8 spins. Arrows going out from a vertex show the possible values of the total spin $S^{(\text{tot})}$ when a spin is added to the chain.

As shown on the diagram, each vertex $(N, S^{(\text{tot})})$ is assigned a number showing the number of states, or more precisely, the degeneracy of the state, represented by this vertex. In other words, this number is the dimensionality of $\mathcal{H}_N^{(S^{(\text{tot})})}$, the spin- $S^{(\text{tot})}$ sector of the total Hilbert space corresponding to a chain of (even) N spins. (Of course there is an additional trivial $2S^{(\text{tot})} + 1$ -fold degeneracy associated with the possible values of the z -component of the total spin.) In this diagram, a state of $\mathcal{H}_N^{(S^{(\text{tot})})}$ is represented by a *path* going from the origin to the vertex $(N, S^{(\text{tot})})$. For example, the blue path in Figure 1.1 is a state of a chain of $N = 8$ spins and total spin $S^{(\text{tot})} = 1$. A crucial feature of this diagram is that a “state path” can go as high as possible, given that it starts from the origin and ends at the desired vertex.

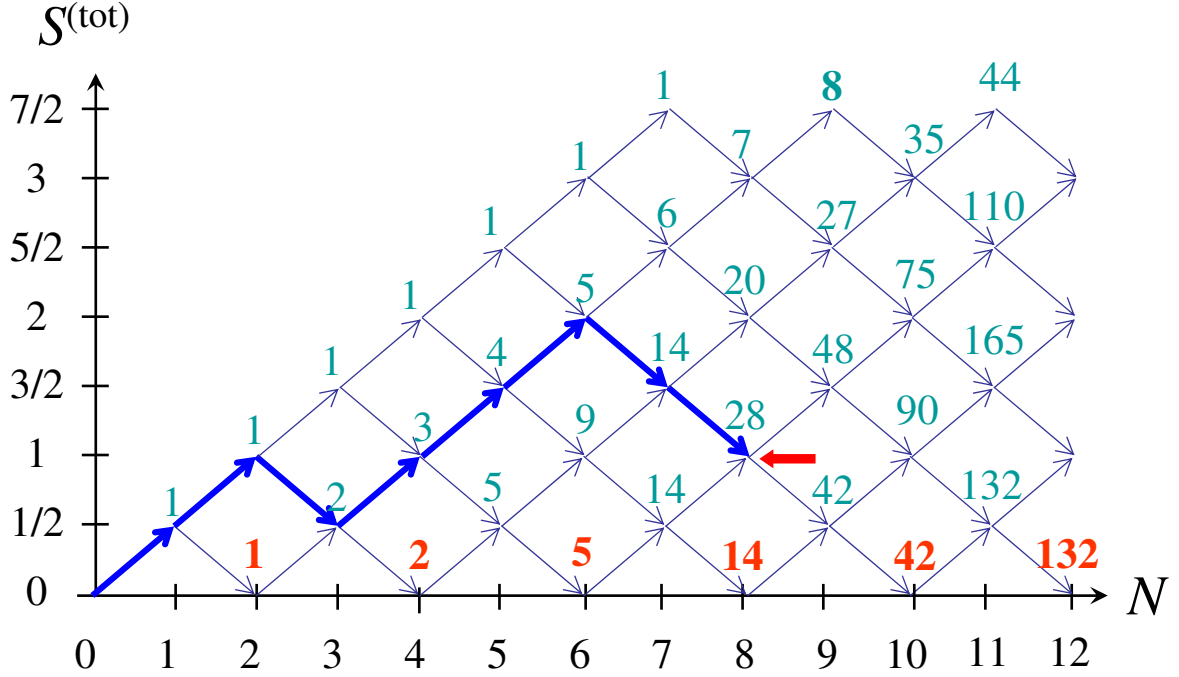


Figure 1.1: Bratteli diagrammatic representation of the Hilbert space of a chain of N spin- $1/2$ particles. The horizontal axis is the number N of spins in the chain while the vertical axis is the total spin $S^{(\text{tot})}$ of the chain. The number attached to a vertex shows the number of states represented by this vertex, which is, by definition, the number of paths going from the origin to the vertex. Blue path is an example of such states where the chain size is $N = 8$ spins and the total spin $S^{(\text{tot})} = 1$. The red numbers along the horizontal axis are the dimensionality of the singlet sector $\mathcal{H}_N^{(0)}$ of the total Hilbert space corresponding to given values of N .

The ground state $|0\rangle$ of the Heisenberg chain described by the Hamiltonian (1.1), according to a theorem by Marshall [1], is a singlet state with total spin zero. The singlet subspace $\mathcal{H}_N^{(0)}$ corresponding to the chain size N and the total spin zero is shown on the horizontal axis of the Bratteli diagram. The dimensionality of $\mathcal{H}_N^{(0)}$ with a given (even) value of N , given by the red numbers along the horizontal axis, by definition, is the number of state paths going from the origin to the corresponding point on the axis. It can be proved (see, for example, Ref. [12]) that this dimensionality is related to the so-called Catalan number as

$$\dim(\mathcal{H}_N^{(0)}) = C_{N/2} = \frac{N!}{(N/2)!(N/2 + 1)!}. \quad (1.4)$$

In the limit $N \rightarrow \infty$, it is readily shown that the Catalan number $C_{N/2}$ and hence, the dimensionality $\dim(\mathcal{H}_N^{(0)})$ grow as

$$\lim_{N \rightarrow \infty} C_{N/2} \sim \frac{2^N}{(N/2)^{3/2} \sqrt{\pi}} \sim 2^N. \quad (1.5)$$

Thus, the dimensionality of the singlet Hilbert space $\mathcal{H}_N^{(0)}$ grows asymptotically as 2^N as $N \rightarrow \infty$.

We now introduce the so-called *quantum dimension* d of the spins, defined so that for a chain of $N \gg 1$ spins, the dimensionality of the singlet Hilbert space $\mathcal{H}_N^{(0)}$ grows asymptotically as

$$\dim \mathcal{H}_N^{(0)} \sim d^N. \quad (1.6)$$

The quantum dimension characterizing spin-1/2 particles is thus $d = 2$ while for other kinds of “particles” that will also be studied in this dissertation, $d \neq 2$. For this reason, d is an important parameter which characterizes the models studied in my dissertation.

1.2 Valence-bond basis

1.2.1 Valence-bond states

The ground state $|0\rangle$ of a spin AFM Heisenberg chain described by the Hamiltonian (1.1) is a singlet state with total spin zero [1], so it can be very conveniently visualized by valence-bond states, the states in which pairs of spins are correlated into singlet states over arbitrary distances. These states are easy to compute with, and are useful to describe many physically interesting systems [13]. In particular, the valence-bond basis, the basis of valence-bond states, can be used for Monte Carlo simulations [14], as first shown in the context of variational Monte Carlo for square-lattice Heisenberg models by Liang, Doucot, and Anderson in 1988 [15].

The concept of a valence bond was introduced in the 1930s by Pauling and collaborators [16] to describe the spin singlet state of two localized (spin-1/2) electrons on different sites. In a spin chain, the singlet state $|s_{ij}\rangle$ of two spins localizing at sites i and j is defined by

$$|s_{ij}\rangle = \frac{1}{\sqrt{2}} (|\uparrow_i \downarrow_j\rangle - |\downarrow_i \uparrow_j\rangle), \quad (1.7)$$

where, as usual, $|\uparrow_i\rangle$ and $|\downarrow_i\rangle$ denote the eigenstates corresponding to the eigenvalues $\pm \frac{1}{2}$ of the spin component S^z of the spin at site i (the reduced Planck constant \hbar is set to unity).

Throughout this work, a valence bond, as shown on Figure 1.2, is usually illustrated by a (red) curve connecting two (blue) circles for two spins. Because $|s_{ij}\rangle = -|s_{ji}\rangle$, it is necessary to emphasize the order of two sites i and j in the definition (1.7) of the singlet state. This order is specified by an arrow in association with the valence bond representing the singlet, pointing from site i to site j (see Figure 1.2). However, the arrow associated with a valence bond is not really necessary in this Dissertation and this will be discussed in the context of bipartite valence-bond states at the end of this subsection.



Figure 1.2: The singlet state of two spins localizing at site i and j (two solid blue circles) is represented by a red curve connecting them. The arrow pointing from site i to site j implies that this bond represents the singlet state $|s_{ij}\rangle$, which differs from $|s_{ji}\rangle$ by a minus sign: $|s_{ij}\rangle = -|s_{ji}\rangle$.

The valence-bond state $|\alpha\rangle$ that can be used to describe chains of (even) N spins (e.g. electrons), is defined as a direct product of $N/2$ singlet states $|s_{i_k, j_k}\rangle$ as

$$|\alpha\rangle = \bigotimes_{k=1}^{N/2} |s_{i_k, j_k}\rangle. \quad (1.8)$$

The valence-bond state $|\alpha\rangle$, for convenience, is sometimes written as

$$|\alpha\rangle = |(i_1, j_1) \cdots (i_{N/2}, j_{N/2})\rangle \quad (1.9)$$

where round parentheses (i_k, j_k) is used for the singlet state $|s_{i_k, j_k}\rangle$, emphasizing that there is a valence bond connecting sites i_k and j_k . This representation is useful for describing the actions of a singlet projection operator on a given valence-bond state, which is discussed in section 1.2.5.

The models studied here are all *bipartite*, i.e., the lattice is composed of two sublattices, \mathcal{A} and \mathcal{B} , with the same size $N_{\mathcal{A}} = N_{\mathcal{B}} = N/2$. Specifically, all the odd sites belong to the sublattice \mathcal{A} while all the even sites belong to the sublattice \mathcal{B} . In a valence-bond state, for

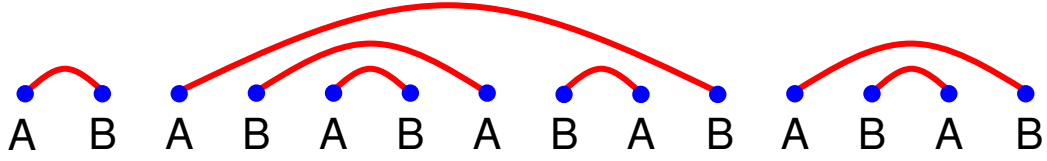


Figure 1.3: A typical valence-bond state used for describing chains of anyons and chains of spins. Blue circles are the anyons/spins while red curves are valence bonds. Letters “A” and “B” label the sublattices of the chain. Any valence bond of this state connect sites from *different* sublattices. Arrows are not necessary because they are always assumed to point from a site belonging to the sublattice \mathcal{A} and a site belonging to the sublattice \mathcal{B} .

example the state written as in Eq. (1.9), for any valence bond (i_k, j_k) , which describes the singlet state $|s_{i_k, j_k}\rangle$, $i_k \in \mathcal{A}$ and $j_k \in \mathcal{B}$. Such states are called bipartite valence-bond states, and one of them is illustrated on the Figure 1.3. For the reason of simplicity, in this figure and in what follow, the arrow which is used to specify the order of the two sites of a valence bond as illustrated on the Figure 1.2 can be removed. Instead, when considering a valence bond, it is automatically implied that the associated arrow always points from the site that belongs to the sublattice \mathcal{A} to the site that belongs to the sublattice \mathcal{B} .

1.2.2 Singlet projection operator

It is convenient to write the Hamiltonian (1.1) in terms of the singlet projection operator Π_i^0 , which is defined as

$$\Pi_i^0 = |s_{i, i+1}\rangle\langle s_{i, i+1}|. \quad (1.10)$$

In this definition $|s_{i, i+1}\rangle$ is the singlet state of two spins at sites i and $i + 1$, which can be written in the S_z eigenstate basis as

$$|s_{i, i+1}\rangle = \frac{1}{\sqrt{2}} (|\uparrow_i \downarrow_{i+1}\rangle - |\downarrow_i \uparrow_{i+1}\rangle). \quad (1.11)$$

It has been shown (see, for example the Appendix A.1) that Π_i^0 can be written in terms of the local Hamiltonian $H_i = \vec{S}_i \cdot \vec{S}_{i+1}$ as

$$\Pi_i^0 = \frac{1}{4} - \vec{S}_i \cdot \vec{S}_{i+1}. \quad (1.12)$$

It can be seen from the Eq. (1.12) that there is only a constant difference between Π_i and $\vec{S}_i \cdot \vec{S}_{i+1}$, so the Hamiltonian (1.1), up to a constant, can be written in terms of the singlet projection operators Π_i^0 as follow

$$H = - \sum_i J_i \Pi_i^0. \quad (1.13)$$

The Hamiltonian (1.13) is used throughout the rest of this dissertation because it is convenient for generalizing the Heisenberg chain to a wider class of models, including chains of interacting non-Abelian anyons, the transverse field Ising model, and higher spin chains.

For more detailed discussions on the singlet projection operator Π_i^0 , readers are referred to the Appendix A.1. In addition, a useful diagrammatic representation for Π_i^0 is given in section 1.2.5.

1.2.3 Valence-bond basis

The basis of all the valence-bond states is massively overcomplete, given that these states are not linearly independent. However, if we work only with non-crossing valence-bond states — states in which valence bonds do not cross others (see Figure 1.3 for an example of such states), the basis is *complete*, i.e., it spans the singlet Hilbert subspace $\mathcal{H}_N^{(0)}$ described in the section 1.1.2, and is *linearly independent*. In other words, the number of non-crossing valence-bond states is also the Catalan number

$$C_{N/2} = \frac{N!}{(N/2)!(N/2 + 1)!}, \quad (1.14)$$

which grows asymptotically as 2^N for large N , as we have discussed in regard to the dimensionality of the singlet subspace $\mathcal{H}_N^{(0)}$ of the spin-1/2 systems.

As a proof for the result that the number of non-crossing valence-bond state is also the Catalan number, on the Figure 1.4 a one-to-one correspondence between a state path of the Bratteli diagram with total spin zero of 10 sites and a non-crossing valence-bond state. Having a state path shown on the diagram, which represents a state of total spin zero, the procedure for constructing the corresponding non-crossing valence-bond state is as follows. At each spin, depending on whether the *incoming arrow goes up or down*, a valence bond is *opened or closed*, respectively, at this site. Consider, for example, site 1 at which the incoming arrow goes up, thus a valence bond is opened at the site 1. The incoming arrow at

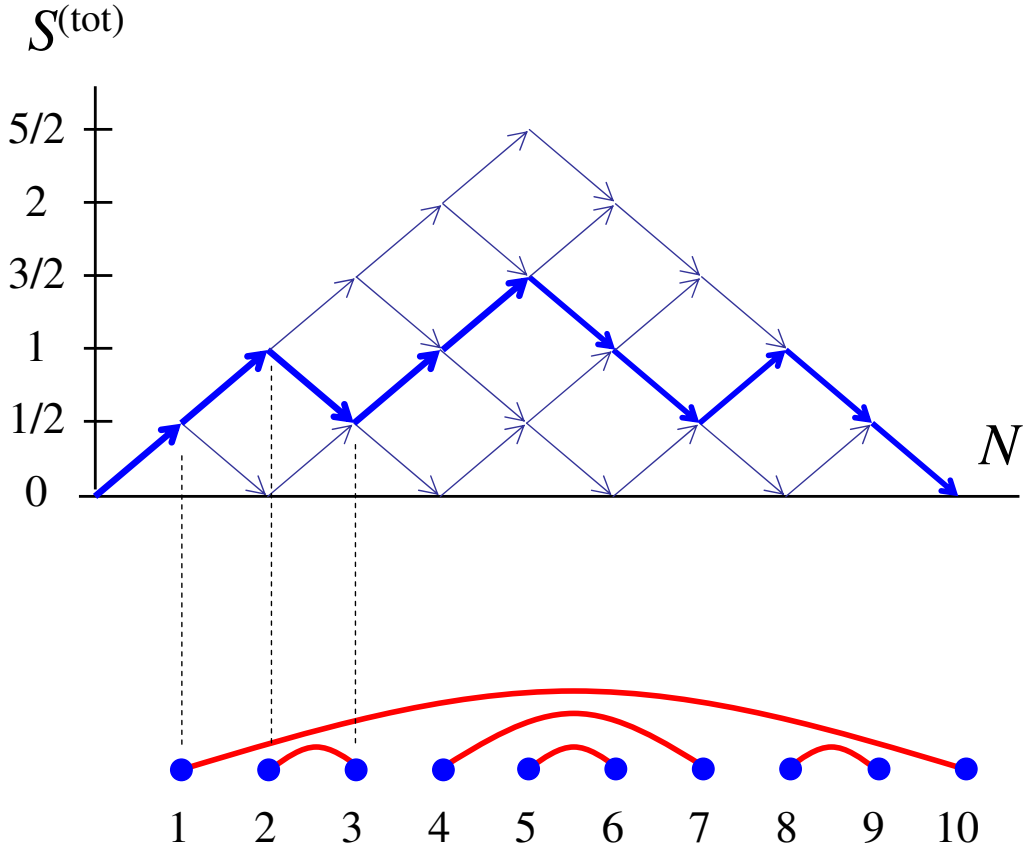


Figure 1.4: A one-to-one correspondence between a state path with total spin zero on the Bratteli diagram and a non-crossing valence-bond state of 10 spins.

site 2 also goes up, thus another valence bond is opened at site 2. Now, the arrow at site 3 goes down, implying that a valence bond is closed at this site. Among two opening valence bonds, which are opened at sites 1 and 2 as mentioned above, which bond is closed at site 3? The answer is the bond starting at site 2, the opening bond opened at the *nearest site from the left*. This criteria guarantees that the bonds constructed by this procedure are non-crossing. This procedure is iterated until the last site is reached. At the end, the non-crossing valence bond obtained is *unique*. This procedure can also be reverted to obtain a unique state path starting from a non-crossing valence-bond state. This one-to-one correspondence implies that the number of all the non-crossing valence-bond states is equal to the number of all the state paths going from the diagram origin to the vertex $(N, 0)$ on the horizontal

axis, which describes a state with total spin zero. The number of such valence-bond states, therefore, is $C_{N/2}$, a Catalan number.

A very important property of this basis is that it is not orthogonal, i.e., the overlap of any two basis states is non-zero (see section (1.2.4)). This is one of the foundations of valence-bond Monte Carlo, the numerical method used in this dissertation. For describing this numerical method, actions of a singlet projection operator Π_i^0 on a given valence-bond state is also necessary. In the next sections, the overlap of two arbitrary valence-bond states as well as the actions of the singlet projection operators Π_i^0 on valence-bond states are described.

1.2.4 Overlap of two valence-bond states

A formal derivation of the overlap of two given valence-bond states describing a chain of spins can be found elsewhere, for example, in Ref. [17]. I will describe here a very simple procedure for calculating the overlap, which is easy to be implemented in a valence-bond Monte Carlo simulation.

Being shown on the Figure 1.5 is the procedure for determining the overlap of two valence-bond states $|\alpha\rangle$ and $|\beta\rangle$ of a chain of N spins. Having the bond configurations corresponding to states $|\alpha\rangle$ and $|\beta\rangle$, one simply superimposes one onto the other, and counts the number of closed loops N_{loops} formed by the bonds. The overlap $\langle\beta|\alpha\rangle$ of the states $|\alpha\rangle$ and $|\beta\rangle$ is then determined by a very simple formula:

$$\langle\beta|\alpha\rangle = d^{N_{loops}-N/2} \quad (1.15)$$

where d is the quantum dimension, which equals 2 for spins. In this case, the overlap of $|\alpha\rangle$ and $|\beta\rangle$ is $2^{N_{loops}-N/2}$. Note that determined by the formula (1.15), the overlap of any two valence-bond states $|\alpha\rangle$ and $|\beta\rangle$ is always non-zero.

1.2.5 Actions of singlet projection operators on a valence-bond state

I will explain in this section a simple rule for diagrammatically describing the actions of a singlet projection operator Π_i^0 on a given valence-bond state. A proof of this rule can be found in Ref. [18] for arbitrary d , of which the value $d = 2$ is relevant for spins.

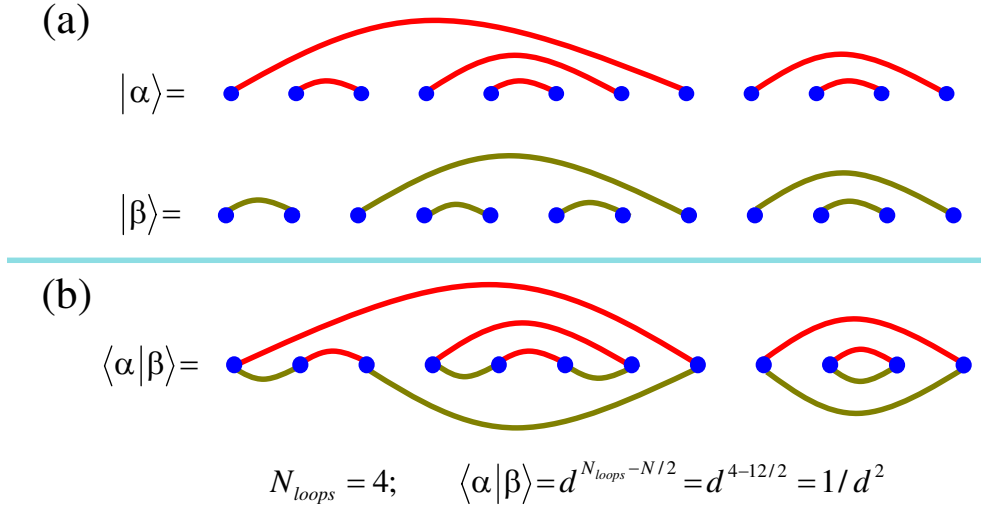


Figure 1.5: (a) Two non-crossing valence-bond states $|\alpha\rangle$, $|\beta\rangle$ with $N = 12$ sites. (b) To determine the overlap of these states one simply overlays the two bond configurations and counts the number of closed loops, N_{loops} , which is equal 4 on this figure. The overlap $\langle \beta | \alpha \rangle$ of the two states is then determined by $d^{N_{\text{loops}} - N/2}$ where d is the quantum dimension, which equal 2 for spins. For the states $|\alpha\rangle$ and $|\beta\rangle$ shown on this figure, the overlap is $\langle \beta | \alpha \rangle = d^{4-6} = d^{-2}$.

For simply describing this rule, we use the notation (i, j) for the singlet state $|s_{ij}\rangle$ of spins at sites i and j . A valence-bond state represented as $|\cdots (i, j) \cdots\rangle$ implies that spins at sites i and j are in a singlet. The actions of a singlet projection operator Π_i^0 on a valence-bond state can be classified into two cases. In the first case when the spins at sites i and $i + 1$ are in a singlet state, operating Π_i^1 on $|\cdots (i, j) \cdots\rangle$ yields $|\cdots (i, j) \cdots\rangle$ itself

$$\Pi_i^0 |\cdots (i, i + 1) \cdots\rangle = |\cdots (i, i + 1) \cdots\rangle, \quad (1.16)$$

i.e., the (diagonal) action of Π_i^0 leaves no change on the state. On the other hand, when the spins at sites i and $i + 1$ are not in a singlet state, the (off-diagonal) action of Π_i^0 re-organizes the bond configuration and introduce an additional factor of $\frac{1}{d}$ (note that for spins, the quantum dimension is $d = 2$)

$$\Pi_i^0 |\cdots (i, j) \cdots (i + 1, k) \cdots\rangle = \frac{1}{d} |\cdots (i, i + 1) \cdots (j, k) \cdots\rangle. \quad (1.17)$$

The rule described in (1.16) and (1.17) can be described in a diagrammatic way which is very useful for the subsequent parts of this dissertation. We first discuss the diagrammatic

$$\Pi_i^0 = \frac{1}{d} \left| \begin{array}{c} | \\ | \\ \dots \\ | \end{array} \right. \begin{array}{c} \text{---} \\ \text{---} \\ \text{---} \\ \text{---} \end{array} \left. \begin{array}{c} | \\ | \\ \dots \\ | \end{array} \right|$$

Figure 1.6: A diagrammatic representation of a singlet projection operator Π_i^0 . Operating on a given valence-bond state, Π_i^0 creates a singlet bond connecting two spins at sites i and $i + 1$ and introduces an additional factor of $1/d$ (for spins, $d = 2$). Time direction goes from the bottom to the top of the diagram. For more interpretations of this diagrammatic representation of Π_i^0 , see Figure 1.7 for the actions of Π_i^0 on two given valence-bond states.

representation of a singlet projection operator Π_i^0 which is shown on the Figure 1.6 where the time direction goes from the bottom to the top of the diagram. It is shown on this figure that Π_i^0 creates a valence bond connecting two sites i and $i + 1$ and introduces an additional factor $1/d$. We note that for spins, $d = 2$.

$$\begin{aligned} \text{(a)} \quad \Pi_1^0 \begin{array}{c} 1 \quad 2 \quad 3 \quad 4 \\ \bullet \text{---} \bullet \quad \bullet \text{---} \bullet \end{array} &= \frac{1}{d} \begin{array}{c} \text{---} \\ \text{---} \\ \text{---} \\ \text{---} \end{array} \begin{array}{c} \text{---} \\ \text{---} \\ \text{---} \\ \text{---} \end{array} = \begin{array}{c} \bullet \text{---} \bullet \quad \bullet \text{---} \bullet \end{array} \\ \text{(b)} \quad \Pi_2^0 \begin{array}{c} 1 \quad 2 \quad 3 \quad 4 \\ \bullet \text{---} \bullet \quad \bullet \text{---} \bullet \end{array} &= \frac{1}{d} \begin{array}{c} \text{---} \\ \text{---} \\ \text{---} \\ \text{---} \end{array} \begin{array}{c} \text{---} \\ \text{---} \\ \text{---} \\ \text{---} \end{array} = \frac{1}{d} \begin{array}{c} \bullet \text{---} \bullet \text{---} \bullet \text{---} \bullet \end{array} \end{aligned}$$

Figure 1.7: Actions of two projection operators Π_1^0 and Π_2^0 on a given valence-bond state. The spins are numbered for easily describing the actions of Π_i^0 , which directly operates on sites i and $i + 1$. The actions of Π_1^0 make one closed loop (see the (a) panel), which introduces a factor of d so the overall factor raised by Π_1^0 is $\frac{1}{d} \times d = 1$. On the other hand, the actions of Π_2^0 makes no closed loop (see the (b) panel), so in this case, the overall factor $\frac{1}{d}$. For spins, the quantum dimension $d = 2$.

The actions of a singlet projection operator Π_i^0 on a given valence-bond state $|\alpha\rangle$ can then be described by overlaying the diagram for Π_i^0 on the bond configuration of $|\alpha\rangle$. The resulting state is determined by the open loops which terminate at the top of the diagram

while an additional factor is given by considering two sites i and $i + 1$ in the initial state $|\alpha\rangle$. If they are already connected by a valence bond, then a closed loop is formed (see Figure 1.7 (a)). For the closed loop, a factor of d is introduced [18], resulting in the overall factor is $1/d \times d = 1$, as described on the Eq. (1.16). On the other hand, if the two sites are not in a singlet state, there is no closed loop (see Figure 1.7 (b)), so the factor is just $1/d$, as in the Eq. (1.17). The overall factor, which is either 1 or $1/d$, is a very important quantity in the numerical method used in my dissertation.

1.3 Random singlet phase

1.3.1 Roles of disorders

With no disorder ($J_i = J$), the uniform spin-1/2 AFM Heisenberg chain described by the Hamiltonian (1.13) can be solved exactly by Bethe ansatz [3, 4] and has been shown to have a gapless quasi-long-range-ordered phase. In the valence-bond basis, the ground state $|0\rangle$ of this chain can be thought of as a linear combination of all the possible valence-bond states in which bonds are strongly resonating on all length scales and are characterized by a power law bond length distribution. This strong resonance reproduces the translational invariance of the “spin-liquid” ground state, which is directly implied from the Hamiltonian of the uniform chain.

It has been shown by Doty and Fisher [9] that any amount of disorder of J_i is relevant and destroys the quasi-long-range order while the translational invariance is also completely broken. Consequently, many unusual phenomena are realized from the presence of disorder, showing a key role of the interplay between strong interactions and disorder [10, 19, 20, 21, 22, 23, 24].

In 1979, Dasgupta, Ma and Hu [21, 22] introduced a real space renormalization group (RG) procedure to study the disordered spin-1/2 AFM Heisenberg chains. The procedure, which is simple and useful, consists of eliminating in an iterative way the degrees of freedom of high-energy scales, to obtain in the end a single non-crossing valence-bond state as the ground state of the disordered chain in low-energy scales, and the associated phase is referred as “random singlet phase” [10]. At zero temperature, each spin forms a singlet pair with another spin, making a valence bond connecting them. While most of the bonds are short, bonds of arbitrary long length also exist. The work of Fisher [10] has thus generated a great

interest in using this method to study the random singlet phases in spin-1/2 Heisenberg chains [25], spin-1 Heisenberg chains [26], and chains of interacting non-Abelian anyons, the model which can be viewed as a generalization of the quantum spin-1/2 chains.

1.3.2 Random singlet phases

The RG procedure introduced by Dasgupta, Ma and Hu [21, 22] for the spin-1/2 AFM Heisenberg chain is described as follow. We first identify the strongest coupling of the chain, say, J_2 and consider the block of four contiguous spins labeled by 1, 2, 3, and 4 with the local Hamiltonian given by

$$\mathcal{H}_{1234} = J_1 \vec{S}_1 \cdot \vec{S}_2 + J_2 \vec{S}_2 \cdot \vec{S}_3 + J_3 \vec{S}_3 \cdot \vec{S}_4. \quad (1.18)$$

We then make an assumption that

$$J_2 \gg J_1 \quad (1.19)$$

$$J_2 \gg J_3,$$

so \mathcal{H}_{1234} can be separated into two terms as $\mathcal{H}_{1234} = \mathcal{H}_0 + \mathcal{H}$ where the unperturbed term \mathcal{H}_0 is given by

$$\mathcal{H}_0 = J_2 \vec{S}_2 \cdot \vec{S}_3 \quad (1.20)$$

and the perturbation term \mathcal{H} is

$$\mathcal{H} = J_1 \vec{S}_1 \cdot \vec{S}_2 + J_3 \vec{S}_3 \cdot \vec{S}_4. \quad (1.21)$$

At zero temperature, perturbation calculations are performed for the ground state energy of the local Hamiltonian \mathcal{H}_{1234} . First, we note that the ground state of the unperturbed Hamiltonian \mathcal{H}_0 is the singlet state $|s_{23}\rangle$ of \vec{S}_2 and \vec{S}_3 corresponding to the ground state energy $\epsilon_s = -\frac{3}{4}J_2$. The two spins at sites 2 and 3, therefore, are connected by a valence bond, as can be seen on the figure (1.8).

We then include the effects of the perturbation \mathcal{H} on the ground state energy of the local Hamiltonian \mathcal{H}_{1234} . Being noted that \mathcal{H}_0 has three more triplet eigenstates $|t_{23}^{(1)}\rangle = \frac{1}{\sqrt{2}}(|\uparrow_i \downarrow_{i+1}\rangle + |\downarrow_i \uparrow_{i+1}\rangle)$, $|t_{23}^{(2)}\rangle = \frac{1}{\sqrt{2}}|\uparrow_i \uparrow_{i+1}\rangle$, and $|t_{23}^{(3)}\rangle = \frac{1}{\sqrt{2}}|\downarrow_i \downarrow_{i+1}\rangle$, all with the same eigenvalue $\epsilon_t = \frac{1}{4}J_2$, the second order perturbation expression for the modified ground state energy of \mathcal{H}_{1234} is

$$\epsilon_0 = \epsilon_s + \langle s_{23} | \mathcal{H} | s_{23} \rangle + \sum_{i=1}^3 \left| \langle s_{23} | \mathcal{H} | t_{23}^{(i)} \rangle \right|^2 \frac{1}{\epsilon_s - \epsilon_t}. \quad (1.22)$$

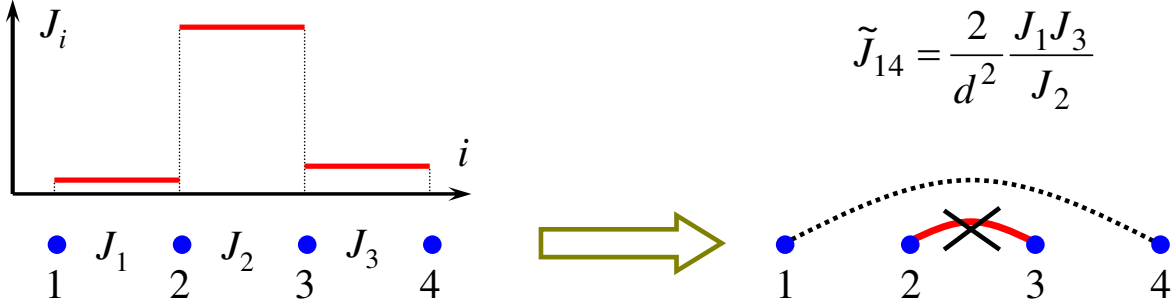


Figure 1.8: An illustration for the decimation procedure. J_2 is assumed to be the strongest coupling of the chain, so J_2 is much larger than the two adjacent coupling $J_2 \gg J_1$ and $J_2 \gg J_3$ (see the sub-figure of J_i vs i). Two spins 2 and 3 are frozen into a singlet state, and can be crossed out from the Hamiltonian. The effective interaction between spins 1 and 4 is then given by $\tilde{J}_{14} = \frac{2}{d^2} \frac{J_1 J_3}{J_2}$. The “quantum dimension” d of spin-1/2 particles, which is used extensively in this dissertation, is equal 2, thus $\tilde{J}_{14} = \frac{1}{2} \frac{J_1 J_3}{J_2}$.

Now the two spins at sites 1 and 4 enter the stage and play a role. The expression (1.22) is expected to be written as

$$\epsilon_0 = \epsilon'_0 + \tilde{J}_{14} \vec{S}_1 \cdot \vec{S}_4. \quad (1.23)$$

A little calculation which makes (1.23) become equivalent to (1.22) gives

$$\epsilon'_0 = -\frac{3}{4} J_2 - \frac{3}{16 J_2} (J_1^2 + J_3^2) \quad (1.24)$$

and

$$\tilde{J}_{14} = \frac{1}{2} \frac{J_1 J_3}{J_2}. \quad (1.25)$$

After this step, two spins at sites 2 and 3 are *frozen* in the singlet state, so they can be removed from the chain. In the *effective* Hamiltonian which describes the reduced chain, the effective coupling \tilde{J}_{14} is added while the constant ϵ'_0 is removed. This procedure is iterated to eliminate the spins corresponding to the next strongest remaining coupling so at the end of the iteration and at the limit of very strong disorder, a valence-bond state (see Figure (1.9)) is obtained as the ground state of this random chain [10, 21, 22].

A crucial feature of this procedure is that the effective coupling \tilde{J}_{14} is not correlated with the remaining couplings of this chain, so J_i are always statistically independent during the decimation procedure. Consequently, one can safely work with $P(J, \Omega)$, defined as the

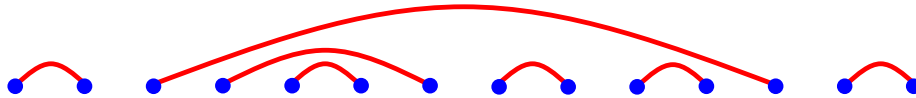


Figure 1.9: An ideal random singlet ground state which is represented by a single valence-bond state. The two spins of a singlet pair can be arbitrary remote and the effective interaction between them is rapidly decreasing with the distance.

probability distribution of the renormalized coupling J , given that the strongest remaining coupling is Ω . This is an important concept in the sense that it determines various physical properties of the chain, for example, the magnetic susceptibility and specific heat when the effects of non-zero temperature are considered [10, 22]. We denote Ω_0 as the strongest initial coupling and introduce

$$\Gamma = \ln \left(\frac{\Omega_0}{\Omega} \right) \quad (1.26)$$

as the flow parameter and

$$\beta = \ln \left(\frac{\Omega}{J} \right) \quad (1.27)$$

is a new variable, the renormalized coupling distribution becomes $P_\Gamma(\beta)$, which is governed by the so-called flow equation [10, 21, 22]

$$\frac{dP_\Gamma(\beta)}{d\Gamma} = P_\Gamma(0) \int_0^\infty d\beta_1 \int_0^\infty d\beta_2 \delta_{\beta_1 + \beta_2 - \beta} P_\Gamma(\beta_2) P_\Gamma(\beta_1) + \frac{\partial P_\Gamma(\beta)}{\partial \beta}. \quad (1.28)$$

In the limit of infinite chain size, Fisher has shown [10] that an arbitrary initial random coupling distribution $P(\beta)$, according to the Eq. (1.28), flows to the infinite randomness fixed point distribution given by

$$P_\Gamma(\beta) = \frac{1}{\Gamma} e^{-\beta/\Gamma}. \quad (1.29)$$

Consequently, disorder with any strength in the random spin-1/2 AFM Heisenberg chains is usually relevant and hence drives the original model into the so-called random singlet phase at low-energies. An illustration for the renormalization group flow is given on figure 1.10.

At zero temperature, the random singlet ground state of a random chain is a single valence-bond state with two important characters: the singlet bonds can be formed at arbitrary long distance as Ω is low enough and no singlet bond can cross each other. In

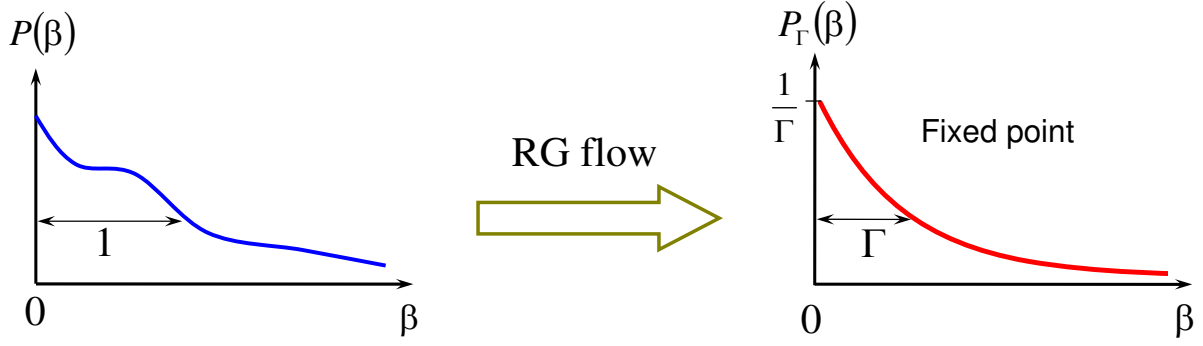


Figure 1.10: An illustration of the renormalization group flow under which an arbitrary distribution of coupling strength $P(\beta)$ (left panel) is driven to a fixed point distribution $P_\Gamma(\beta) = \frac{1}{\Gamma}e^{-\beta/\Gamma}$ (right panel).

addition, it can be found [25] that the relation between the typical singlet bond length λ and the energy scale, on average, is

$$\lambda \sim \Gamma^2 \quad (1.30)$$

where $\Omega = \Omega_0 e^{-\Gamma}$. So at lower Ω , the flow parameter Γ is larger and the length scale of the corresponding singlet bond is also longer.

The scaling of length with energy results directly to the forms of the susceptibility and specific heat at low temperatures. The key point here is that at a low temperature T , spins with bond energies $\Omega > T$ are frozen (paired) into singlets, while temperature T breaks valence bonds with $\Omega \leq T$, so the spins associated with these bonds are free. The number of unpaired (remaining) spins is

$$N_R = \frac{N}{\Gamma^2} \sim \frac{1}{|\ln \Omega|^2} \propto \frac{1}{|\ln T|^2}. \quad (1.31)$$

Because these spins are essentially free, they contribute to physical quantities such as specific heat and susceptibility, and therefore N_R determines the forms of these quantities. From the number of unpaired spins (1.31), it was found [10] that the low-energy specific heat is given by

$$C = \frac{TdS}{dT} \sim \frac{1}{|\ln T|^3} \quad (1.32)$$

while the susceptibility of the random singlet phase is

$$\chi \sim \frac{1}{T[\ln(\Omega/T)]^2}. \quad (1.33)$$

1.3.3 Essential features

There are two essential features that characterize a random single ground state and are relevant to the work in my dissertation. The *first feature* implies that valence bonds in a random singlet ground state can have any length. More precisely, the probability to have a long bond decreases with an inverse-square power law of the bond length. This feature, which is illustrated on figure 1.9, is directly implied by the RG scheme on a given disorder.

For a sufficiently strong disorder, the approximation (1.19) used for the RG analysis is well satisfied, i.e., the criteria (1.19) holds for all the decimation steps of the RG analysis. Therefore, the random singlet ground state is precisely a single valence-bond state, of which valence bonds do not fluctuate. In a more realistic model with finite disorder strength, the picture is somewhat different. In particular, the valence bonds are “locked” into given bond configuration on long-length scales, while, at the same time, they strongly resonate on short-length scales. For an illustration of this feature, a movie that visualizes a random singlet state is available online [here](#) [27], which clearly shows that the bonds fluctuate only on short-length scales. This feature implies that although the RG analysis described in section 1.3.2 is less effective for short-length scales, it is asymptotically correct on long-length scales or equivalently, on low-energy scales. The low-energy physics of the model is therefore adequately described by the random singlet ground state obtained by the RG approach.

1.4 Generalized models

1.4.1 Non-Abelian anyons

A spin-1/2 AFM Heisenberg chain can be viewed as a special case of a model which describes chains of interacting non-Abelian anyons (or simply anyons in what follows), the exotic quasiparticle excitations believed to exist in some two-dimensional quantum systems and obey non-Abelian statistics — the statistics described by unitary matrices [18, 28]. The model, defined by Feiguin *et al.* in 2007 [29], is characterized by a single parameter d so that for $d = 2$, it corresponds to a spin-1/2 AFM Heisenberg chain. Random chains of anyons, similar to random spin-1/2 AFM Heisenberg chains, have been shown to enter random singlet phases, as pointed out by Bonesteel and Yang [30].

Non-Abelian anyons are of particular interest due to a possibility to be used in the so-called topological quantum computers, where braiding of the anyons is used to perform the

unitary transformations of a quantum computation scheme [31, 18, 28]. Physically, non-Abelian anyons can be realized [18, 32] by collective excitations in some condensed matter systems, such as the fractional quantum Hall states of two dimensional electron systems [33]. For example, Ising anyons and Fibonacci anyons are the non-Abelian anyons corresponding to the so-called *levels* $k = 2$ and $k = 3$, which can be relevant to the fractional quantum Hall states with $\nu = 5/2$ [34, 35] and $\nu = 12/5$ [36], respectively. Mathematically, properties of non-Abelian anyons with level k can be described by the $SU(2)_k$ Chern-Simon effective field theory. In this theory, non-Abelian anyons are characterized by a “angular-momentum-like” quantum number called topological charge s which can take the values $0, \frac{1}{2}, 1, \dots, \frac{k}{2}$ [18, 28, 32].

The anyons may interact. For a system of N anyons, there is an associated low-energy Hilbert space whose dimensionality grows exponentially with N . If the anyons are well separated, this Hilbert space is degenerate, however, bringing them closed enough will lift the degeneracy, and the anyons are said to interact. When two anyons with topological charge s_1 and s_2 interact, they can either annihilate, or form a new anyon with a total topological charge. The fuse rule, which specifies the possible values of the total topological charge is given as [18, 28]

$$s_1 \otimes s_2 = |s_1 - s_2| \oplus \dots \oplus \min(s_1 + s_2, k - s_1 - s_2), \quad (1.34)$$

where each value of possible total topological charge occurs with multiplicity 1. This fusion rule implies that for a collection of non-Abelian anyons of level k , the total topological charge of the collection can not exceed $k/2$. Note that according to Eq. (1.2), there is no such limit for spins. For an example, consider two anyons with $s_1 = s_2 = \frac{1}{2}$, so the fusion rule is

$$\frac{1}{2} \otimes \frac{1}{2} = 0 \oplus 1, \quad (1.35)$$

i.e., if one has two anyons with topological charges $\frac{1}{2}$, the topological charge of their resulting state is either 0 or 1. We note that this fusion rule is similar to that for spins described in Eq. (1.2) according to which two spins may form a singlet or a triplet. Following Refs. [29, 30], the resulting state with total topological charge 0 or 1 are referred as a “singlet” or a “triplet”, respectively. Note that while the spin triplet state is 3-fold degenerated, the anyonic “triplet” is non-degenerated. The terminologies of anyonic singlet and triplet are useful in generalizing from chains of spins to chains of anyons.

1.4.2 Chains of non-Abelian anyons

Chains of non-Abelian anyons

In 2007, Feiguin *et al.* [29] introduced a simple, exactly solvable model which is an analogue of the spin-1/2 AFM Heisenberg chain. This model, which describes a chain of anyons, is defined by, similar to spin-1/2 particles, assigning an energy gain $J_i > 0$ if two anyons at site i and $i + 1$ fuse to triplet state (total topological charge 1) instead of singlet state (total topological charge 0) (see figure 1.11 for an illustration). The Hamiltonian describing this model is then given by:

$$H = - \sum_i J_i \Pi_i^0, \quad (1.36)$$

where the anyonic “singlet” projection operator Π_i^0 , again, is defined to project the anyons at sites i and $i + 1$ onto the singlet state — the state with total topological charge zero. Similar to the spin singlet projection operator, the anyonic singlet projection operator Π_i^0 can be diagrammatically described by Figure 1.6 in which d is the quantum dimension of the anyons, and will be defined right below.

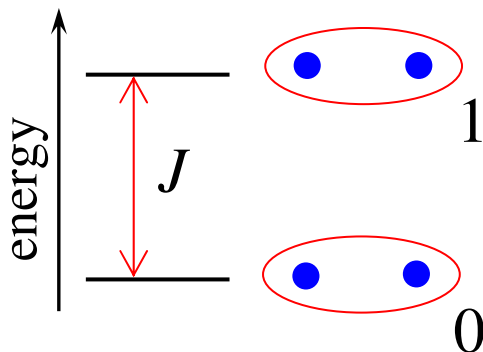


Figure 1.11: Two non-Abelian anyons (solid blue circles) can fuse into a state with total topological charge 0 or 1, corresponding to the anyonic singlet or triplet states, respectively. It is assumed that there is an energy cost J for the anyons to be in the triplet state instead of the singlet state.

While the Hamiltonian (1.36) for a chain of interacting anyons is mathematically identical to the Hamiltonian (1.13) for a spin-1/2 AFM Heisenberg chain, the chain of anyons can

be viewed as a generalization of the spin-1/2 Heisenberg chains. In order to discuss this generalization, we will discuss the Hilbert space of a chain of anyons.

Hilbert space

Similar to that for spins, the fusion rule (1.34) with a truncation at $k/2$ for anyons is the starting point for using Bratteli diagram to represent the Hilbert space $\mathcal{H}_N^{(0)}$ corresponding to a chain of N anyons. On the Figure 1.12, a truncated Bratteli diagram corresponding to a chain of N anyons with $k = 3$ is shown. According to the fusion rule (1.34), the total topological charge of the chain is limited by the value of $k/2$ which is shown on the Figure 1.12 as the red line. State paths (the blue path is an example), therefore, can not exceed this limit. The dimensionality of $\mathcal{H}_N^{(0)}$, again, is the number of state paths starting from the origin and ending at the point $(N, 0)$. Being shown on the Figure (1.12), the red numbers corresponds to the values of $\dim(\mathcal{H}_N^{(0)}) = 1, 2, 5, 13, 34, 89$ with the chain sizes $N = 2, 4, 6, 8, 10, 12$.

Due to the truncation of the total topological charge at $k/2$, $\dim(\mathcal{H}_N^{(0)})$ for a chain of N anyons is different from that of a chain of N spins. It can be shown that for $N \gg 1$, the dimensionality $\dim(\mathcal{H}_N^{(0)})$ depends on N as [18, 28]

$$\dim(\mathcal{H}_N^{(0)}) \sim d^N \quad (1.37)$$

where

$$d = 2 \cos \frac{\pi}{k+2} \quad (1.38)$$

is called the “quantum dimension” of the anyons at level k [37, 18, 28, 32]. A derivation for the relations (1.37) and (1.38) by counting the state paths in the Bratteli diagram can be found, for example, in Ref. [12].

In the limit $k \rightarrow \infty$, the quantum dimension $d = 2$ and the anyons can be viewed as spins in the sense that there is no truncation on the total topological charge. Fibonacci anyons with $k = 3$ have the quantum dimension is $d = \phi = \frac{1}{2}(\sqrt{5} + 1)$, the golden mean, are of particular interest for quantum computation [18]. Another kind of anyons which is also of great interest is the so-called the Ising anyon. Ising anyons are characterized by the level $k = 2$ or, equivalently, the quantum dimension $d = \sqrt{2}$.

With the introduction of “anyonic singlet” which is energetically favorable over the anyonic triplet in section 1.4.1, valence bonds can be used to describe the singlet state

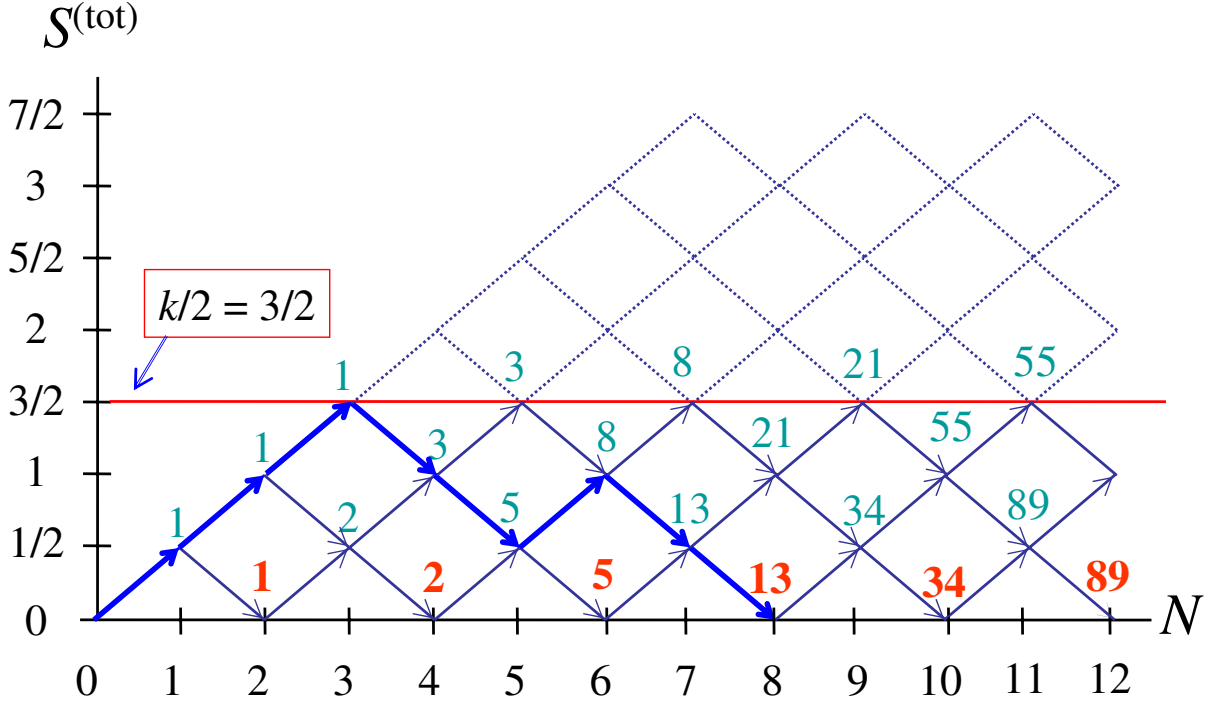


Figure 1.12: A Bratteli diagram for the Hilbert space of a chain of N non-Abelian anyons with $k = 3$ — a chain of Fibonacci anyons. The horizontal axis shows the number of anyons N of the chain while the vertical axis shows the total topological charge of the chain. The dotted lines form a “prohibited area” where state paths can not enter due to the limit at $k/2$ of the total topological charge shown by the red line. The number attached to a given vertex shows the number of states represented by this vertex, which is, again, the number of state paths going from the origin to the vertex. For example, the blue path represents a state of a chain of 8 anyons with total topological charge 0. The red numbers along the horizontal axis show the dimensionality of $\mathcal{H}_N^{(0)}$.

of pairs of anyons. Consequently, the valence-bond basis can also be used to describe chains of interacting anyons. Determined by Eq. (1.38), the quantum dimension d of an anyon with any k is smaller than 2, which is the quantum dimension of spins, so the dimensionality of the relevant Hilbert space of an anyon chain is smaller than that of a spin chain. Consequently, the non-crossing valence-bond basis described in the section 1.2 is over-complete when describing the Hilbert space $\mathcal{H}_N^{(0)}$ of chains of anyons. However, the Hilbert space $\mathcal{H}_N^{(0)}$ spanned by this basis is still perfectly well-defined, and can still be used for describing chains of anyons. For the values of d given by Eq. (1.38), the Hilbert space

$\mathcal{H}_N^{(0)}$ can be interpreted physically as describing the “topological charge 0” sector of the chains of N interacting anyons.

Special cases and related models

Chains of anyons described by the Hamiltonian (1.36) can be viewed as certain deformations of a spin-1/2 AFM Heisenberg chain. For certain values of d , model (1.36) corresponds to various known models. For integer k , i.e., $k = 2, 3, \dots, \infty$, the uniform chain of anyons described by (1.36) with $d = 2 \cos \frac{\pi}{k+2}$ corresponds to the so-called conformally invariant Andrews-Baxter-Forrester (ABF) models [38]. Model (1.36) with $k = 2$ or, equivalently, with quantum dimension $d = \sqrt{2}$ describes a chain of Ising anyons, the non-Abelian anyons believed to exist in the fractional quantum Hall state with $\nu = 5/2$ [34, 35]. This model can be mapped onto the transverse field Ising model, the known model described by:

$$H = \sum_i J_i S_i^z S_{i+1}^z + \sum_i h_i S_i^z. \quad (1.39)$$

Moreover, when $k = 3$, the quantum dimension $d = \frac{1}{2}(\sqrt{5} + 1)$, which is the golden mean ϕ . In this case, the Hamiltonian (1.36) describes chains of Fibonacci anyons [29], the non-Abelian anyons which may be relevant in the fractional quantum Hall state with $\nu = 12/5$ [39]. Finally, in the limit $k \rightarrow \infty$, the quantum dimension $d = 2$ so the Hilbert space $\mathcal{H}_N^{(0)}$ corresponds to the spin-1/2 AFM Heisenberg chain.

Going beyond the specific values of d given by Eq. (1.38), model (1.36) can also be generalized to the case of arbitrary d . If one defines the operators $U_i = d\Pi_i^0$, it can be verified that that U_i are generators of a Temperley-Lieb algebra [40, 41], i.e.

$$\begin{aligned} U_i^2 &= dU_i, \\ U_i U_{i\pm 1} U_i &= U_i, \\ [U_i, U_j] &= 0, \quad \text{for } |i - j| > 1. \end{aligned} \quad (1.40)$$

The Temperley-Lieb algebra is known [41] to characterizes many important models, including the 1+1 dimensional Q -state Potts model with $Q = d^2$, which is described by the Hamiltonian:

$$H = - \sum_i U_i. \quad (1.41)$$

The Hamiltonian (1.41) is equivalent to the Hamiltonian (1.36) with constant J_i . Consequently, the Hamiltonian (1.36) with arbitrary d and $J_i = 1$ describes the 1+1 dimensional quantum $Q = d^2$ -state Potts model. In addition, chains of higher spin particles, i.e., particles with spin 1 or higher can also be described by the model (1.36) is with $d > 2$.

1.4.3 Random singlet phases in random chains of anyons

Random chains of interacting anyons described by the Hamiltonian (1.36) with $d = 2 \cos \frac{\pi}{k+2}$ have recently been studied using real-space RG analysis [30]. Because this method is initially developed for spin-1/2 models, modifications are needed to include the quantum dimension $d \neq 2$. In particular, instead of (1.25), the effective coupling \tilde{J}_{14} is determined by [30]

$$\tilde{J}_{14} = \frac{2}{d^2} \frac{J_1 J_3}{J_2}, \quad (1.42)$$

i.e., the factor 1/2 in (1.25) is replaced by $2/d^2$ in (1.42). For $d = 2$, $2/d^2 = 1/2$ so (1.42) becomes (1.25). For $d \geq \sqrt{2}$ as $k = 2, 3, \dots \infty$, $2/d^2 \leq 1$ so one has $\tilde{J}_{14} \ll J_2$ which implies that the decimation procedure reduces the energy scale along the RG flow.

As a consequence of the real-space RG analysis described above, random chains of interacting non-Abelian anyons with any disorder strength all flow to the random singlet phases associated with the same fixed point (1.29) for random spin-1/2 AFM Heisenberg chains [30], at which the ground state is a single valence-bond state. The random singlet phases for random chains of anyons, like that for random spin-1/2 Heisenberg AFM chains, also exhibit the essential features which are discussed in subsection 1.3.3.

1.5 Goals and outline

My work presented in this dissertation is motivated in part by Ref. [29] which gives a definition of chains of interacting non-Abelian anyons, which are described by the Hamiltonian (1.36) with $d = 2 \cos \frac{\pi}{k+2}$ and Ref. [30] which showed that these models enter random singlet phases when disorder is present. In particular, I will present a numerical study of the random singlet phases which appear in disordered models (1.36) with *arbitrary* value of d , which can be thought of describing a chain of fictitious particles characterized by quantum dimension d . This picture is useful for visualizing random singlet ground states by valence-bond states, focusing on the features (see subsection 1.3.3) which are thought to be the essential characteristics of a random single ground state.

The numerical method used in my dissertation is a version of valence-bond Monte Carlo, which was initially developed for spin-1/2 models [14], with some modifications to incorporate the quantum dimension $d \neq 2$. As one of the main results of this work, we have shown that the modified valence-bond Monte Carlo can be used to study the model (1.36) with arbitrary d [42]. For justification, various quantities, e.g., ground state energy, triplet state energy, singlet-triplet energy gap, valence-bond entanglement entropy, bond length distributions, have been calculated and compared with known exact results [42]. Our results using valence-bond Monte Carlo also provide numerical verifications [43] for various very recent exact results, e.g., the so-called valence-bond entanglement entropy and related fluctuations of the Q -state Potts models [44].

Because of the very visual nature of the valence-bond states, valence-bond Monte Carlo is an ideally suited method for studying the two essential features of a random singlet ground state. One of the features, the one which implies that valence bonds in a random singlet ground state can take any length can be probed by the so-called valence-bond entanglement entropy [45, 46]. The other feature which indicates that valence bonds of a random singlet ground state are locked into a particular bond configurations, has not previously been studied by valence-bond Monte Carlo, and is one of the main original contributions of the work presented in this dissertation.

Specifically, we propose a new quantity, the so-called valence-bond fluctuation, which is related to the valence-bond entanglement entropy, and is easy to calculate using valence-bond Monte Carlo. The main advantage of calculating this quantity is that it can be used to actually “see” and then quantitatively analyze the “locking” of the random singlet ground states into a particular single valence-bond state on long-length scales [43, 27]. The formation of the random singlet phases in the limit of no disorder (the uniform chain) can then be studied quantitatively with the use of this new quantity.

While the present Chapter has set up the models and introduced some of the fundamental concepts, Chapter 2 describes in detail the valence-bond Monte Carlo method with some modifications for studying the model (1.36) with arbitrary d . The ground state energy per site of the uniform chains of non-Abelian anyons are also calculated and compared to exact results by Bethe ansatz as evidence for the applicability of the modified valence-bond Monte Carlo. In Chapter 3, we discuss the concept of von Neumann entanglement entropy and calculate a related quantity, the so-called valence-bond entanglement entropy. This quantity

has initially been introduced for spin-1/2 systems [45, 46], but can be straightforwardly generalized for the model (1.36) with arbitrary d . Results in this chapter are compared with various known results by other methods [25, 29, 30, 44] and provide evidence for the random singlet phases associated with the corresponding random models. Valence-bond fluctuation, the new quantity which can be used as a new approach to study random singlet phases, is introduced and calculated in Chapter 4. The fluctuation length scale, the length scale that is relevant to the bond fluctuations of the ground state of the model (1.36) is also introduced and discussed in some detail. The dissertation is completed with an Appendix A for the proofs of some basic results used in our dissertation.

CHAPTER 2

VALENCE-BOND MONTE CARLO

The present chapter describes the valence-bond Monte Carlo simulation method, the numerical method which is proved to be ideally suited for studying random singlet phases. Valence-bond Monte Carlo is a projection Monte Carlo method, initially introduced to sample singlet ground states of spin models (for which the quantum dimension introduced in Chapter 1 is $d = 2$) directly from the valence-bond basis. By introducing some suitable modifications, the version of valence-bond Monte Carlo described in this chapter can be directly applied to the models (1.36) with *arbitrary* d . This chapter begins with a presentation of the key idea of how to project out the ground state of a given Hamiltonian from a starting trial state. This is followed by a description of a detailed procedure for applying such a projection to simulate the model (1.36) with *arbitrary* d . To test the method, section 2.3 presents some numerical calculations which have been done to compare with known results calculated by other methods. The excellent agreement observed in section 2.3 implies that valence-bond Monte Carlo can indeed be used for simulations of the model (1.36) with arbitrary d . This sets the stage for my work on the random singlet phases in disordered models, presented in Chapters 3 and 4.

2.1 Ground state projection

The valence-bond Monte Carlo method, which was introduced by Sandvik in 2005 [14], is basically a projection Monte Carlo method that samples the ground state of spin models directly from valence-bond basis. Various models, for example, in Refs. [14, 42, 43, 45, 46, 47, 48], have been studied using valence-bond Monte Carlo, showing its advantages in some certain ways over traditional Monte Carlo methods.

The idea of valence-bond Monte Carlo is that starting from a given initial valence-bond

state $|S_0\rangle$ one can operate $(-H)^n$ with $n \rightarrow \infty$ on $|S_0\rangle$ to project out the ground state $|0\rangle$ of the model. The key here is that because $|S_0\rangle$ is a non-crossing valence-bond state, its overlap with the ground state $|0\rangle$ is always non-zero so this idea works with any initial state $|S_0\rangle$. In describing the method in more a detailed way, assume that the initial state $|S_0\rangle$ can be written in terms of the energy eigenstates $|E_i\rangle$ as

$$|S_0\rangle = \sum_i C_i |E_i\rangle. \quad (2.1)$$

Because $\langle S_0|0\rangle \neq 0$, the coefficient C_0 is guaranteed to be non-zero. With this expansion, the action of $(-H)^n$ on $|S_0\rangle$ is

$$(-H)^n |S_0\rangle = \sum_i C_i |E_i|^n |E_i\rangle = |E_0|^n \sum_i C_i \left| \frac{E_i}{E_0} \right|^n |E_i\rangle \quad (2.2)$$

In the system described by the Hamiltonian (1.13), the ground state energy E_0 has the largest magnitude, thus the quantity $|E_i/E_0| < 1$ for all $i > 0$. In the limit $n \rightarrow \infty$, all the terms with $i > 0$ of (2.2) becomes small and can be completely negligible, thus the ground state $|0\rangle \equiv |E_0\rangle$ is obtained

$$\lim_{n \rightarrow \infty} (-H)^n |S_0\rangle \sim |0\rangle \quad (2.3)$$

The value of n , which is called in this dissertation the *power number*, according to Eq. (2.3), must be chosen so that $|E_1/E_0|^n \ll 1$. While there are some choice of n in earlier studies, for example in Ref. [45] $n/N = 10$, in our work n/N is chosen up to 80.

2.2 Valence-bond Monte Carlo

2.2.1 Ground state sampling

For using the idea of ground state projection method described in section 2.1 to sample the ground state $|0\rangle$ directly from the valence-bond basis, we start from the expression (1.36) for the Hamiltonian H , thus

$$(-H)^n |S_0\rangle = \sum_{(i_1, \dots, i_n)} J_{i_1} \cdots J_{i_n} \Pi_{i_1}^0 \cdots \Pi_{i_n}^0 |S_0\rangle \quad (2.4)$$

where the summation is taken over all the possible permutations (i_1, \dots, i_n) (note that $i_j = 1, \dots, N$ for $j = 1, \dots, n$) and $|S_0\rangle$ is an arbitrary initial valence-bond state. The

central equation (2.3) of valence-bond Monte Carlo now becomes

$$\sum_{(i_1, \dots, i_n)} J_{i_1} \cdots J_{i_n} \Pi_{i_1}^0 \cdots \Pi_{i_n}^0 |S_0\rangle = \sum_{\alpha} w(\alpha) |\alpha\rangle \sim |0\rangle. \quad (2.5)$$

It can be seen that in the Eq. (2.5) we use the propagation described by

$$J_{i_1} \cdots J_{i_n} \Pi_{i_1}^0 \cdots \Pi_{i_n}^0 |S_0\rangle = w(\alpha) |\alpha\rangle \quad (2.6)$$

in which $|\alpha\rangle$ is the valence-bond state resulting from the propagation of $|S_0\rangle$ through the sequence of singlet projection operators $\Pi_{i_1}^0 \cdots \Pi_{i_n}^0$ and $w(\alpha)$ is the corresponding weight factor. Both of them can be determined following a simple procedure, based on the Eqs. (1.16) and (1.17) and the Figure 1.7. While the resulting valence-bond state $|\alpha\rangle$ is determined by the bond reorganizations shown by these equations and on the Figure 1.7, the weight factor $w(\alpha)$ is given by

$$w(\alpha) = \prod_{j=1}^n (J_{i_j} w_{i_j}) \quad (2.7)$$

where w_{i_j} is the factor resulting from the action of $\Pi_{i_j}^0$ on the valence-bond state obtained by applying $\Pi_{i_{j+1}}^0 \cdots \Pi_{i_n}^0$ on $|S_0\rangle$. According to Eqs. (1.16) and (1.17), w_{i_j} is either 1 or $1/d$.

2.2.2 Sampling procedure: a diagrammatic illustration

A diagrammatic illustration of the procedure is shown on the figure 2.1, which is taken from Ref. [42]. On two (top and bottom) diagrams of the Figure 2.1, examples for the propagations of a given valence-bond state $|S_0\rangle$ through two particular sequences $\Pi_{i_1}^0 \cdots \Pi_{i_6}^0$ of six singlet projection operators are illustrated. These diagrams provide a simple procedure to determine the resulting state $|\alpha\rangle$ and its corresponding weight factor $w(\alpha)$. While the resulting state $|\alpha\rangle$ is determined by the open loops which terminate at the top of the diagrams, the weight factor is just the product of $J_{i_1} \cdots J_{i_n}$ with the factors listed on the right of each diagram. Each of these factors is either 1 or $1/d$, depending on whether the corresponding projection operator, listed on the left of each diagram, forms a closed loop or not. For example, the weight factor $w(\alpha_1) = J_5 J_8 J_9 J_{11} J_2 J_4 d^{-4}$ for the top diagram while $w(\alpha_2) = J_5 J_8 J_4 J_{11} J_2 J_4 d^{-3}$ for the bottom diagram of the Figure 2.1.

The top and bottom diagrams on the Figure 2.1 can be viewed as the “before” and “after” pictures of a single Monte Carlo update in which the third projection operator from

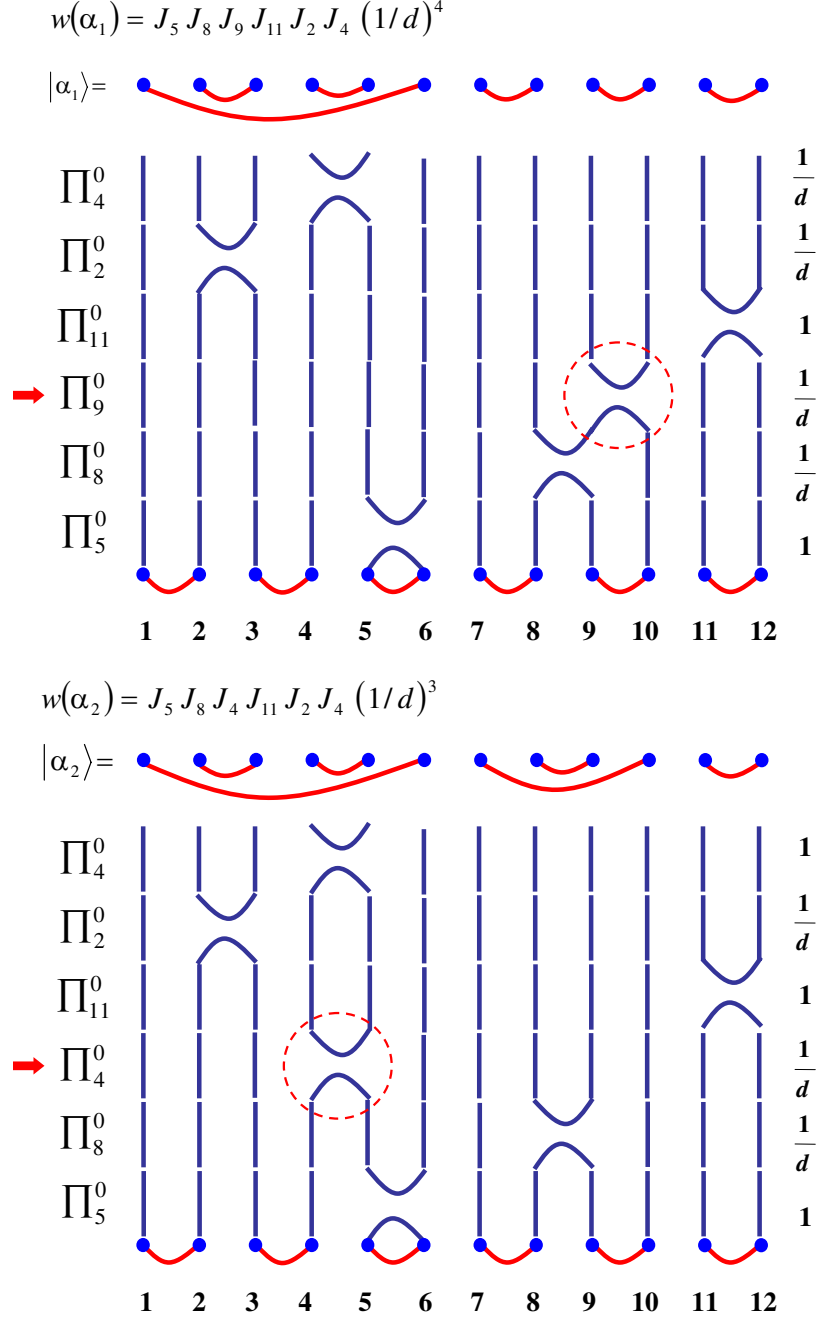


Figure 2.1: (Top) a diagrammatic representation of the action of a sequences of singlet projection operators on $|\alpha_1\rangle$ a given starting valence-bond state. The singlet projection operators act on the initial valence-bond state in a sequence. The resulting state $|\alpha_1\rangle$ and the weight factor $w(\alpha_1)$ are determined using the rules described in section 1.2.5. (Bottom) resulting state $|\alpha_2\rangle$ and the weight factor $w(\alpha_2)$ when the third operator in the sequence on the top panel of this figure, which is Π_9^0 , is updated by Π_4^0 (see the red arrows and circles). This update is accepted or rejected according to the usual Metropolis-Hastings algorithm.

the bottom is shifted from Π_4^0 to Π_9^0 (see the red circles shown on Figure 2.1). The weight factors $w(\alpha_l)$ and $w(\alpha_r)$ which correspond to the states $|\alpha_l\rangle$ and $|\alpha_r\rangle$ are then used when implementing the Metropolis-Hastings [49, 50] algorithm to decide if the state $|\alpha_r\rangle$ is accepted or rejected, or more precisely, the sequence $\Pi_5^0\Pi_8^0\Pi_4^0\Pi_{11}^0\Pi_2^0\Pi_4^0$ is accepted or rejected. In particular, having $w(\alpha_1)$ and $w(\alpha_2)$, one accepts the new state $|\alpha_2\rangle$ with the probability

$$P_{\text{accept}} = \min \left[\frac{w(\alpha_2)}{w(\alpha_1)}, 1 \right]. \quad (2.8)$$

It should be noted here that the quantum dimension d is introduced in this section for valence-bond Monte Carlo as the modification which allows our version of valence-bond Monte Carlo to simulate the (1.36) with arbitrary d . This value in the original valence-bond Monte Carlo [14] is 2, which is the quantum dimension of spins, as discussed on section 1.4.1. The replacement of 2 by d is originated from the Ref. [30] where the authors formulated the actions of the singlet projection operators Π_i^0 acting on valence-bond states.

2.2.3 Sampling procedures: a summary

The detailed procedure of a valence-bond Monte Carlo simulation, based on the discussion above, can be summarized as follow:

1. Choose an initial valence-bond state $|S_0\rangle$ (see the section 2.2.4) and a sequence of n singlet projection operators $(\Pi_1^0, \dots, \Pi_n^0)$.
2. Propagate the initial state $|S_0\rangle$ through the sequence $(\Pi_1^0, \dots, \Pi_n^0)$ to determine the resulting state $|\alpha\rangle$ and its corresponding weight factor $w(\alpha)$, using the procedure illustrated on Figure 2.1.
3. Randomly choose a singlet projection operator Π_j^0 , $j \in [1, n]$ and assign an random value between 1 and N to it. We now have a trial sequence of singlet projection operators.
4. Propagate the initial state $|S_0\rangle$ through the *trial* sequence of singlet projection operators to determine the resulting state $|\alpha'\rangle$ and its corresponding weight factor $w(\alpha')$.
5. Randomly generate a real number r uniformly distributed in $[0, 1)$ and compare it with $P_{\text{accept}} = \min \left[\frac{w(\alpha')}{w(\alpha)}, 1 \right]$.

6. If $P_{\text{accept}} > r$, accept the trial sequence of singlet projection operators. Otherwise, i.e., $P_{\text{accept}} \leq r$, reject the trial sequence.
7. Repeat the steps 2 \rightarrow 6, and measure when the equilibration is reached.

2.2.4 Initial valence-bond state

As mentioned above, because the overlap of any two valence-bond states is non-zero, in principle, valence-bond Monte Carlo works with any initial state $|S_0\rangle$. However, the efficiency of a valence-bond Monte Carlo simulation can be much better if a good initial state $|S_0\rangle$ is selected. A good initial state $|S_0\rangle$ is the state which maximize its overlap with the ground state $|0\rangle$, i.e., the quantity $\langle S_0|0\rangle$ should be as closed to 1 as possible.

Starting from the above criteria for a good initial valence-bond state $|S_0\rangle$, it is clear that $|S_0\rangle$ must be chosen depending on whether the models are uniform or random. For random chains with a given disorder realization, i.e., a given set of the couplings J_1, \dots, J_N , as discussed in the section 1.3.2, the valence-bond state obtained by the decimation procedure is a good approximation of the ground state $|0\rangle$, especially in the limit of strong disorder [10]. Therefore, for each disorder realization of a random model, this valence-bond state should be chosen as the initial state $|S_0\rangle$. However, the decimation procedure does not applicable in uniform models. There are several ways to choose the initial state $|S_0\rangle$, e.g., the amplitude-product state [15, 51]. In our work, a random non-crossing valence-bond state is used as the initial state $|S_0\rangle$.

2.2.5 Sampling average

The valence-bond Monte Carlo method described above allows for sampling the ground state of a models with arbitrary d . Given an observable O which takes the values

$$O(\alpha) = \frac{\langle \alpha|O|\alpha\rangle}{\langle \alpha|\alpha\rangle} \quad (2.9)$$

in a non-crossing valence-bond states $|\alpha\rangle$, valence-bond Monte Carlo can be used to compute the weighted average

$$\langle O \rangle = \frac{\sum_{\alpha} w(\alpha)O(\alpha)}{\sum_{\alpha} w(\alpha)} \quad (2.10)$$

for any state $|0\rangle$ of the form (2.5), provided $w(\alpha) > 0$, (angle brackets will always denote this average in what follows). While $\langle O \rangle$ is not the usual quantum mechanical expectation value of the observable O , both because of the nonorthogonality of valence-bond states and the fact that the weight factors used in the averaging are amplitudes and not probabilities, it is a well-defined quantity.

2.3 Method benchmarks

While the valence-bond Monte Carlo method is developed for spin-1/2 systems with $d = 2$, it is desirable to verify that the modified version described in the above section can be used for any value of d . For a justification, we use this method to calculate some quantities and then compare the obtained data with various known results using other methods.

2.3.1 Ground state energy

The ground state energy E_0 of the model (1.36) is one of the quantities which is easily computed using valence-bond Monte Carlo. In this section, we use valence-bond Monte Carlo to calculate the ground state energy per site E_0/N of the uniform ($J_i = J$) model (1.36) as a function of quantum dimension d . The procedure given in [14] to calculate E_0/N for spin-1/2 systems can be trivially generalized [42] for arbitrary d . On each valence-bond state $|\alpha\rangle$, one first calculate a quantity $\varepsilon(\alpha)$ by

$$\varepsilon(\alpha) = \sum_{i=1}^N w_i(\alpha) \quad (2.11)$$

where $w_i(\alpha)$ is determined by

$$w_i(\alpha) = \begin{cases} 1 & (i, i+1) \text{ if } i, j \text{ are in a singlet} \\ \frac{1}{d} & \text{if } i, j \text{ are not in a singlet.} \end{cases} \quad (2.12)$$

Given that $\varepsilon(\alpha)$ is determined, the ground state energy per site E_0/N is then calculated by average $\varepsilon(\alpha)$ over $|\alpha\rangle$ with the corresponding weight $w(\alpha)$:

$$E_0(N) = -J \frac{\sum_{\alpha} w(\alpha) \varepsilon(\alpha)}{\sum_{\alpha} w(\alpha)}. \quad (2.13)$$

On the other hand, the ground state energies of the uniform version ($J_i = J$) of the models (1.36) can be found exactly. This can be done by noting that for any d , the Temperley-Lieb operators U_i can be represented using spin-1/2 operators as [38]

$$U_i = 2 (S_i^x S_{i+1}^y + S_i^y S_{i+1}^x) + d \left(\frac{1}{4} - S_i^z S_{i+1}^z \right) + i \sqrt{1 - \frac{d^2}{4}} (S_{i+1}^z - S_i^z). \quad (2.14)$$

For the case of open boundary conditions the models (1.36) can then be mapped onto spin-1/2 XXZ chains with external (non-Hermitian) fields applied to the two ends (the staggered field term in the expression for U_i cancels in the “bulk” of the chain). In the thermodynamic limit, the ground state energies will not depend on boundary conditions, and the values of E_0 for the models (1.36) with periodic boundary conditions should be the same as that for the corresponding XXZ models. Consequently, one can straightforwardly generalize the expression for the ground state energies of the XXZ models found using Bethe ansatz by Yang and Yang [52, 53] to obtain the following expression for the ground energies of the models (1.36),

$$\lim_{N \rightarrow \infty} \frac{E_0(N)}{N} = J \frac{d^2 - 4}{4d} \int_{-\infty}^{\infty} dx \frac{\operatorname{sech}(\pi x)}{\cosh \left(2x \arccos \frac{d}{2} \right) - \frac{d}{2}}. \quad (2.15)$$

The formula (2.15) returns $-\ln 2 = -0.69315 \dots$ for $J = 1$ and $d = 2$. This value is the ground state energy per site of the spin-1/2 Heisenberg chain shifted by $\frac{1}{4}$ from the exact value $\frac{1}{4} - \ln 2$ obtained by Hulthén using the Bethe ansatz [4, 5, 54], by Lanczos calculations [55, 56] as well as other numerical methods [57, 58]. The shift of $\frac{1}{4}$ is originated from the definition of the singlet projection operator (1.12).

The ground state energy per site $E_0(N)/N$ estimated by Eq. (2.13) is a function of the chain size N , and should agree with the formula (2.15) when $N \rightarrow \infty$. Depicted on the figure 2.2 are the valence-bond Monte Carlo results for $E_0(N)/N$ (in unit of J) of the uniform chain of anyons with $d = \sqrt{2}$, $d = \frac{1}{2}(\sqrt{5} + 1)$, and $d = 2$, which correspond to $k = 2$, $k = 3$ and $k \rightarrow \infty$, respectively. The exact values of $E_0(N)/N$ in the limit $N \rightarrow \infty$ given by the formula (2.15) are also shown by the dashed lines. Figure 2.2 shows that the ground state energy $E_0(N)/N$ converges very quickly to the exact values for $E_0(N)/N$ as N increases. We have also found that within the error bars, the results by valence-bond Monte Carlo simulations shown on the Figure 2.2 are consistent with those calculated by other methods in the Refs. [55, 56, 57, 58].

The ground state energy per site $E_0(N)/N$ of a chain of interacting anyons calculated by valence-bond Monte Carlo as a function of d is depicted on Figure 2.3 in unit of J . Specific values of the quantum dimension d used for my calculations are $d = 2 \cos \frac{\pi}{k+2}$ with $k = 2, 3, 4, 5, 6, 8, 10, 15$ and ∞ . The chain size is $N = 128$, which, as shown on the Figure 2.2, is large enough for $E_0(N)/N$ to converge to the exact values in the thermodynamic limit. The exact value for $E_0(N)/N$ given in Eq. (2.15) is shown on this figure by the red line. The power number is chosen to be $n = 20N$. Although the chain size $N = 128$ is not large, the agreement between the numerical results for $N = 128$ and the exact result for $N \rightarrow \infty$ is remarkable for all the values of d , implying that the valence-bond Monte Carlo method can indeed be used for the model (1.36) with any d [42].

2.3.2 Triplet state simulations

Valence-bond Monte Carlo can be used to calculate not only the ground state energy but also the $m_z = 0$ triplet state energy of the model (1.36). A unique advantage of the valence-bond basis is that the triplet state $|1\rangle$ can be projected out simultaneously with the singlet ground state $|0\rangle$ [14, 59]. Therefore, for another benchmark of the method, I use valence-bond Monte Carlo to calculate $E_1(N)/N$, the triplet state energy per site and $\Delta E(N)$, the singlet-triplet gap of the uniform spin-1/2 AFM Heisenberg chain and compare the obtained results with those from other calculations.

The singlet ground state $|0\rangle$ of a spin-1/2 AFM Heisenberg chain can be viewed as a superposition of valence-bond states $|\alpha\rangle$, each of which has $N/2$ singlet bonds. In the first $m_z = 0$ triplet state $|1\rangle$, excitations break one of the singlet bonds in $|0\rangle$ and promote it to the triplet state $\frac{1}{\sqrt{2}}(|\uparrow\downarrow\rangle + |\downarrow\uparrow\rangle)$. In the thermodynamic limit, the uniform spin-1/2 Heisenberg AFM chain is gapless, i.e., the singlet-triplet gap ΔE between $|0\rangle$ and $|1\rangle$ vanishes [3, 4]. For a chain with finite size N , the singlet-triplet gap $\Delta E(N)$ is, however, non-zero and it scales as $1/N$ when $N \rightarrow \infty$.

A technique usually employed to calculate $E_1(N)$ and $\Delta E(N)$ of a spin-1/2 AFM Heisenberg chain is the Lanczos exact diagonalization algorithm, which gives several lowest eigenvalues of the Hamiltonian to high accuracy. Calculations using this technique can be easily found elsewhere, for example, in Refs. [60, 61]. Because the Lanczos technique has to store a number of requirements which is comparable to the dimensionality of the Hilbert space, it is not easy to use this technique for a sufficiently large chain. Some versions of

Monte Carlo simulation were used for calculating $E_1(N)$ and $\Delta E(N)$, as can be found in the Refs. [57, 58].

The $m_z = 0$ triplet state, similar to the singlet ground state, can be expanded as:

$$|1\rangle = \sum_{\alpha^{(t)}} w(\alpha^{(t)}) |\alpha^{(t)}\rangle \quad (2.16)$$

where $|\alpha^{(t)}\rangle$ is a “valence-bond state” with *one* of $N/2$ bonds is the $m_z = 0$ triplet

$$|t_{ij}^{(1)}\rangle = \frac{1}{\sqrt{2}} (|\uparrow_i \downarrow_j\rangle + |\downarrow_i \uparrow_j\rangle) \quad (2.17)$$

while $w(\alpha^{(t)})$ is the corresponding weight factor which can be determined in a simple way as shown below.

The actions of a singlet projection operator Π_i^0 on a valence-bond state which has one triplet bond can be described by a rule like that described in Eqs. (1.16) and (1.17). If we, for convenience, denote the triplet state $|t_{ij}^{(1)}\rangle$ as $[i, j]$, and a valence-bond state which has *one* triplet bond by $|\cdots [i, j] \cdots\rangle$, the rule can be shown as:

$$\begin{aligned} \Pi_i^0 |\cdots [i, i+1] \cdots\rangle &= 0, \\ \Pi_i^0 |\cdots (i, i+1) \cdots\rangle &= |\cdots (i, i+1) \cdots\rangle \\ \Pi_i^0 |\cdots [i, j] \cdots (i+1, k) \cdots\rangle &= \frac{1}{2} |\cdots (i, i+1) \cdots [j, k] \cdots\rangle. \end{aligned} \quad (2.18)$$

Note that in this subsection we calculated $E_1(N)$ and $\Delta E(N)$ only for uniform spin-1/2 AFM Heisenberg chains with $d = 2$, the factor $1/d$ is replaced by $1/2$ in Eq. (2.18). Thus, on one hand, the action of Π_i^0 on a valence-bond state destroys it if the spins at sites i and $i+1$ are in a triplet. On the other hand, if spins at sites i and $i+1$ are not in a triplet, the state survives and the valence bonds are reorganized in the same fashion as described in Eqs. (1.16) and (1.17). More important, the matrix elements remains the same as in the case of valence-bond states with all singlet bonds. This feature is crucial for carrying out a simulation for the triplet state at the same time with the simulation with the singlet ground state.

As described in the section (2.2), an initial valence-bond state $|S_0\rangle$ is chosen and this state is then propagated through a sequence of singlet projection operators $\Pi_{i_1}^0 \cdots \Pi_{i_n}^0$ to determine the valence-bond state $|\alpha\rangle$ and its amplitude $w(\alpha)$ in the ground state. A simulation of the triplet state is carried out simultaneously with that of the singlet ground state by marking one

of the $N/2$ valence bonds in $|S_0\rangle$ as a triplet. Being propagated by the sequence $\Pi_{i_1}^0 \cdots \Pi_{i_n}^0$, the *surviving* resulting states are denoted by $|\alpha^{(t)}\rangle$ with the corresponding non-zero amplitude by $w(\alpha^{(t)})$.

The bond configurations of the resulting states $|\alpha^{(t)}\rangle$ and $|\alpha\rangle$ corresponding to a given sequence of singlet projection operators $\Pi_{i_1}^0 \cdots \Pi_{i_n}^0$ are identical. While all the bonds of $|\alpha\rangle$ are singlet, *one* of the bonds of $|\alpha^{(t)}\rangle$ is triplet, and its position can be easily determined by keeping track the position of the triplet bond of $|S_0\rangle$ when propagating through $\Pi_{i_1}^0 \cdots \Pi_{i_n}^0$. During the process of determining $|\alpha^{(t)}\rangle$ by operating $\Pi_{i_1}^0 \cdots \Pi_{i_n}^0$ on $|S_0\rangle$, when a singlet projection operator operates on a triplet bond, the weight factor $w(\alpha^{(t)})$ is set to be zero, implying that the valence-bond state $|\alpha^{(t)}\rangle$ has no contribution to the triplet state $|1\rangle$. Typically, most of the times $w(\alpha^{(t)}) = 0$ but, depending on the power number n , there is also a given probability for it to be non-zero. The triplet state $|1\rangle$ can therefore be sampled by the surviving states $|\alpha^{(t)}\rangle$ which correspond to non-zero amplitudes $w(\alpha^{(t)}) \neq 0$.

Having obtained the surviving states $|\alpha^{(t)}\rangle$, similar to the calculations of the ground state, one calculates the quantity $\varepsilon(\alpha^{(t)})$ for estimating the excited state energy $E_1(N)$ by

$$\varepsilon(\alpha^{(t)}) = \sum_{i=1}^N w_i(\alpha^{(t)}) \quad (2.19)$$

where $w_i(\alpha^{(t)})$ is given by

$$w_i(\alpha^{(t)}) = \begin{cases} 1 & \text{if } (i, i+1) \text{ are in a singlet} \\ 0 & \text{if } (i, i+1) \text{ are in a triplet} \\ \frac{1}{2} & \text{otherwise.} \end{cases} \quad (2.20)$$

By doing an weighted average over all the possible states $\varepsilon(\alpha^{(t)})$, one can estimate the triplet state energy $E_1(N)$ by

$$\frac{E_1(N)}{J} = - \frac{\sum_{\alpha^{(t)}} w(\alpha^{(t)}) \varepsilon(\alpha^{(t)})}{\sum_{\alpha^{(t)}} w(\alpha^{(t)})}. \quad (2.21)$$

Having the excited state energy $E_1(N)$ calculated, the finite-size gap $\Delta E(N)$ can be determined by

$$\Delta E(N) = E_1(N) - E_0(N). \quad (2.22)$$

Following the procedures discussed above, valence-bond Monte Carlo simulations were done on uniform spin-1/2 AFM Heisenberg chains of up to $N = 128$ with the power number

Table 2.1: Triplet state energy per bond $E_1(N)/N$ of the uniform spin-1/2 AFM Heisenberg chain for various chain size N . Results from the Lanczos technique were calculated up to $N = 20$ spins while those for $N > 20$ were extrapolated and marked by asterisks. Calculations from a conventional Monte Carlo simulation was done for chains of up to $N = 48$ spins. For comparison, the triplet state energy $E_1(N)$ for the uniform chains of up to $N = 128$ sites was calculated using valence-bond Monte Carlo. Results are given here in unit of $J_i = J$.

N	Lanczos [60, 61]	Monte Carlo [58]	VB Monte Carlo
6	-0.6030	-0.6023(4)	-0.60281 ± 0.00030
8	-0.6411	-0.6403(5)	-0.64107 ± 0.00019
10	-0.6592	-0.6589(5)	-0.65908 ± 0.00017
12	-0.6693	-0.6685(6)	-0.66910 ± 0.00013
14	-0.6755	-0.6746(5)	-0.67558 ± 0.00011
16	-0.6795	-0.6786(8)	-0.67938 ± 0.00008
20	-0.6843	-0.6831(5)	-0.68430 ± 0.00006
24	-0.6870*	-0.6860(6)	-0.68692 ± 0.00005
32	-0.6897*	-0.6887(8)	-0.68957 ± 0.00007
40	-0.6909*	-0.6897(9)	-0.69088 ± 0.00005
48	-0.6916*	-0.6900(9)	-0.69162 ± 0.00004
64			-0.69227 ± 0.00004
96			-0.69272 ± 0.00003
128			-0.69293 ± 0.00004

up to $n = 30N$. Note that for small chain sizes like $N \lesssim 16$, the power number n may be as small as $n = 6N$ for at least one triplet state to survive.

Table 2.1 shows the triplet state energy per site $E_1(N)$ calculated by various methods of a uniform spin-1/2 Heisenberg chain with the chain size N taken from 6 to 128. The triplet state energies calculated by valence-bond Monte Carlo simulations are shown to agree very well with those from other methods, e.g., Lanczos exact diagonalization [60, 61], and Monte Carlo [58].

We now move on to finite-size gap $\Delta E(N)$ calculated using valence-bond Monte Carlo which is shown on the Table 2.2 in comparison to the results calculated by other methods. Calculations using Lanczos technique were done on the chains of up to $N = 20$ sites. Results for chains of $N > 20$ sites were obtained by extrapolating the calculated data and marked by asterisks. Also shown on this table is the results from random walk [57], and Monte Carlo

Table 2.2: Finite-size gap $\Delta E(N)$ of the uniform spin-1/2 AFM Heisenberg chain for various chain size N . Results from the Lanczos technique were calculated up to $N = 20$ sites while those for $N > 20$ were extrapolated and marked by asterisks. Calculations from two Monte Carlo simulations were done for chains of up to $N = 48$ sites. For comparison, the finite-size gap $\Delta E(N)$ for chains of up to $N = 128$ sites was calculated using valence-bond Monte Carlo. Results are given here in unit of $J_i = J$.

N	Lanczos [60, 61]	Random walk [57]	Monte Carlo [58]	VB Monte Carlo
6	0.6847	0.6854 ± 0.0020	0.683(5)	0.6863 ± 0.0019
8	0.5227	0.5236 ± 0.0046	0.522(11)	0.5219 ± 0.0016
10	0.4232	0.4247 ± 0.0062	0.419(10)	0.4248 ± 0.0018
12	0.3558	0.345 ± 0.012	0.366(10)	0.3582 ± 0.0016
14	0.3071	0.319 ± 0.013	0.312(11)	0.3052 ± 0.0015
16	0.2702	0.273 ± 0.004	0.270(19)	0.2720 ± 0.0013
20	0.217	0.220 ± 0.006	0.232(24)	0.2186 ± 0.0010
24	0.182*	0.189 ± 0.008	0.199(20)	0.1832 ± 0.0010
32	0.137*	0.164 ± 0.017	0.17(5)	0.1384 ± 0.0019
40	0.110*	0.166 ± 0.026	0.13(5)	0.1108 ± 0.0015
48	0.092*	0.132 ± 0.038	0.13(8)	0.0914 ± 0.0013
64				0.0686 ± 0.0011
96				0.0448 ± 0.0008
128				0.0335 ± 0.0022

simulations, which were done for chains of up to $N = 48$ sites [58].

The result for $\Delta E(N)$ we obtained from valence-bond Monte Carlo is shown on the Table (2.2) to be in an excellent agreement with that from Lanczos calculations. The results from valence-bond Monte Carlo have some advantages over the other methods [57, 58] in the sense that our result agrees better with those from the Lanczos calculations.

2.4 Concluding remarks

Two benchmarks for the modified version of valence-bond Monte Carlo described here all return positive results. For the ground state energy per site $E_0(N)/N$ of chains of anyons with $k = 2, 3, 4, 5, 6, 8, 10, 15$ and ∞ , the result calculated by valence-bond Monte Carlo agrees very well with the exactly calculated result by Bethe ansatz [52, 53] for the whole range of d examined (see figure 2.3). This excellent agreement should be regarded as a strong evidence that the modified valence-bond Monte Carlo method can indeed be used to simulate

the models (1.36) with arbitrary d [42].

In addition, the triplet excited state energy $E_1(N)/N$ and the finite-size gap $\Delta E(N)$ have also been calculated with valence-bond Monte Carlo. Results for $E_1(N)/N$ and $\Delta E(N)$ are shown on Table 2.1, and 2.2, respectively. Similar to the case of the ground state energy E_0/N , calculated results for both $E_1(N)/N$ and $\Delta E(N)$ are shown to be in very good agreements with the results previously calculated by other methods. This feature of the valence-bond Monte Carlo can be used to study other versions of the Heisenberg chain, for example spin-1/2 alternating Heisenberg chains, in which energy gaps are opened and capture some recent interests [62, 63].

In conclusion, it has been shown that with modifications, the valence-bond Monte Carlo method can indeed be used to simulate the model (1.36) with arbitrary d . In the next chapters, I will use this numerical method to focus on random singlet phases, the interesting phases appearing as a consequence of disorders in model (1.36) with arbitrary d [10, 30].

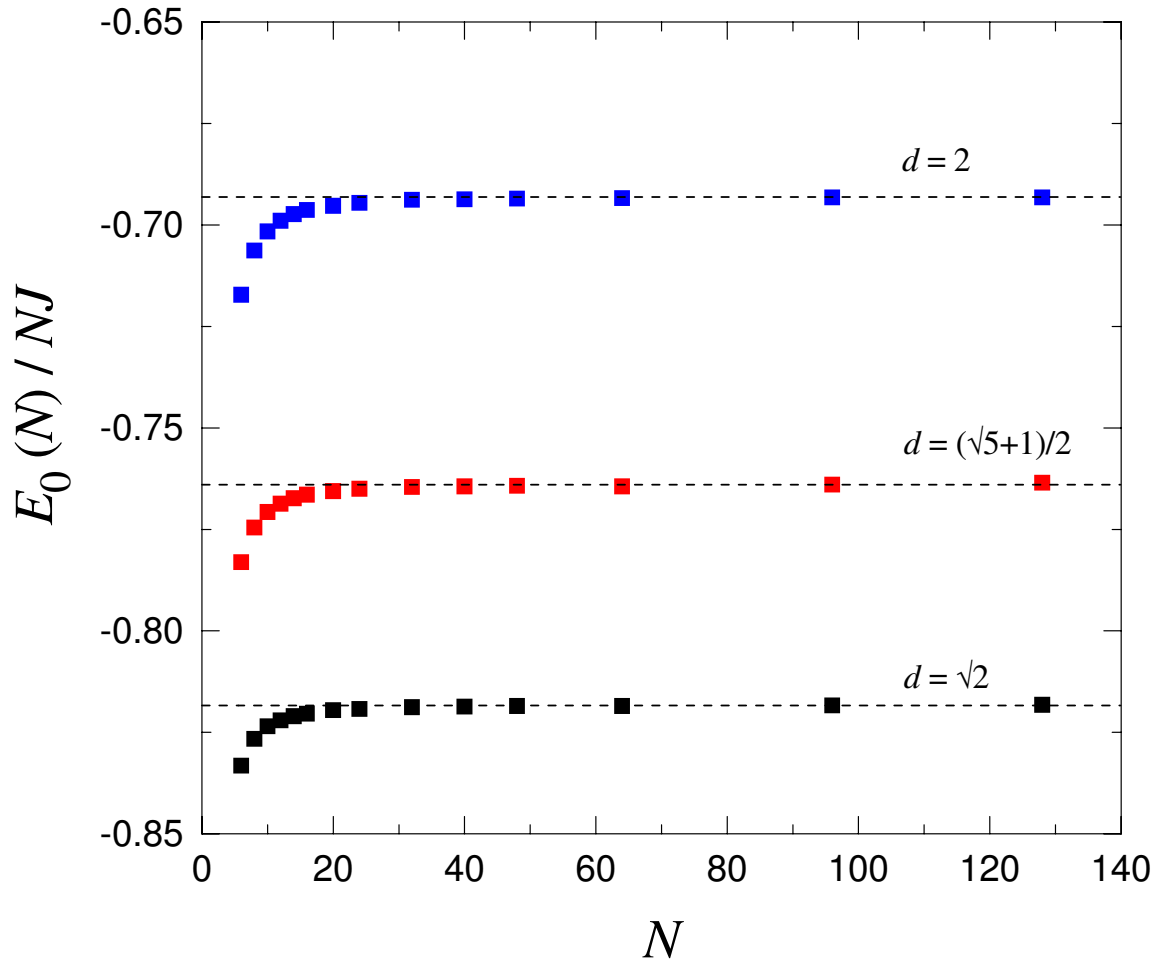


Figure 2.2: Ground state energy per site $E_0(N)/N$ (in unit of J) as functions of N , the size of the uniform chains of anyons with $d = \sqrt{2}$, $\frac{1}{2}(\sqrt{5} + 1)$ and 2 which correspond to $k = 2$, $k = 3$ and $k \rightarrow \infty$. Error bars are smaller than the symbol size. The specific values of chain size taken are $N = 6, 8, 10, 12, 14, 16, 20, 24, 32, 40, 48, 64, 96, 128$. Dashed lines represent the exact results using Bethe ansatz (2.15).

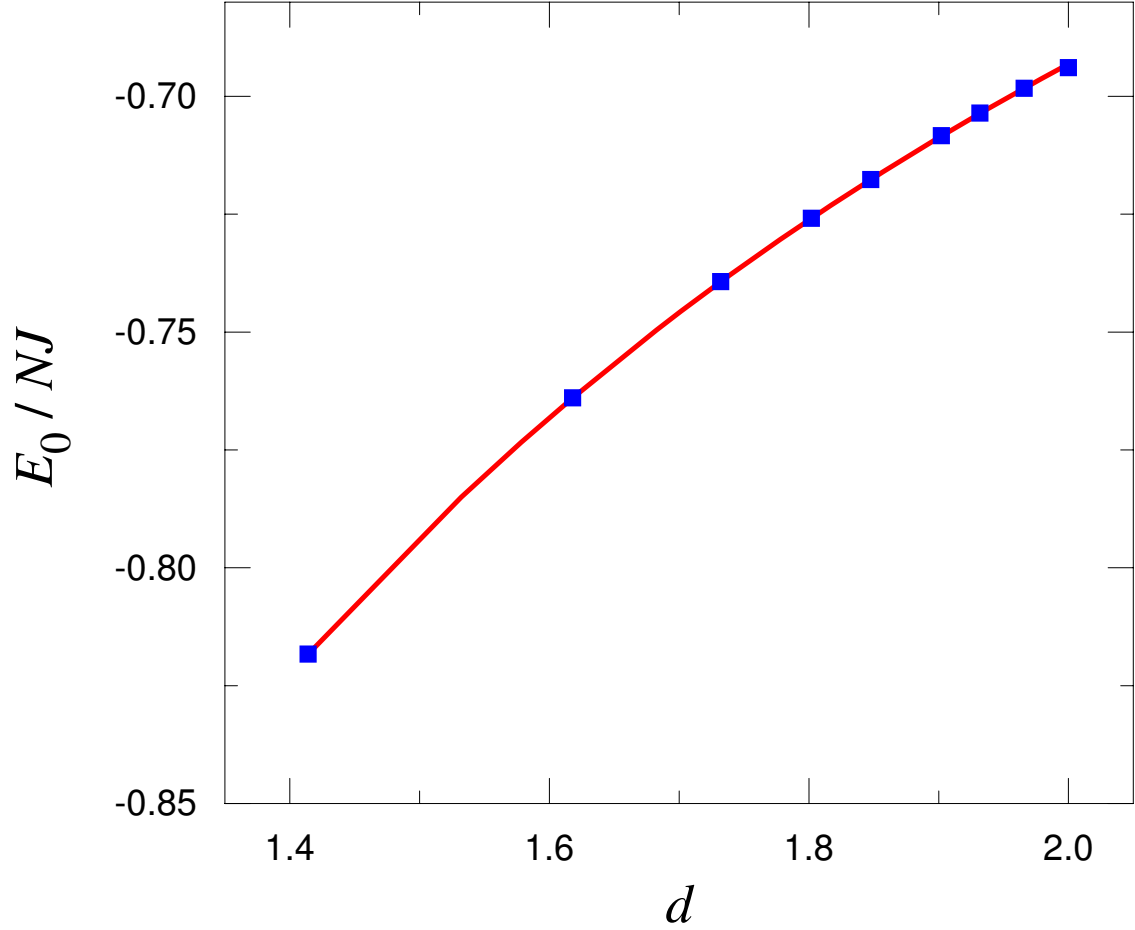


Figure 2.3: Ground state energy per bond $E_0(N)/N$ (in unit of J) of a uniform chain of interacting non-Abelian anyons as a function of quantum dimension d . Solid red line is the exact results using Bethe ansatz (2.15) while blue squares are the results from valence-bond Monte Carlo calculations for the values of d corresponding to $k = 2, 3, 4, 5, 6, 8, 10, 15$ and ∞ . Numerical results are estimated at the chain size $N = 128$. Error bars are smaller than the symbol size.

CHAPTER 3

VALENCE-BOND ENTANGLEMENT ENTROPY

In 2004, Refael and Moore [25] showed that the so-called block entanglement entropy (a particular example of von Neumann entanglement entropy) in certain random singlet phases scales logarithmically with block size with a universal coefficient. This work was generalized by Bonesteel and Yang [30] to the anyon chain models described in Chapter 1 of this dissertation. Unfortunately, von Neumann entanglement is difficult to compute numerically, however a closely related quantity, the so-called valence-bond entanglement entropy was introduced by Alet *et al.* [45], and independently, by Chhajlany *et al.* [46], both in 2007. Similar to von Neumann entanglement entropy, valence-bond entanglement entropy can be used to study the random singlet phase associated with random spin-1/2 AFM Heisenberg chains, i.e., the model (1.36) with $d = 2$, and related models. e.g., random chains of interacting non-Abelian anyons. This chapter begins by introducing the von Neumann entanglement entropy and block entanglement entropy, the specific quantity which is relevant to random singlet phases. I then review the concept of valence-bond entanglement entropy, a quantity which shares some features with block entanglement entropy in studying random singlet phases. Both block entanglement entropy and valence-bond entanglement entropy, which are initially introduced for spin-1/2 systems, can all be generalized for the models (1.36) with arbitrary d . Finally, numerical calculations using valence-bond Monte Carlo for the valence-bond entanglement entropies and bond length distributions of these models are carried out and compared with various known results. Discussions on the essential features of random singlet phases based on these results are also given.

3.1 von Neumann entanglement entropy

3.1.1 Definition

Entanglement is the property of a quantum system in which the quantum state of any subsystem is linked to those of the others so that one subsystem can not be adequately described without full mention of the others. This fundamental concept has been described for the first time in the context of Einstein-Podolsky-Rosen paradox [64]. Entanglement plays a central role in the study of strongly correlated quantum systems, since a highly entangled ground state is at the heart of a large variety of collective quantum phenomena. Entanglement can also be used for a possible quantum computer in the future [65].

One of the most important concepts that quantifies the entanglement is von Neumann entanglement entropy. Assume that the quantum system of interest is composed by a subsystem A and its complement, the subsystem B . In general, there is no way to associate a pure state to either the subsystem A or B , however, a reduced density matrix can be used for either A or B . Let $|0\rangle\langle 0|$ be the full density matrix of the whole system, the subsystem A can be described by the reduced density matrix ρ_A obtained by tracing out the full density matrix over the degrees of freedom of the subsystem B :

$$\rho_A \equiv \sum_j \langle \varphi_j^{(B)} | 0 \rangle \langle 0 | \varphi_j^{(B)} \rangle = \text{Tr}_B |0\rangle\langle 0| \quad (3.1)$$

where the summation is taken over the orthonormal basis states $|\varphi_j^{(B)}\rangle$ of the Hilbert space associated with the subsystem B . The von Neumann entanglement entropy of the subsystem A is then defined as the von Neumann entropy associated with the reduced density matrix ρ_A

$$S_A = -\text{Tr}[\rho_A \log_2 \rho_A]. \quad (3.2)$$

It is straightforward to check that $S_A = S_B$. Some more information on the von Neumann entanglement entropy can be found in the Appendix A.2.

3.1.2 Entanglement per bond

Spin singlet

As an example, let us consider a quantum system composed of two spin-1/2 particles in the singlet state — a pure state. If one spin is taken to be the subsystem A while the other

spin is taken to be B (see Figure 3.1), one can determine the von Neumann entanglement entropy S_A or S_B according to the definition in Eq. (3.2).

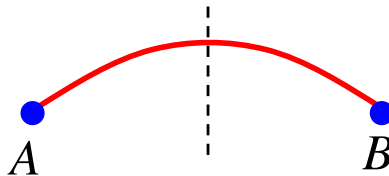


Figure 3.1: A system of two spin-1/2 particles forming a singlet state which can be decomposed into two regions A and B and then the von Neumann entanglement entropy can be determined.

Starting from the singlet state

$$|s\rangle = \frac{1}{\sqrt{2}} (|\uparrow_A \downarrow_B\rangle - |\downarrow_A \uparrow_B\rangle), \quad (3.3)$$

the spectral decomposition of the reduced density matrix can then be obtained as:

$$\rho_A = \frac{1}{2} (|\uparrow_A\rangle\langle\uparrow_A| + |\downarrow_A\rangle\langle\downarrow_A|). \quad (3.4)$$

From the spectral decomposition (3.4), the von Neumann entanglement entropy S_A defined in (3.2) is determined in terms of Schmidt coefficients (see the Appendix A.2) as:

$$S_A = - \left[\frac{1}{2} \log_2 \left(\frac{1}{2} \right) + \frac{1}{2} \log_2 \left(\frac{1}{2} \right) \right] = 1. \quad (3.5)$$

Finally, the entanglement per bond for the case of spin-1/2 singlet is

$$S_{\text{bond}} = 1. \quad (3.6)$$

Anyonic singlet

The concept of von Neumann entanglement entropy can be straightforwardly generalized to a system of interacting anyons, as did in the Ref. [30], where the entanglement per anyonic singlet bond is calculated asymptotically. The calculation was carried out on a state $|\alpha\rangle$ of $2\mathcal{N}$ anyons, which form \mathcal{N} singlets. The subsystem A is chosen to include \mathcal{N} anyons at the ends of \mathcal{N} singlet bonds, while its complement is the other \mathcal{N} ends of these bonds. For a detailed illustration of this state, see the Figure 3.2 which is taken from the Ref. [30].

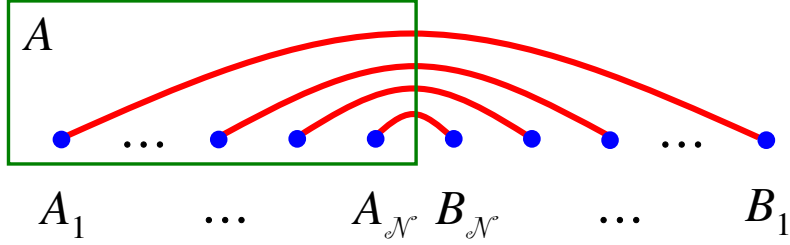


Figure 3.2: A state $|\alpha\rangle$ of $2\mathcal{N}$ anyons which pair up to \mathcal{N} singlets. The subsystem A is taken to include \mathcal{N} ends of the \mathcal{N} singlet bonds.

Following the standard procedure for calculating von Neuman entanglement entropy, the corresponding Schmidt coefficients are determined in terms of $d = 2 \cos \frac{\pi}{k+2}$, the quantum dimension of the anyons. At the final, one finds the following asymptotic result in the limit of $\mathcal{N} \rightarrow \infty$ [30]

$$S_A^{|\alpha\rangle} \simeq \mathcal{N} \log_2 d, \quad (3.7)$$

so the entanglement per anyonic singlet bond is given asymptotically as [30]

$$S_{\text{bond}} \simeq \log_2 d. \quad (3.8)$$

Throughout this dissertation, inspired by this result, the entanglement per bond for the case of arbitrary d is also taken to be $\log_2 d$. For spin-1/2 models with $d = 2$, $S_{\text{bond}} = 1$ which is consistent with the entanglement per bond determined by Eq. (3.6).

3.1.3 Block entanglement entropy

Block entanglement entropy S_L of a chain of, either spins or anyons, is defined as the von Neumann entanglement entropy of a given block of L contiguous sites with the rest of the chain. An illustration for the geometry of the definition is given on the Figure 3.3, where the (dark) green block of $L = 5$ sites is regarded as the subsystem A while the rest of the chain is the subsystem B .

Recently the scaling of the block entanglement entropy S_L of quantum spin chains at quantum critical points, at which the length scale over which different spins are entangled, diverges, has been of special interest. One of many reasons is that the *universal* scaling law

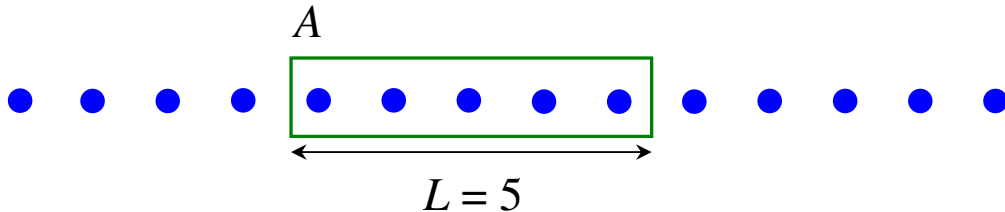


Figure 3.3: An illustration for a block A of $L = 5$ contiguous spins embedded in a spin chain. The complement of the block (subsystem) A is defined as the subsystem B for calculating the block entanglement entropy.

of random chains [25] is different from that of the uniform chain [66, 67], so one can use it as a signature of the random singlet phase associated with random chains.

Uniform chain and the central charge

The block entanglement S_L of the uniform spin-1/2 AFM Heisenberg chain at the quantum critical point obeys an universal scaling law which is related to the central charge of the corresponding conformal field theory [66, 67, 68]. A comprehensive derivation of S_L using conformal field theory and the second law of thermodynamics is out of the scope of this dissertation, and can be found in the Ref. [67] by Korepin. The final result is

$$S_L = \frac{c}{3} \ln L + \mathcal{C} \quad (3.9)$$

where c is the central charge of the corresponding conformal field theory and \mathcal{C} is a non-universal constant. In this dissertation, \mathcal{C} is always used for non-universal constants of scaling laws, of which (3.9) is an example.

For the uniform spin-1/2 AFM Heisenberg chain, the central charge $c = 1$. The central charge of the uniform chains of interacting anyons with $d = 2 \cos \frac{\pi}{k+2}$, which are also conformally invariant, is given by [29]

$$c = 1 - \frac{6}{(k+1)(k+2)}. \quad (3.10)$$

It is worth to check that in the limit $k \rightarrow \infty$, the central charge determined by Eq. (3.10) is 1, which is consistent with that of the uniform spin-1/2 AFM Heisenberg chain. Another

special case is the chain of anyons with $k = 2$ in which the model (1.36) corresponds to the transverse field Ising model. The central charge determined by Eq. (3.10) is $1/2$, which is equal to the known value of the central charge of the uniform transverse field Ising model [66].

Random chains and effective central charge

Disorders in the model (1.36) has many interesting effects on the block entanglement entropy [69]. Different from the uniform chain, random chains have no conformal symmetry, thus one can not derive the block entanglement entropy S_L from the corresponding conformal field theory. Instead, using the real-space RG analysis, this quantity has been derived for the first time by Refael and Moore [25] for critical random spin-1/2 AFM Heisenberg chains, and was then generalized for random chains of interacting anyons [30]. The following derivation, which is taken from Ref. [25], is essentially for random spin-1/2 AFM Heisenberg chains.

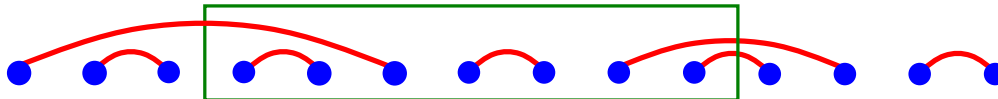


Figure 3.4: The random singlet ground state of a random chain. Given a block A of $L = 7$ sites, the number of bonds n_L leaving the block is determined to be $n_L = 3$ so in this state, the block entanglement entropy is $S_L = n_L \log_2 d = 2 \log_2 d$.

The starting point of the derivation of S_L for random chains is the approximated ground state obtained by the real-space RG analysis and the fixed point distribution (1.29). As discussed in the section 1.3.2, the random singlet ground state of a random chain is approximated by a single valence-bond state, which can be written in the form of (1.8) so the block entanglement S_L of a given block A of size L (see Figure 3.4) can be determined in a very simple way:

$$S_A = n_L \log_2 d \quad (3.11)$$

where n_L is the number of valence bond crossing the ends of the block A . A proof for this formula can be found in the Appendix A.2.

Having determined the block entanglement entropy for a given random realization of disorder by such an easy procedure described above, one average them over many random realizations of disorder to find the final result [25, 30]:

$$S_L = \overline{n_L} \log_2 d, \quad (3.12)$$

where the overbar denote a disorder average.

In order to estimate $\overline{n_L}$, one finds the element of the number of couplings decimated when the energy scale Ω (define in section 1.3.2) is lowered an amount of $d\Omega$ as $\Omega \rightarrow \Omega - d\Omega$ or, equivalently, $\Gamma \rightarrow \Gamma + d\Gamma$. During this process, all the couplings with $0 < \beta < d\Gamma$ are decimated and the corresponding singlet bonds are created. The element $d\bar{\nu}$ of the average number of singlet bonds created, therefore, is

$$d\bar{\nu} = P(\beta = 0)d\Gamma = \frac{d\Gamma}{\Gamma} \quad (3.13)$$

which leads to

$$\bar{\nu} = \ln \Gamma. \quad (3.14)$$

It should be emphasized here that among the $\bar{\nu}$ singlet bonds created, only the bonds with length up to L contribute to n_L . Therefore, in order to estimate $\overline{n_L}$, we should count only the bond up to the length $L = \Gamma^2$, so

$$n_L \sim \ln L. \quad (3.15)$$

More detailed analysis, which can be found in the Refs. [25, 30], found that the pre-factor of this logarithmic scaling is $1/3$. Therefore, the block entanglement entropy S_L of the critical random chains depends on the block size L is

$$S_L = \frac{\ln d}{3} \log_2 L + \mathcal{C} \quad (3.16)$$

where \mathcal{C} is, again, a non-universal constant. This very interesting result reveals that although the critical random chains have no conformal invariance, the block entanglement entropy scales logarithmically with the block length L in the same fashion with that of the uniform chain (3.9). Therefore, the pre-factor $\frac{\ln d}{3}$ in the Eq. (3.16) is said to be connected to the so-called ‘‘effective’’ central charge \tilde{c} defined as

$$\tilde{c} = \ln d \quad (3.17)$$

so that

$$S_L = \frac{\tilde{c}}{3} \log_2 L + \mathcal{C}. \quad (3.18)$$

The result (3.18) for random spin-1/2 AFM Heisenberg chains has been confirmed numerically by several methods, for example, by exact diagonalization in Ref. [70]. We note that the effective central charge $\ln d$ is always less than the central charge $c = 1 - 6/(k+1)(k+2)$. This is not always true, e.g., Santachiara [71] has shown that for the parafermionic Potts models for $n \geq 42$, the central charge of the uniform model is smaller than that of the random model.

The difference between the central charge c determined in Eq. (3.10) of the uniform models and the effective central charge \tilde{c} given in Eq. (3.17) of the corresponding random models can be used as a signature of the relevant random singlet phases [25, 30].

3.2 Valence-bond entanglement entropy

3.2.1 Definitions

Inspired by the idea of calculating the block entanglement entropy for random spin-1/2 AFM Heisenberg chains in the Ref. [25], a new quantity called valence-bond entanglement entropy has been introduced for both uniform and random spin-1/2 AFM Heisenberg chains by Alet *et al.* [45] and independently, by Chhajlany *et al.* [46], both in 2007. The advantage of this quantity is that it can be easily calculated using valence-bond Monte Carlo, by which one samples the ground state of the model from the valence-bond basis. This quantity, like the block entanglement entropy, scales logarithmically with the block length L and can be used in studying the random singlet phase.

Assume that we are considering a given block A of size L , i.e., it has L sites, as illustrated on the Figure 3.4. In a given valence-bond state $|\alpha\rangle$, the quantity $n_L(\alpha)$ is defined as the number of valence bonds, each of which connects a site in the block A and a site which is not in block A . This implies that these valence bonds cross the ends of the block A , thus n_L is the number of valence bonds crossing the ends of the block. In the example shown on the Figure 3.4, $n_L(\alpha) = 3$ since there are 3 valence bonds crossing the ends of the block A .

It is recalled that in valence-bond Monte Carlo, the ground state of a chain can be sampled from the basis of valence-bond states. Therefore, the number of bonds $n_L(\alpha)$ for a given state $|\alpha\rangle$ is then averaged with the corresponding weight $w(\alpha)$ in the ground state to have

the weighted average $\langle n_L \rangle$ in the ground state as

$$\langle n_L \rangle = \frac{\sum_{\alpha} w(\alpha) n_L(\alpha)}{\sum_{\alpha} w(\alpha)}. \quad (3.19)$$

From $\langle n_L \rangle$, the valence-bond entanglement entropy is defined as [45, 46]

$$S_L^{\text{VB}} = \langle n_L \rangle, \quad (3.20)$$

given that the entanglement entropy per bond for the spin-1/2 AFM Heisenberg chains with $d = 2$ is $\log_2 d = 1$. For random chains, in addition to the weighted average over states $|\alpha\rangle$, one has to do another average over disorders, i.e., average over many random realizations of J_i , thus

$$S_L^{\text{VB}} = \overline{\langle n_L \rangle}, \quad (3.21)$$

where the overbar denotes the disorder average.

As discussed in the section 3.1.2, the asymptotic entanglement entropy per bond with arbitrary d when $N \gg 1$ is $\log_2 d$, thus one can define the valence-bond entanglement entropy for the uniform chains as [44, 43]

$$S_L^{\text{VB}} = \langle n_L \rangle \log_2 d \quad (3.22)$$

and for random chains as

$$S_L^{\text{VB}} = \overline{\langle n_L \rangle} \log_2 d. \quad (3.23)$$

The introduction of the factor $\log_2 d$ in (3.22) and (3.23) is the generalization of the definition (3.20) and (3.21) for spin-1/2 chains with $d = 2$. With this generalization, the valence-bond entanglement entropy S_L^{VB} of model (1.36) with arbitrary d can also be easy to calculate using valence-bond Monte Carlo.

Because the non-crossing valence-bond basis is complete, the valence-bond entanglement entropy is a perfectly well-defined quantity [45]. Even in two-dimensional systems when the valence-bond basis used is over-complete, it has been shown [45] that this quantity is conserved in any linear combination of the valence-bond state used for the definitions (3.20) and (3.22). Valence-bond entanglement entropy can also be shown to be well-defined for the model (1.36) with arbitrary $d < 2$, with which the valence-bond basis is over-complete.

While S_L^{VB} is easy to calculate, it is generally *not* equal to the block entanglement entropy S_L of uniform and random models determined by Eqs. (3.9) and (3.16), respectively. The reason here is that for both cases, the ground state of these models is not precisely a single valence-bond state, the only case in which block entanglement entropy and valence-bond entanglement entropy are equal.

3.2.2 Bond length distribution

Before closing the section of valence-bond entanglement entropy S_L^{VB} , it is noted here that this quantity is closely related to the bond-length distribution, $P(l)$, for valence bonds. A valence bond connecting site i and site j is said to have a length $l = |i - j|$. By defining $b_l(\alpha)$ as the number of bonds with length l in the state $|\alpha\rangle$ and $\langle b_l \rangle$ is the weighted average of $b_l(\alpha)$

$$\langle b_l \rangle = \frac{\sum_{\alpha} w(\alpha) b_l(\alpha)}{\sum_{\alpha} w(\alpha)}, \quad (3.24)$$

the bond length distribution $P(l)$ is defined by

$$P(l) = \frac{1}{N/2} \langle b_l \rangle. \quad (3.25)$$

Note that $P(l) = 0$ for even l because there is no bond with even length in a non-crossing valence-bond state. Bond length distribution, as named, provides information of the probability distribution of the bond length in the ground state of the model. This distribution is interesting in our work because its *power-law* dependence on l is useful in showing that valence bonds with any length exist in a certain ground state of either the uniform chain or a random chain.

It is readily shown [72] that $P(l)$ is related to S_L^{VB} by

$$S_L^{\text{VB}} = 2 \log_2 d \sum_{l=1}^{N/2} P(l) \min(l, L). \quad (3.26)$$

This relation is useful when one has to determine the scaling of $P(l)$ from the scaling of S_L^{VB} and vice versa.

Defined by (3.22) and (3.23), valence-bond entanglement entropy of the model (1.36) with arbitrary d can be easily calculated using valence-bond Monte Carlo. In particular, using the

modified valence-bond Monte Carlo, one can sample the ground state of this model from the valence-bond basis. For each sampling state $|\alpha\rangle$, one counts the number n_L of bond crossing the boundaries of a given block of size L , and then perform the averages described in Eqs. (3.22) and (3.23). At the same time and on the same way, the bond length distribution $P(l)$ can also be calculated. Detailed discussions on scalings of $P(l)$ are given in the next sections when scalings of S_L^{VB} can be determined via some methods.

3.3 Valence-bond Monte Carlo results

3.3.1 Uniform model

Valence-bond entanglement entropy

The asymptotic logarithmic scaling of the valence-bond entanglement entropy S_L^{VB} has been determined exactly by Jacobsen and Saleur in 2008 [44] using the loop model representation of the Temperley-Lieb algebra which defines the quantum $Q = d^2$ -state Potts models [40]. The averaged value $\langle n_L \rangle$ of n_L is determined via the correlation function of a pair of the so-called vertex operators V_{\pm} which are inserted at two ends of the block of length L . These operators assign an weight of w for a bond crossing the ends of the block, but an weight of $\sqrt{Q_b}$ (defined in (3.30)) for the bonds which do not cross the ends. The correlation function is then determined as [44]

$$\langle V_+(0)V_-(L) \rangle = \frac{\sum_C d^{n_{\text{loops}}} (\sqrt{Q_b})^{N/2 - n_L} w^{n_L}}{\sum_C d^{n_{\text{loops}}} (\sqrt{Q_b})^{N/2}} \propto L^{-2h(w,d)}, \quad (3.27)$$

where the sums over C taken over the possible loop configurations is equivalent to the weighted average taken over sampling states $|\alpha\rangle$ with the weight

$$w(\alpha) = d^{n_{\text{loops}}} (\sqrt{Q_b})^{N/2}. \quad (3.28)$$

In the Eqs. (3.27) and (3.28), n_{loops} is the number of closed loops appearing on the diagram of the representation of the algebra. In addition,

$$h(w, d) = \frac{4 \arccos^2(w/2) - \arccos^2(d/2)}{4\pi^2[1 - (\arccos(d/2))/\pi]} \quad (3.29)$$

and

$$Q_b = 2 + d. \quad (3.30)$$

The quantity $\langle n_L \rangle$ can be extracted from the correlation function $\langle V_+(0)V_-(L) \rangle$ by operating $w \frac{\partial}{\partial w}$ on both sides of (3.27) and then set $w = \sqrt{Q_b} = \sqrt{2+d}$. The left hand side thus becomes

$$w \frac{\partial}{\partial w} \left(\frac{\sum_c d^{n_{loops}} (\sqrt{Q_b})^{N/2 - n_L} w^{n_L}}{\sum_c d^{n_{loops}} (\sqrt{Q_b})^{N/2}} \right) \Big|_{w=\sqrt{Q_b}} = \frac{\sum_c d^{n_{loops}} (\sqrt{Q_b})^{N/2} n_L}{\sum_c d^{n_{loops}} (\sqrt{Q_b})^{N/2}} = \langle n_L \rangle. \quad (3.31)$$

Operating $w \frac{\partial}{\partial w}$ on the right hand side yields

$$w \frac{\partial}{\partial w} L^{-2h(w,d)} \Big|_{w=\sqrt{Q_b}} = \left(w L^{-2h(w,d)} \frac{\partial}{\partial w} [-2h(w,d)] \right) \Big|_{w=\sqrt{Q_b}} \ln L. \quad (3.32)$$

Note that $h(w,d) = 0$ when $w = \sqrt{Q_b}$ so $L^{-2h(w,d)} = 1$. From the results (3.31) and (3.32), the valence-bond entanglement entropy S_L^{VB} which is defined to be $\langle n_L \rangle \log_2 d$ can now be written as [44]

$$S_L^{\text{VB}} = \frac{c_1}{3} \log_2 L + \mathcal{C}, \quad (3.33)$$

where the coefficient c_1 is given by [44]

$$c_1 = \frac{6 \ln d}{\pi} \sqrt{\frac{2+d}{2-d}} \frac{\arccos(d/2)}{\pi - \arccos(d/2)}. \quad (3.34)$$

It can be verified that c_1 is generally not equal to the ‘‘true’’ central charge $c = 1 - 6/(k+1)(k+2)$ as determined by Eq. (3.10), implying that the valence-bond entanglement entropy S_L^{VB} is indeed different from the block entanglement entropy S_L as expected. In particular, for $d = 2$, $c_1 = 12 \ln 2/\pi^2 \approx 0.843$, showing that S_L^{VB} is considerably smaller than S_L with $c = 1$. For $d = \sqrt{2}$, $c_1 \approx 0.533$, slightly larger than the central charge $c = 0.5$ determined from Eq. (3.10), which is the central charge of the transverse field Ising model [66]. Whereas this difference can be expected from the qualitative discussion connecting with the superposition of valence-bond states and can be calculated exactly by mapping the Q -state Potts model onto the Temperley-Lieb algebra, it is definitely desirable to have a numerical confirmation for the exact asymptotic scaling given in Eq. (3.33).

We have calculated, using valence-bond Monte Carlo, the valence-bond entanglement entropy S_L^{VB} of the uniform chain described by (1.36) with $d = 2$, $d = \frac{1}{2}(\sqrt{5} + 1)$ and $d = \sqrt{2}$. Note that the chain with these values of d corresponds to the spin-1/2 AFM Heisenberg chain, the golden chain, and the transverse field Ising model, respectively. For

an independent simulation, a non-crossing valence-bond state was generated stochastically and was then used as the initial state $|S_0\rangle$. Other detailed parameters are the chain size $N = 1024$, the power number $n = 20N$, the value I found to be large enough for random non-crossing initial valence-bond state $|S_0\rangle$. Results shown here are obtained by averaging over 50 independent simulations.

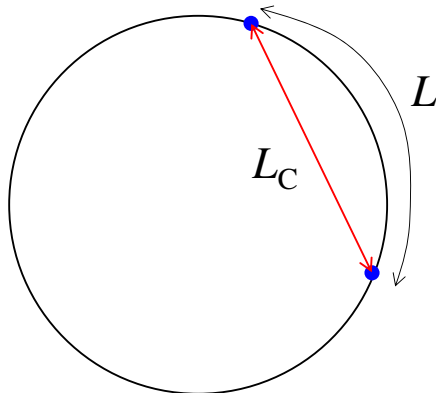


Figure 3.5: Conformal distance L_C , the concept which is introduced to minimize finite-size effect. For a chain of N sites and the periodic boundary condition, the conformal distance of a block of L sites in the chain is given by $L_C = N/\pi \sin(\pi L/N)$.

Semi-log plots for valence-bond entanglement entropy S_L^{VB} as functions of L_C are depicted on the Figures 3.6, 3.7, and 3.8, for the model (1.36) with $d = 2$, $d = \frac{1}{2}(\sqrt{5} + 1)$ and $d = \sqrt{2}$, respectively. Here

$$L_C = \frac{N}{\pi} \sin\left(\frac{\pi L}{N}\right) \quad (3.35)$$

is the so-called block conformal length which we use to minimize the finite size effect when L is nearly equal to $N/2$, a half of the system size (see Figure 3.5 for an illustration of L_C). Also shown on these figures are the exact asymptotic scalings of S_L^{VB} determined by Eq. (3.33) with the coefficient c_1 given by Eq. (3.34). The constant \mathcal{C} is adjusted for the best fit for the calculated data.

In the scaling regime $1 \ll L \ll N/2$, our data agrees very well with the exact asymptotic scaling (3.33) [44], especially for $d = \frac{1}{2}(\sqrt{5} + 1)$ and $d = \sqrt{2}$. The agreement for $d = 2$ is not very good because, as will be seen on the Figure 3.19, the finite size effect in this case is quite strong. In order to observe a better agreement, one has to simulate much bigger chains, as

pointed out by the Ref. [43]. Historically, c_1 was first claimed to equal c by a simulation of a small-size uniform chain with $N = 128$ spins using valence-bond Monte Carlo [45]. However, this conjecture has quickly been disproved by the Ref. [44]. The finite-size effect for $d \neq 2$, implied by the excellent agreements shown on Figures 3.7, and 3.8, is not strong like that for $d = 2$.

Our results, which are shown on the Figures 3.6, 3.7, and 3.8 can be regarded as the first (and non-trivial) numerical confirmation for the exact asymptotic logarithmic scaling (3.33) of S_L^{VB} recently found by Jacobsen and Saleur [44].

Bond length distribution

Starting from the expression (3.26) for the connection between S_L^{VB} and $P(l)$, the logarithmic divergence of S_L^{VB} mentioned in Eq. (3.33) implies that the bond length distribution $P(l)$ should follow an inverse-square power law for $1 \ll l \ll N/2$:

$$P(l) = \frac{2c_1}{3 \ln 2} l^{-2}. \quad (3.36)$$

Similar to S_L^{VB} , the bond length distribution $P(l)$ is an interesting quantity which is easy to calculate using valence-bond Monte Carlo. We have calculated $P(l)$ as functions of the bond conformal length $l_C = N/\pi \sin(\pi l/N)$ and the results are shown on the on Figures 3.9, 3.10, and 3.11 for $d = 2$, $d = (\sqrt{5} + 1)/2$, and $d = \sqrt{2}$, respectively. The results shown on these figures are obtained by averaging over 50 independent simulations. Other parameters of the system used for simulations are $N = 1024$, $n = 20N$, and the periodic boundary condition. The predicted inverse-square power law (3.36) are also shown on these figures by the red lines. We note that c_1 is a function of d thus the predicted inverse-square power law (3.36) on the figures are quantitatively different.

The finite-size effect for $d = 2$ can be seen clearly on the Figure 3.9 as the calculated $P(l)$ is slightly shifted from the red line for the scaling (3.36), indicating that the calculated value of c_1 is slightly larger than the predicted value in Eq. (3.34). On the other hand, the very good agreement observed on Figures 3.10 and 3.11 for $d = \frac{1}{2}(\sqrt{5} + 1)$ and $d = \sqrt{2}$ implies that the finite-size effect is not quite strong for $d \neq 2$. The results for $P(l)$ shown on Figures 3.9, 3.10, and 3.11 can be used as a justification for the predicted power-law scaling given in Eq. (3.36).

It should be emphasized here that the logarithmic divergence of S_L^{VB} and the inverse-square power law dependence of $P(l)$ readily imply that in the ground state of the uniform chain, valence bonds can have *any length*.

3.3.2 Random models

Valence-bond entanglement entropy

It has been mentioned above (section 1.3.2) that valence bonds of a random singlet ground state are locked into a single valence-bond state on long-length scales while they strongly resonate on short-length scales. Therefore, although S_L^{VB} and S_L are generally different, they share the same behavior on long-length scales, where both of them are essentially characterized by a particular single valence-bond state, of which block entanglement entropy and valence-bond entanglement entropy are equal. In particular, S_L^{VB} should also diverge logarithmically in the scaling regime $1 \ll L \ll N$ as

$$S_L^{\text{VB}} = \frac{\ln d}{3} \log_2 L + \mathcal{C}. \quad (3.37)$$

The logarithmic scaling (3.37) has been confirmed numerically by Alet *et al.* [45] for random spin-1/2 AFM Heisenberg chains ($d = 2$) up to 128 sites. In this work, we use valence-bond Monte Carlo to calculate S_L^{VB} of the random model (1.36) of 1024 sites with some particular values of d which correspond to the quantum dimensions of some anyons.

In order to specify the disorder strength of the disorders used in this dissertation, we use the parameter u which is defined so that the coupling J_i are confined and uniformly distributed on the interval $[1 - u, 1 + u]$, i.e., the probability distribution $P(J)$ of the coupling J is

$$P(J) = \begin{cases} \frac{1}{2u} & \text{if } J \in [1 - u, 1 + u] \\ 0 & \text{otherwise.} \end{cases} \quad (3.38)$$

Consequently, the uniform chain which has no disorder is characterized by $u = 0$ while a stronger disorder is specified by a larger u , i.e., the disorder with $u = 1.0$ is stronger than the disorder with $u = 0.5$. An illustration of the definition is sketched on the Figure 3.12.

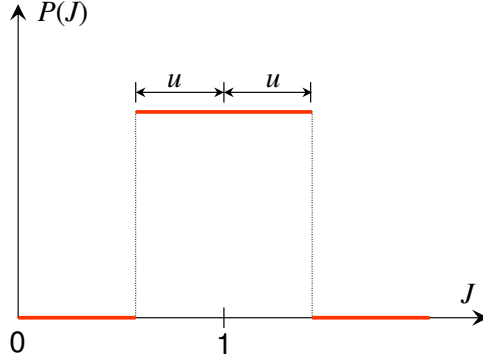


Figure 3.12: Definition of disorder strength u , the parameter which specifies the distribution $P(J)$ of the couplings J_i in such a way in which J_i are uniformly distributed on $[1 - u, 1 + u]$.

I have simulated random chains of $N = 1024$ interacting non-Abelian anyons with $d = 2$, $d = \frac{1}{2}(\sqrt{5} + 1)$, and $d = \sqrt{2}$ and calculated S_L^{VB} using Eq. (3.23). Results are averaged over 2000 random realizations of disorders, each of which with strength $u = 1.0$. For each disorder, i.e., a random realization of J_i , the decimation procedure was executed to obtain a singlet non-crossing valence-bond state, which maximizes the overlap with the ground state. This state was then used as the initial valence-bond state $|S_0\rangle$ for a valence-bond Monte Carlo simulation with power number $n = 20N$. Data for S_L calculated for $d = 2$, $d = \frac{1}{2}(\sqrt{5} + 1)$, and $d = \sqrt{2}$ are depicted as functions of the block conformal length $L_C = N/\pi \sin(\pi L/N)$ on Figures 3.13, 3.14 and 3.15, respectively. For giving a numerical confirmation of (3.37), the predicted scaling (3.37) is also shown on these figures by the red lines.

Figures 3.13, 3.14 and 3.15 clearly demonstrate that S_L^{VB} , similar S_L , also scales logarithmically with L on long-length scales in the fashion given in Eq. (3.37). The “effective” central charge $\tilde{c} = \ln d$ which characterizes the scaling (3.37) is also confirmed by our calculated data. Whereas results shown here are for the disorder strength $u = 1.0$, calculations done with other disorder strengths, e.g., $u = 0.5$, show the same agreements, although the scaling regime is different. The results for S_L^{VB} of random models shown on the Figures 3.13, 3.14 and 3.15 can be used as an evidence of the random singlet phases of the random model (1.36) with arbitrary d , specifically, the random transverse field Ising model with $d = \sqrt{2}$ [73] and random chains of non-Abelian anyons with $d = 2 \cos \frac{\pi}{k+2}$ [30].

Bond length distribution

Similar to the uniform models, in random models, $P(l)$ is predicted to have an inverse-square power law dependence but with a d -independent coefficient

$$P(l) = \frac{2}{3}l^{-2}. \quad (3.39)$$

In the same way like that of the logarithmic scaling of S_L^{VB} , the power-law bond length distribution directly demonstrates that in a random singlet ground state, valence bonds can take any lengths.

In order to reproduce this power-law dependence, the bond length distributions $P(l)$ of the same random models, i.e., $d = 2$, $d = \frac{1}{2}(\sqrt{5} + 1)$, and $d = \sqrt{2}$, are also calculated numerically. On Figures 3.16, 3.17 and 3.18, numerical results for the bond length distribution $P(l)$ is shown as functions of the bond conformal length $l_C = N/\pi \sin(\pi l)/N$ for, again, minimizing the finite-size effects. The calculated results which are shown on the Figures 3.16, 3.17 and 3.18 clearly agree very well with the predicted inverse-square power law (3.39), clearly demonstrating the existence of valence bonds with any length in a random singlet ground state.

3.3.3 Valence-bond central charges

As discussed in the previous sections, the logarithmic scaling of the block entanglement entropy S_L is related to the central charge c or the effective central charge \tilde{c} , depending on whether the chain in which S_L is determined is uniform or random. Because the valence-bond entanglement entropy S_L^{VB} , similar to S_L , also scales logarithmically with L , it is convenient to introduce the so-called valence-bond central charge c^{VB} , defined as

$$S_L^{\text{VB}} \simeq \frac{c^{\text{VB}}}{3} \log_2 L + \mathcal{C} \quad (3.40)$$

in the scaling regime $1 \ll L \ll N$. For the uniform model, the valence-bond central charge c^{VB} defined here is identical to the coefficient c_1 of the valence-bond entanglement entropy calculated exactly by Jacobsen and Saleur and given by Eq. (3.34)

$$c^{\text{VB}} = \frac{6 \ln d}{\pi} \sqrt{\frac{2+d}{2-d}} \frac{\arccos(d/2)}{\pi - \arccos(d/2)}. \quad (3.41)$$

For random chains, as discussed above, since the valence-bond entanglement entropy S_L^{VB} share the same logarithmic scaling with the block entanglement entropy S_L , the valence-bond central charge c^{VB} is equal the effective central charge \tilde{c} , which is $\ln d$ [25, 30].

Defined by Eq. (3.40), the valence-bond central charge c^{VB} can be easily extracted either from S_L^{VB} or $P(l)$. With the valence-bond central charge c^{VB} , the discussions in the sections 3.3.1 and 3.3.2 can be summarized in a condensed figure. On Figure 3.19, the central charge c , the effective central charge \tilde{c} , and the valence-bond central charge c^{VB} for both uniform and random chains are all shown in unit of $\log_2 d$, the unit of entanglement entropy. Results for the valence-bond central charge c^{VB} were obtained by fitting S_L^{VB} to $a_0 + (c^{\text{VB}}/3) \log_2 x$ over the range $N/16 < L < N/4$, where $x = (N/\pi) \sin(L\pi/N)$ is the conformal distance defined on the chain (see Figure 3.5 for an illustration). The higher part of the figure shows the results for the uniform chain while the lower part of the figure shows that for random chains.

On the higher part, the valence-bond central charge c^{VB} obtained from valence-bond Monte Carlo simulation with various values d corresponding to $k = 2, 3, 4, 5, 6$ and ∞ , are shown by blue full circles. It should be noted here that c^{VB} for $k \rightarrow \infty$ was determined by a finite-size extrapolation, which is shown in the inset of the Figure 3.19 together with that for the case of $k = 2$. The extrapolations clearly shows the much stronger finite-size effects for the $k \rightarrow \infty$ case with $d = 2$. The calculated c^{VB} is found to agree very well with the exact c^{VB} determined by the formula (3.41) shown on this figure as the red curve. This positive result can be used as a numerical confirmation for the exact formula (3.41) of the valence-bond central charge c^{VB} as a function of d .

The higher part of the Figure 3.19 also shows the central charge $c = 1 - 6/(k+1)(k+1)$ [29] for the conformally invariant uniform model with $k = 2, 3, 4, 5, 6$ and ∞ as the black full squares. The dotted line is a guide to the eyes. It is clearly demonstrated that c and the c^{VB} are clearly different as mentioned in the previous sections, implying that S_L and S_L^{VB} are generally not equal for the whole range of d examined. On the range of d , $c^{\text{VB}} > c$ for small d while $c^{\text{VB}} < c$ for larger d .

On the lower part of Figure 3.19, the results for the random chains discussed in the section 3.3.2 are shown. The dashed black line is the real-space RG result $\tilde{c}/\log_2 d = \ln 2$ for the random models, and the blue squares are our valence-bond Monte Carlo results for random models with $d = 2 \cos \frac{\pi}{k+2}$ where $k = 2, 3, 4, 5, 6$ and ∞ . The agreement between

S_L^{VB} and S_L observed in section 3.3.2 is shown here as the agreement between c_d^{VB} and \tilde{c} , which is very good.

The concept of valence-bond central charge c^{VB} , therefore, can be used to capture the logarithmic scaling of block and valence-bond entanglement entropies, which are relevant in a discussion of random singlet phases.

3.4 Concluding remarks

To summarize, in this chapter I have reviewed the block entanglement entropy S_L and studied numerically the valence-bond entanglement entropy S_L^{VB} , the quantities which are useful in studying random singlet phases. While the valence-bond entanglement entropy is easy to calculate using valence-bond Monte Carlo, it is generally not equal the block entanglement. Defined by Eq. (3.22) for the uniform chain and Eq. (3.23) for random chains, the logarithmic scaling of S_L^{VB} , which was shown on Figures 3.6, 3.7, and 3.8 for the uniform chain and Figures 3.13, 3.14, and 3.15 for random chains clearly demonstrates the existence of bonds with *any length* in the ground state of these chains. This can also be shown by a more direct way: the power-law bond length distribution $P(l)$, which is predicted in Eqs. (3.36) and (3.39). These power laws of $P(l)$ are confirmed numerically on the Figures 3.9, 3.10 and 3.11 for the uniform chain and 3.16, 3.17 and 3.18 for random chains. This chapter, therefore, has discussed in details one of the essential features of a random singlet ground state.

The other essential feature implies that, as discussed in the subsection 1.3.3, the valence bonds of a random singlet ground state strongly resonate up to a finite length scale while they are locked into a particular valence-bond configuration beyond this length scale. In fact, this feature is reflected in the valence-bond central charge $c^{\text{VB}} = \ln d$ of random chains, which is quantitatively different from the central charge $c = 1 - 6/(k+1)(k+1)$ for the uniform chain. This feature is also implied by the coefficients of the bond length distribution $P(l)$, which is $(2c_1)/(3 \ln 2)$ for the uniform chain and $2/3$ for the random chains. However, the connection between the “locking” assumption and the valence-bond central charge is *indirect* in the sense that it is based on the approximation (1.19), which is less effective for weak disorders. Note that the length scale beyond which valence bonds of a random singlet ground state are locked is an interesting quantity which characterize random singlet phase. However, no information on this length scale can be extracted from valence-bond

entanglement entropy S_L^{VB} and bond length distribution $P(l)$. In the next chapter, these issues will be discussed in a new way.

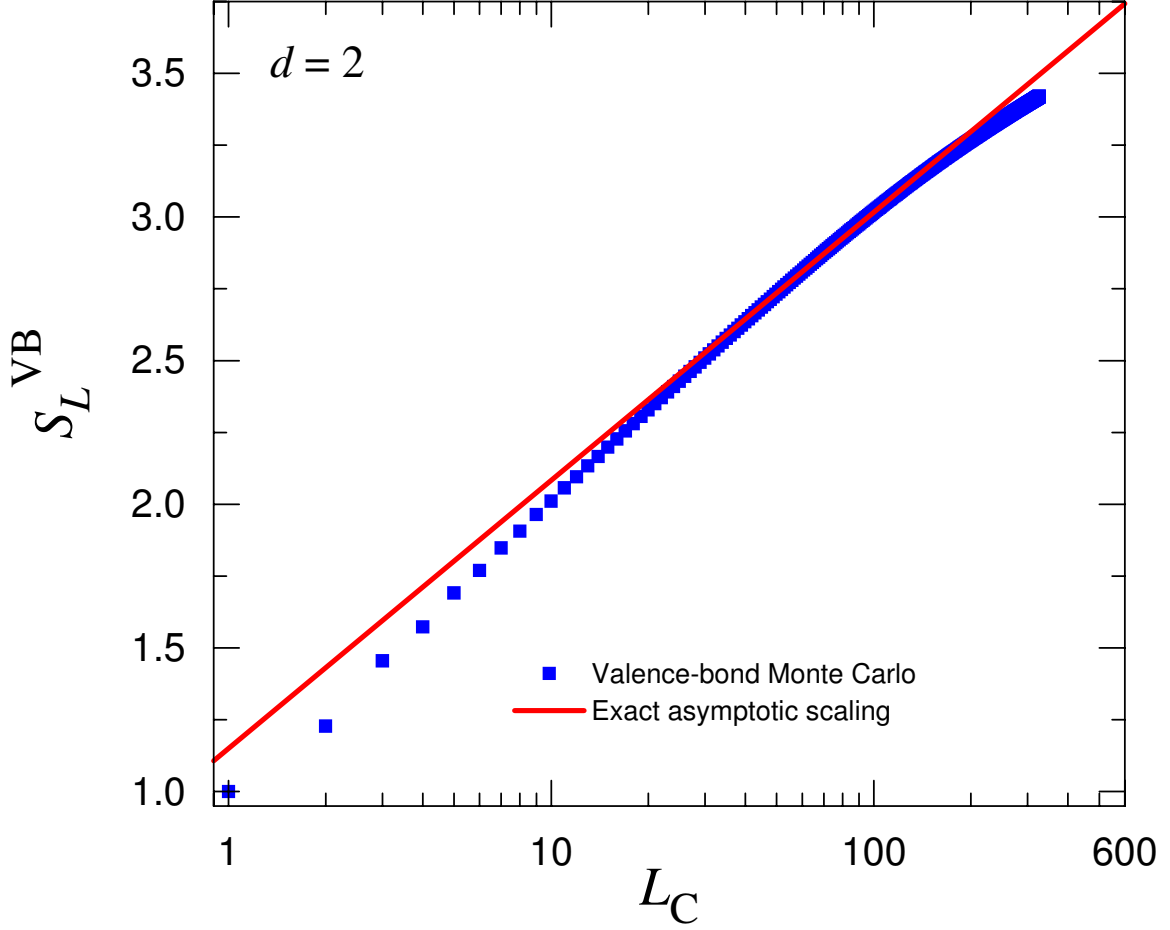


Figure 3.6: Semi-log plot of the valence-bond entanglement entropy S_L^{VB} of the uniform model with $d = 2$ as a function of block conformal length L_C defined as $L_C = N/\pi \sin(\pi L/N)$. System parameters are $N = 1024$, $n = 20N$ with periodic boundary conditions. Data is averaged over 50 independent simulations. The exact asymptotic scaling of S_L^{VB} by Jacobsen and Saleur is sketched by the solid line. Error bars are smaller than the symbol size.

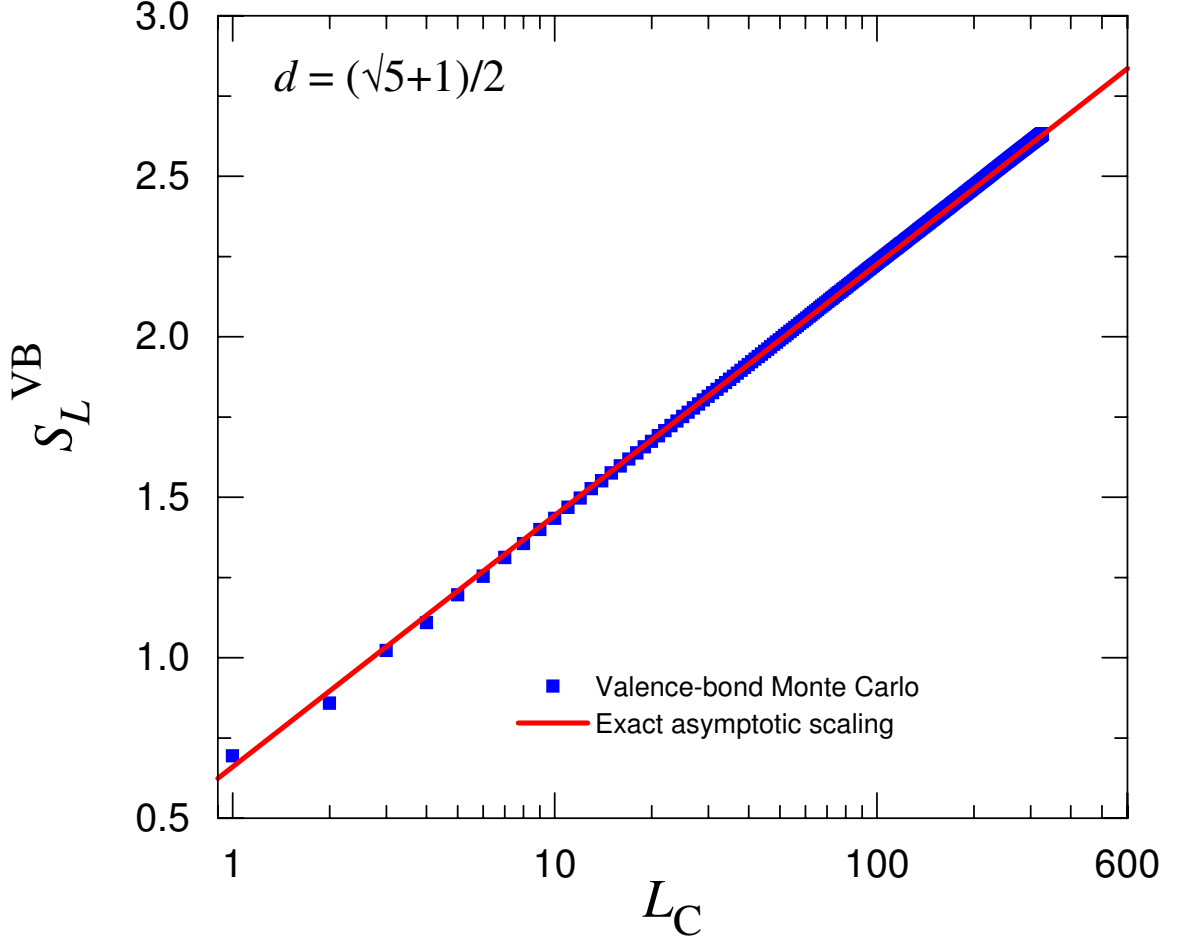


Figure 3.7: Semi-log plot of the valence-bond entanglement entropy S_L^{VB} of the uniform model with $d = \frac{1}{2}(\sqrt{5} + 1)$ as a function of block conformal length L_C defined as $L_C = N/\pi \sin(\pi L/N)$. System parameters are $N = 1024$, $n = 20N$ with periodic boundary conditions. Data is averaged over 50 independent simulations. The exact asymptotic scaling of S_L^{VB} by Jacobsen and Saleur is sketched by the solid line. Error bars are smaller than the symbol size.

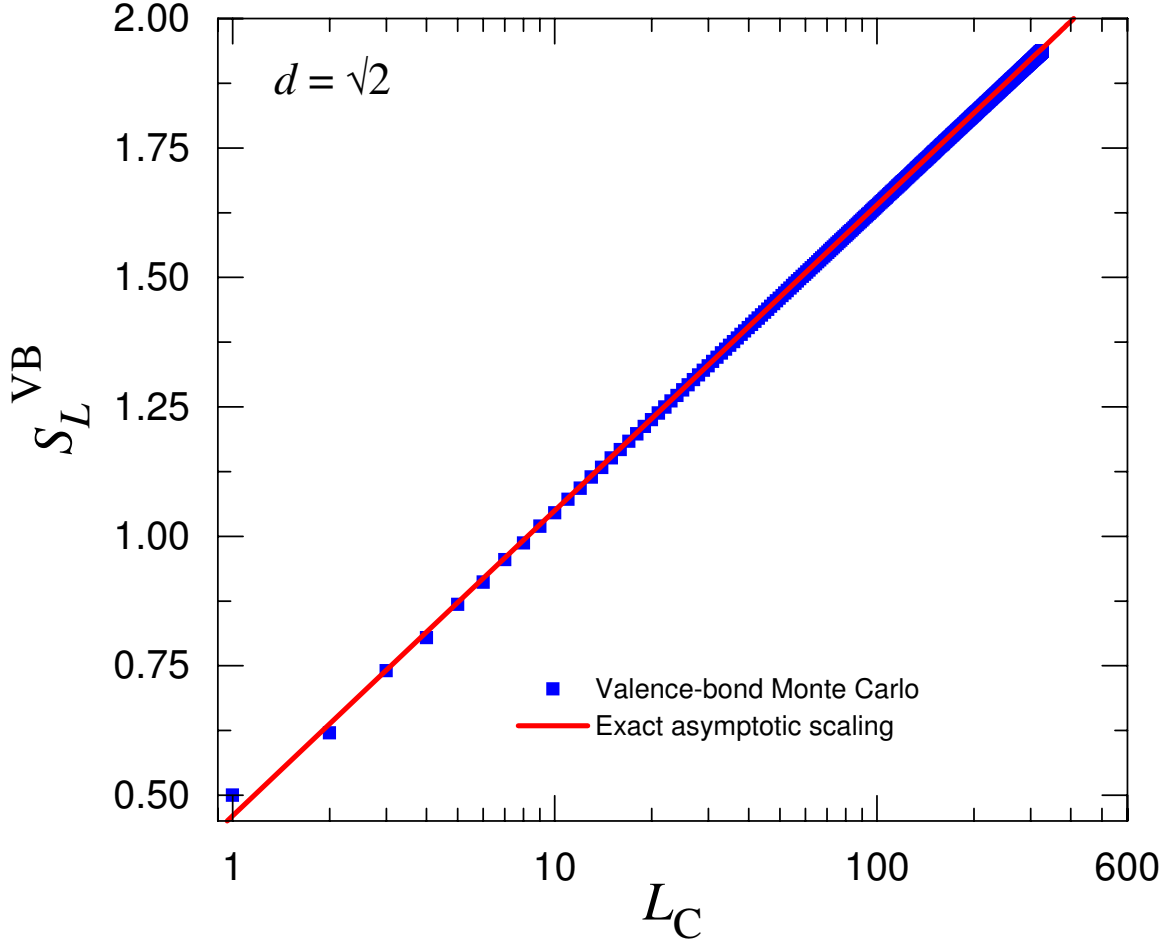


Figure 3.8: Semi-log plot of the valence-bond entanglement entropy S_L^{VB} of the uniform model with $d = \sqrt{2}$ as a function of block conformal length L_C defined as $L_C = N/\pi \sin(\pi L/N)$. System parameters are $N = 1024$, $n = 20N$ with periodic boundary conditions. Data is averaged over 50 independent simulations. The exact asymptotic scaling of S_L^{VB} by Jacobsen and Saleur is sketched by the solid line. Error bars are smaller than the symbol size.

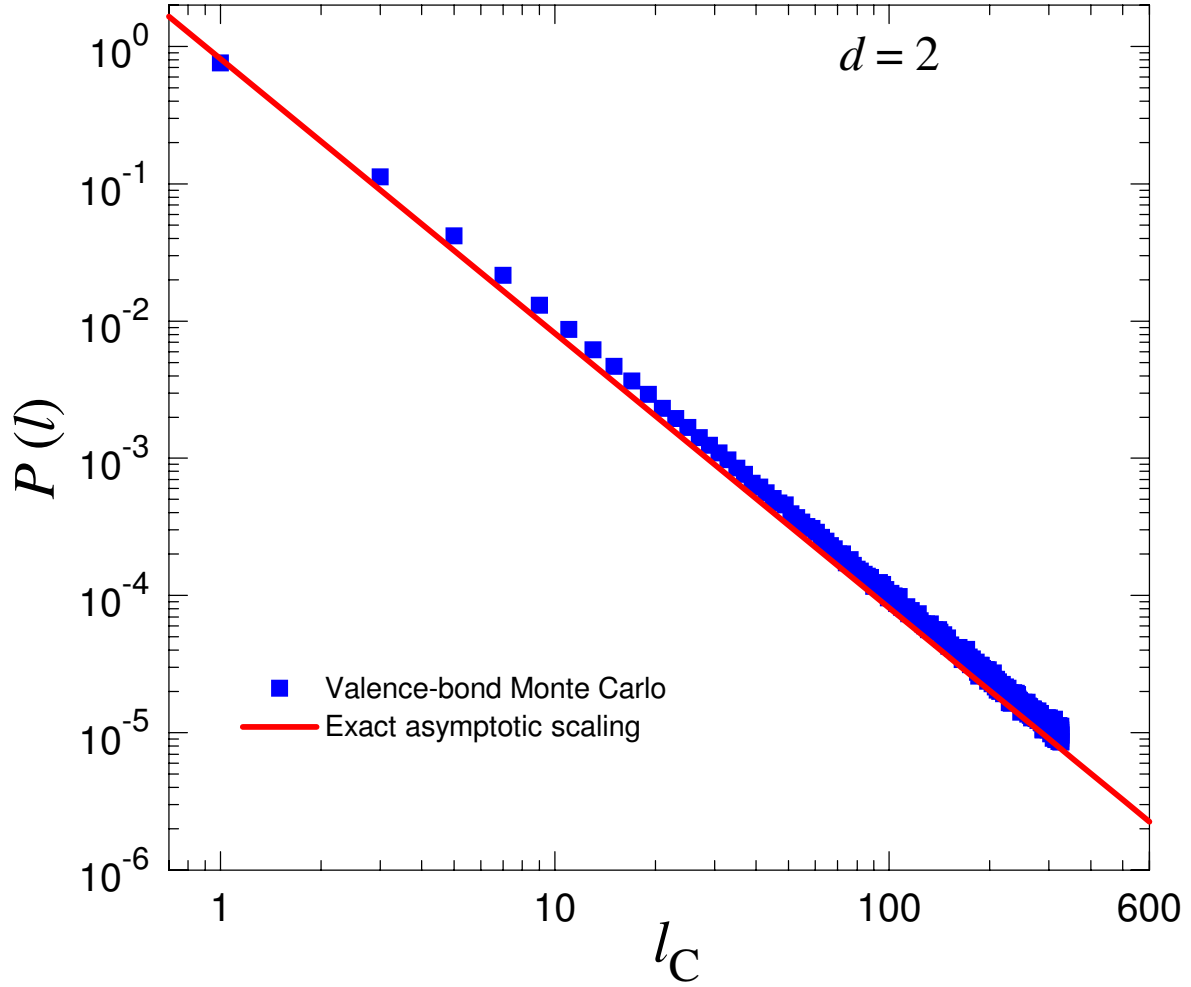


Figure 3.9: Log-log plot of the bond length distribution $P(l)$ of the uniform model with $d = 2$ as a function of bond conformal length l_C . System parameters are $N = 1024$, $n = 20N$. Data is averaged over 50 independent simulations. Periodic boundary condition is employed. The exact asymptotic scaling is sketched by the solid line. Error bars are smaller than the symbol size.

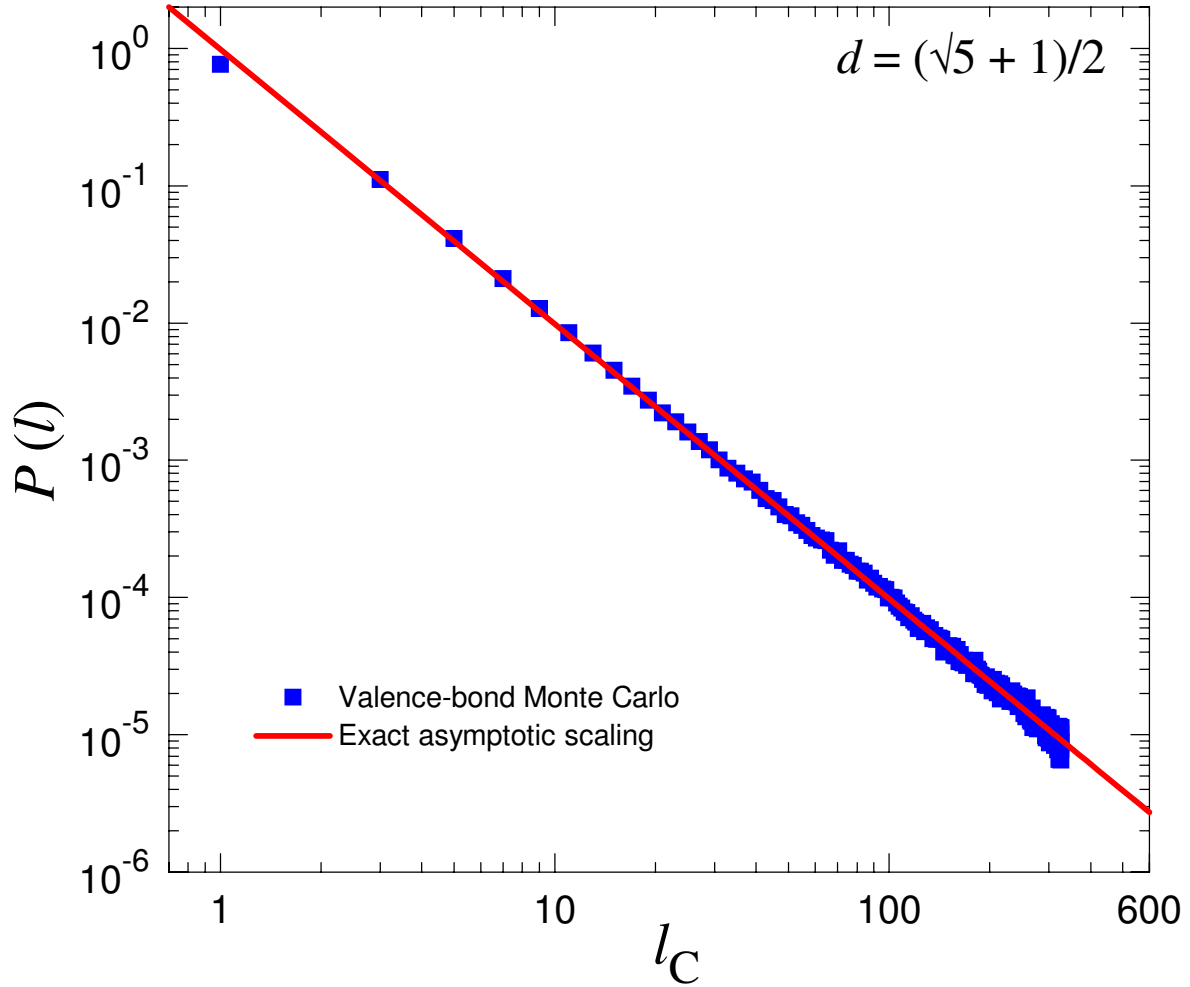


Figure 3.10: Log-log plot of the bond length distribution $P(l)$ of the uniform model with $d = \frac{1}{2}(\sqrt{5} + 1)$ as a function of bond conformal length l_C . System parameters are $N = 1024$, $n = 20N$. Data is averaged over 50 independent simulations. Periodic boundary condition is employed. The exact asymptotic scaling is sketched by the solid line. Error bars are smaller than the symbol size.

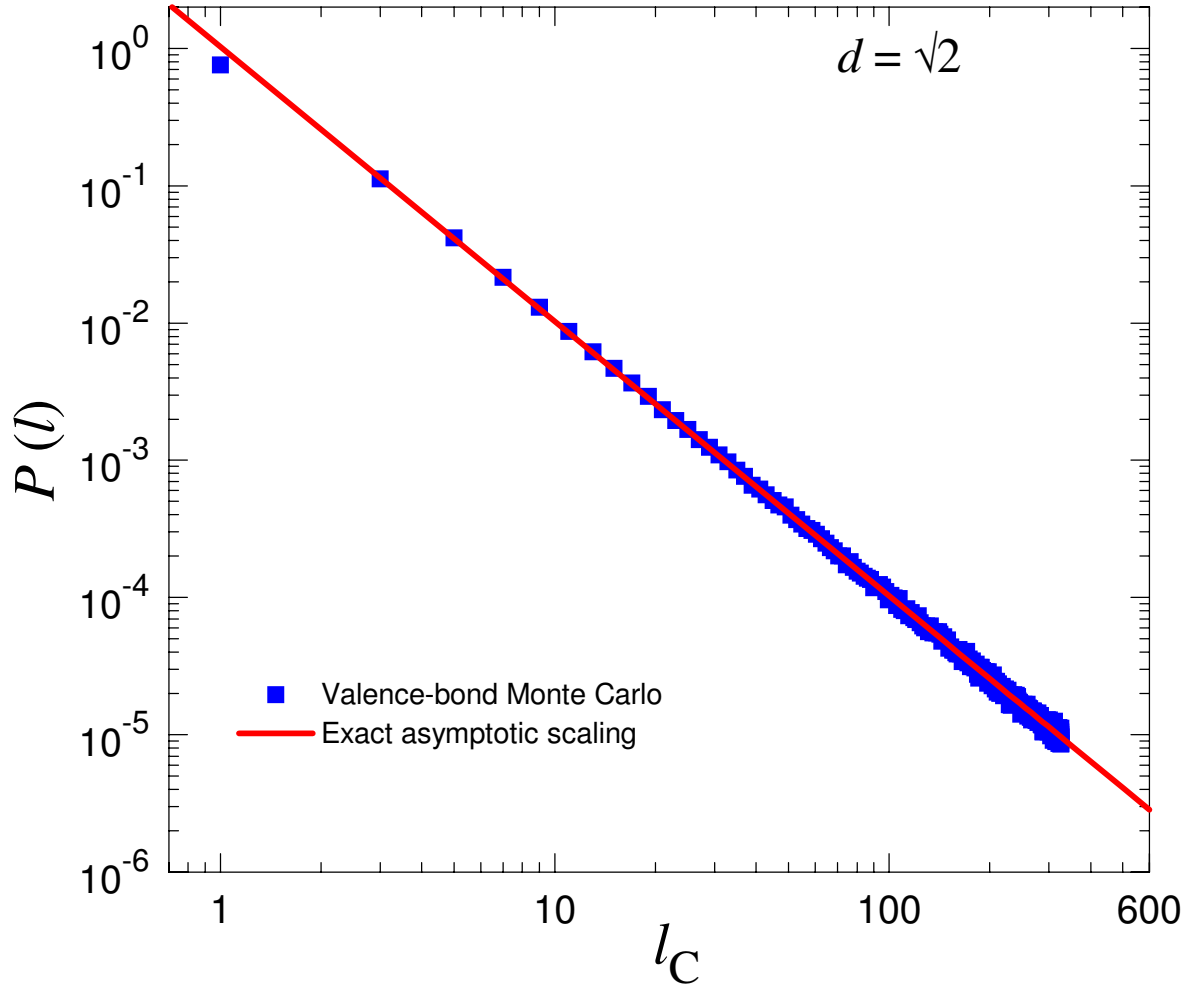


Figure 3.11: Log-log plot of the bond length distribution $P(l)$ of the uniform model with $d = \sqrt{2}$ as a function of bond conformal length l_C . System parameters are $N = 1024$, $n = 20N$. Data is averaged over 50 independent simulations. Periodic boundary condition is employed. The exact asymptotic scaling is sketched by the solid line. Error bars are smaller than the symbol size.

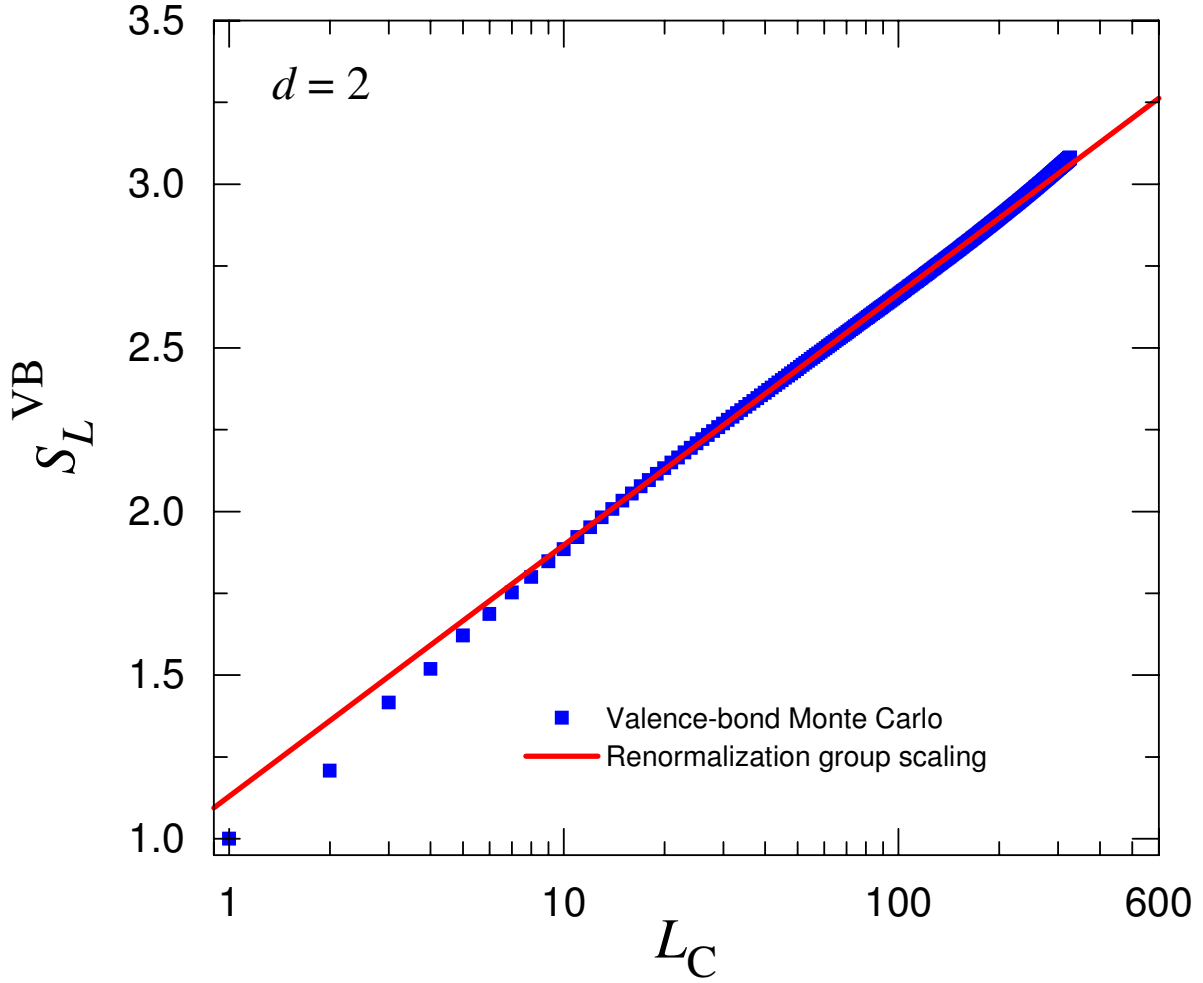


Figure 3.13: Semi-log plots of the valence-bond entanglement entropy S_L^{VB} of a random chain with $d = 2$ as a function of block conformal length L_C . System parameters are $N = 1024$, $n = 20N$, and $u = 1.0$. Results are averaged over 2000 disorders. Periodic boundary condition is employed. RG scaling is sketched by the solid line. Error bars are smaller than the symbol size.

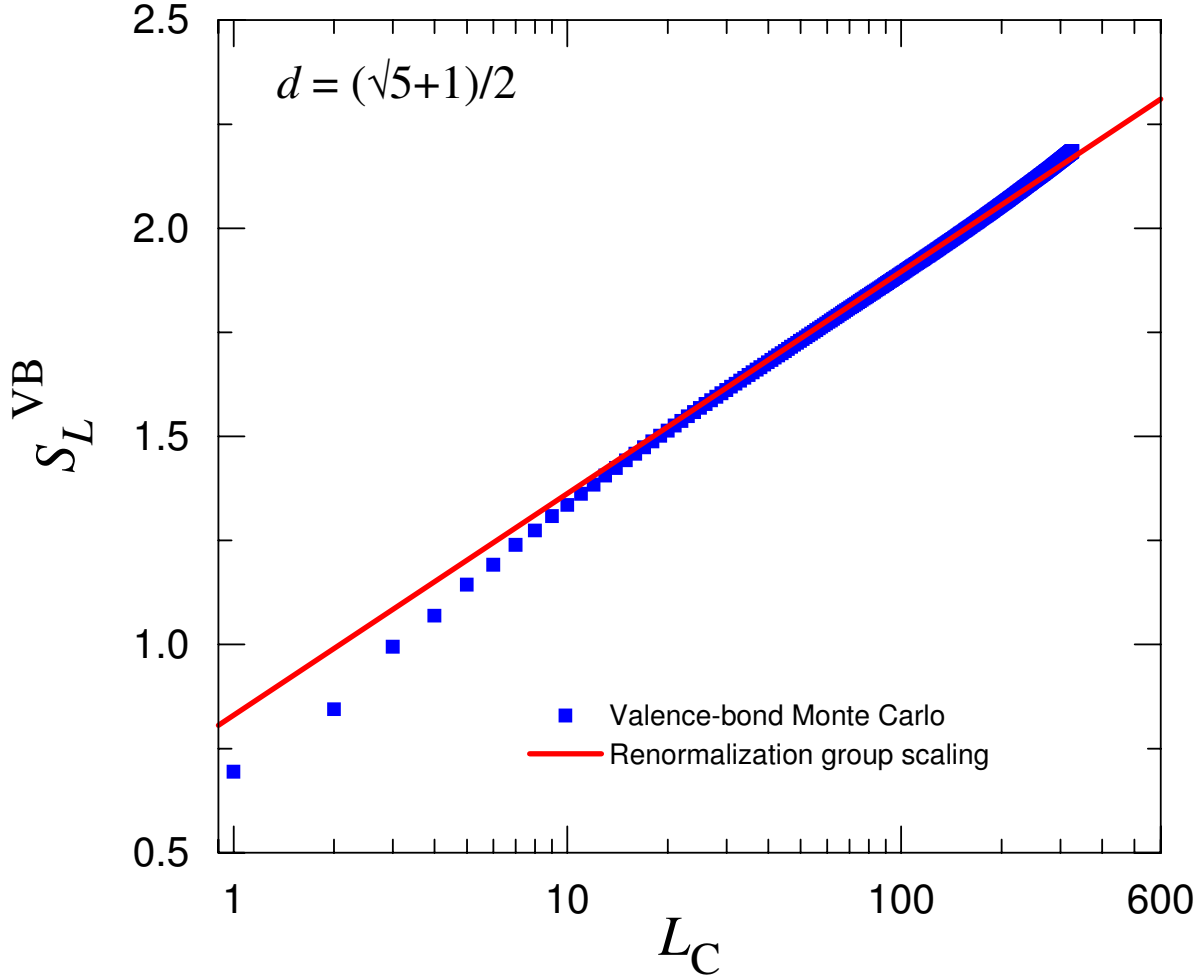


Figure 3.14: Semi-log plots of the valence-bond entanglement entropy S_L^{VB} of a random chain with $d = \frac{1}{2}(\sqrt{5} + 1)$ as a function of block conformal length L_C . System parameters are $N = 1024$, $n = 20N$, and $u = 1.0$. Results are averaged over 2000 disorders. Periodic boundary condition is employed. RG scaling is sketched by the solid line. Error bars are smaller than the symbol size.

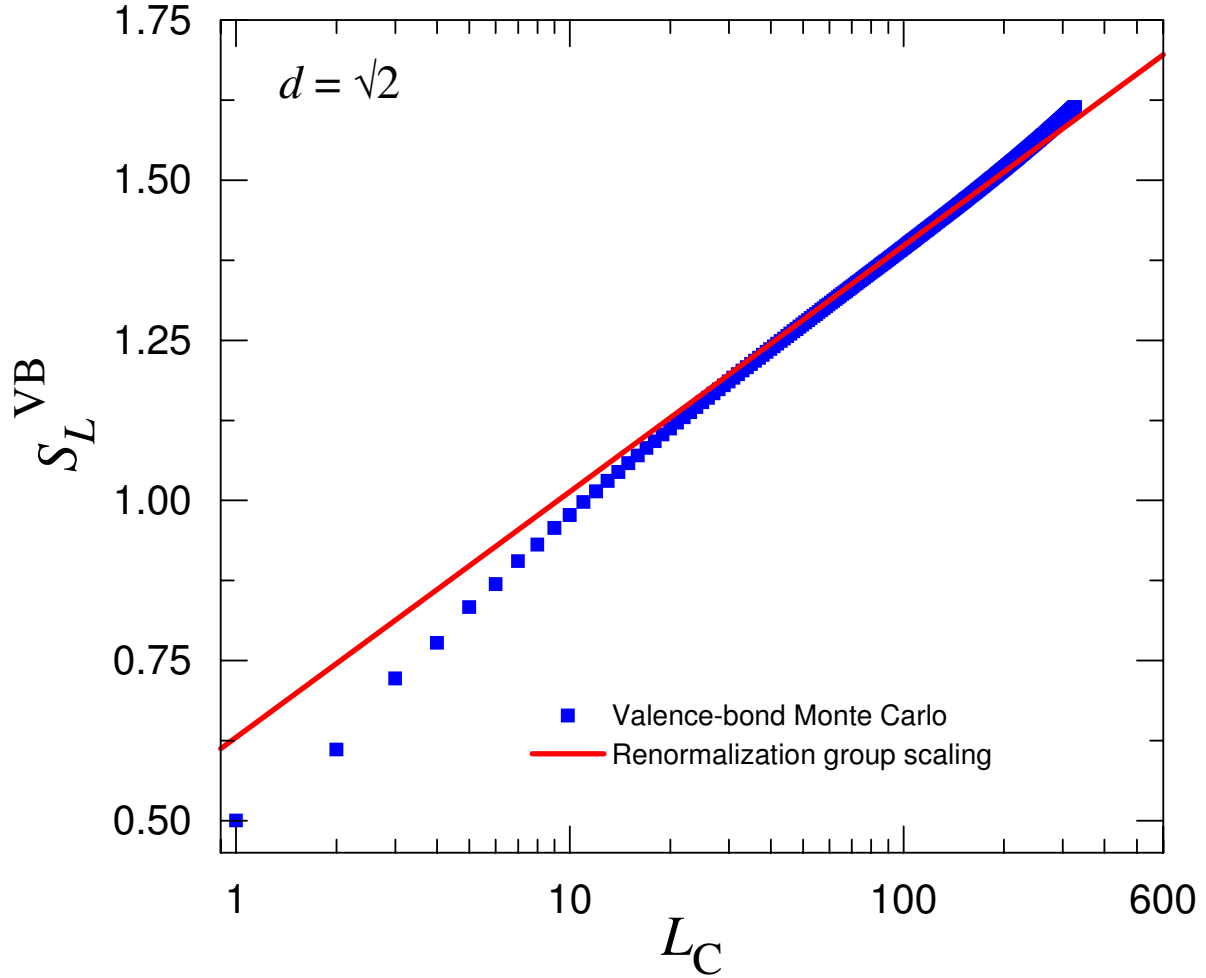


Figure 3.15: Semi-log plots of the valence-bond entanglement entropy S_L^{VB} of a random chain with $d = \sqrt{2}$ as a function of block conformal length L_C . System parameters are $N = 1024$, $n = 20N$, and $u = 1.0$. Results are averaged over 2000 disorders. Periodic boundary condition is employed. RG scaling is sketched by the solid line. Error bars are smaller than the symbol size.

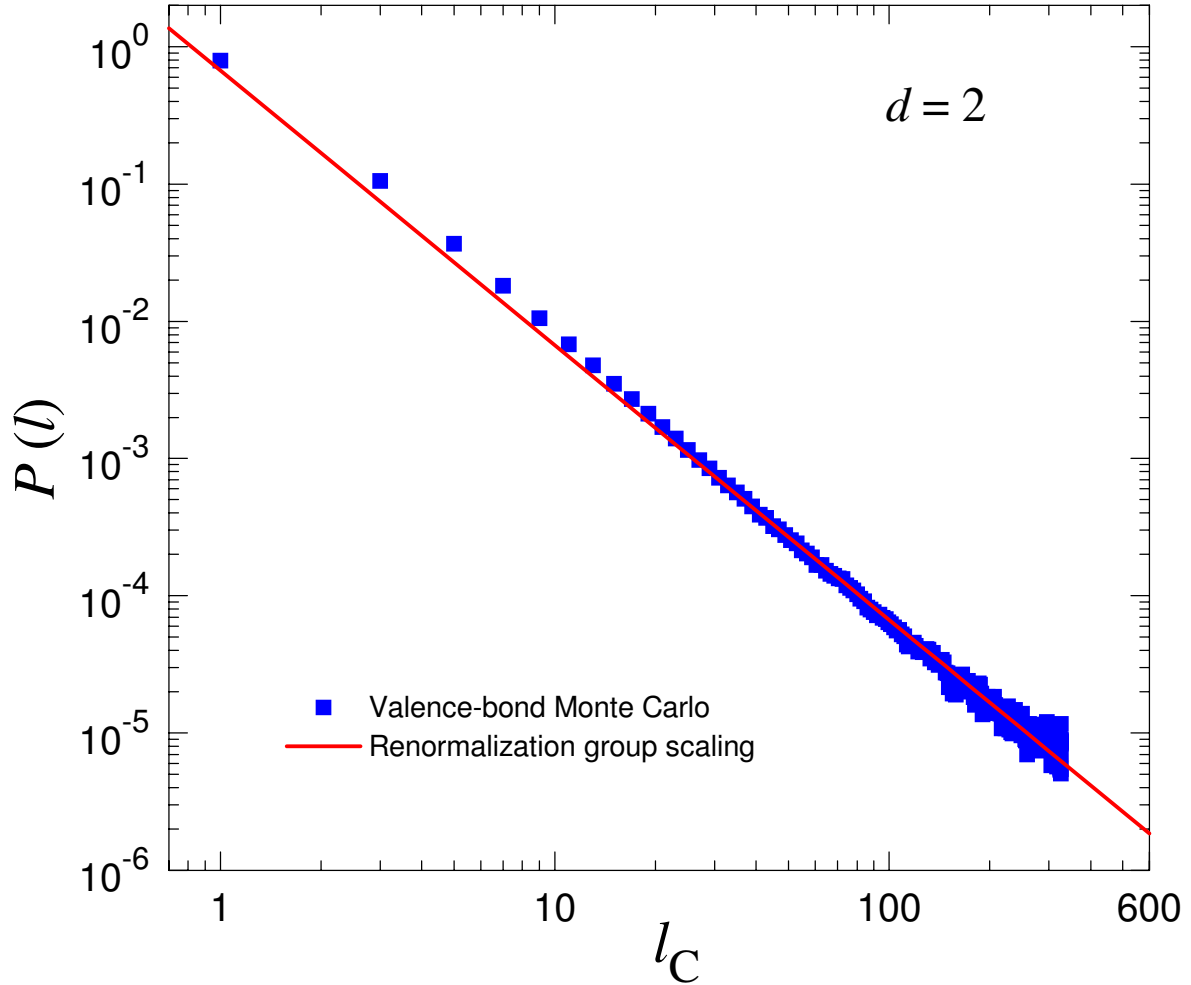


Figure 3.16: Log-log plots of the bond length distribution $P(l)$ of a random chain with $d = 2$ as a function of bond conformal length l_C . System parameters are $N = 1024$, $n = 20N$, and $u = 1.0$. Results are averaged over 2000 disorders. Periodic boundary condition is employed. RG scaling is sketched by the solid line. Error bars are smaller than the symbol size.

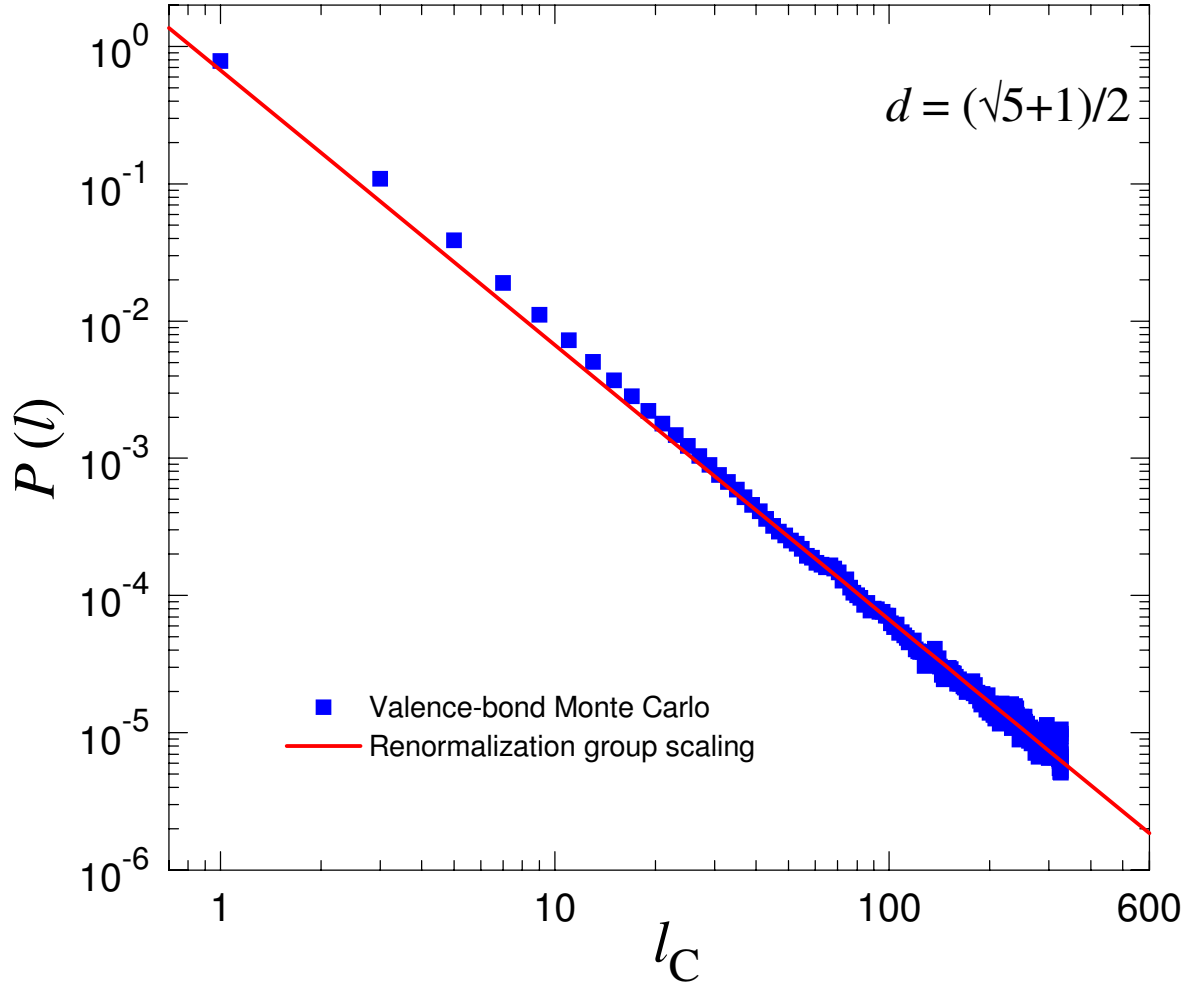


Figure 3.17: Log-log plots of the bond length distribution $P(l)$ of a random chain with $d = \frac{1}{2}(\sqrt{5} + 1)$ as a function of bond conformal length l_C . System parameters are $N = 1024$, $n = 20N$, and $u = 1.0$. Results are averaged over 2000 disorders. Periodic boundary condition is employed. RG scaling is sketched by the solid line. Error bars are smaller than the symbol size.

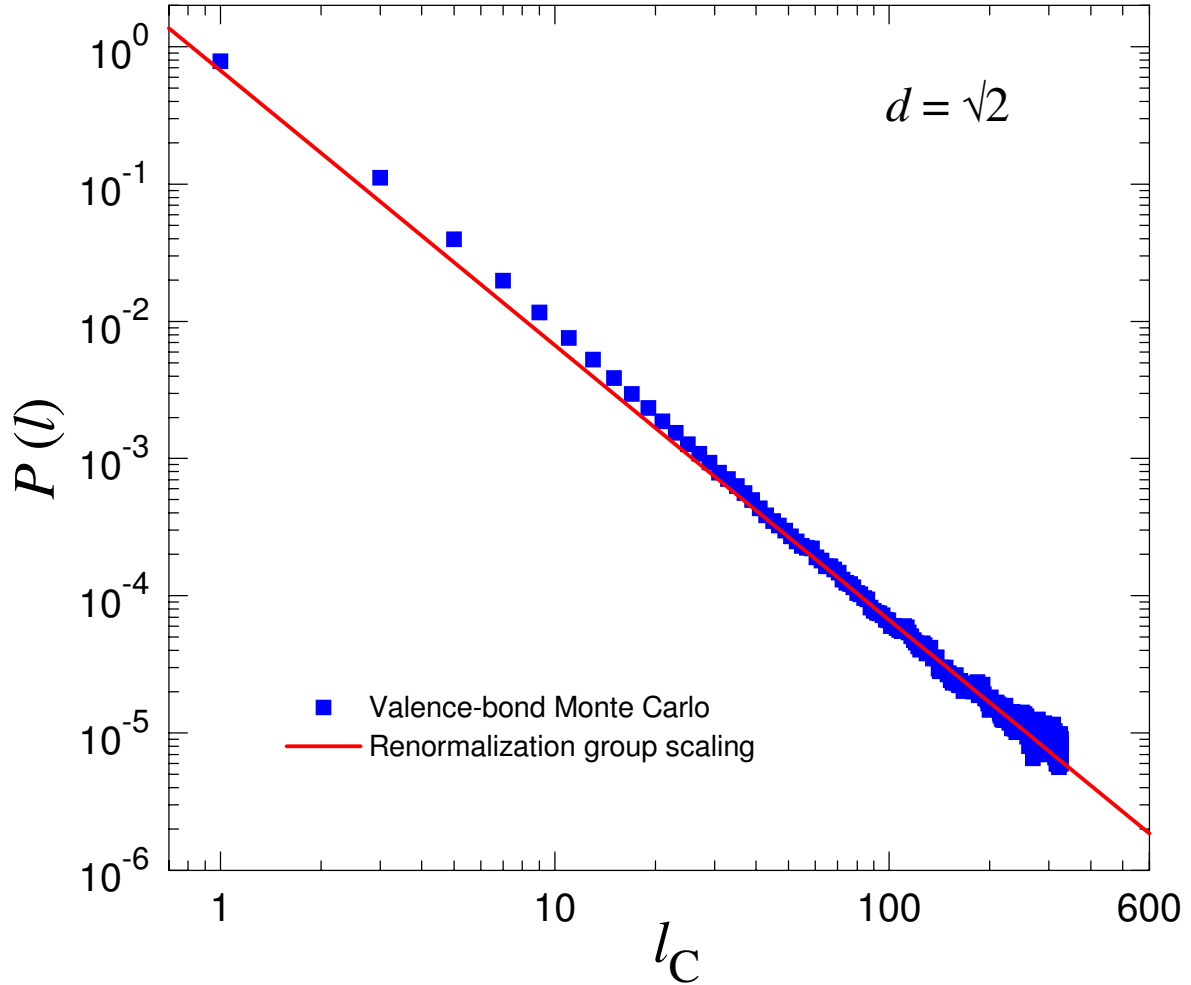


Figure 3.18: Log-log plots of the bond length distribution $P(l)$ of a random chain with $d = \sqrt{2}$ as a function of bond conformal length l_C . System parameters are $N = 1024$, $n = 20N$, and $u = 1.0$. Results are averaged over 2000 disorders. Periodic boundary condition is employed. RG scaling is sketched by the solid line. Error bars are smaller than the symbol size.

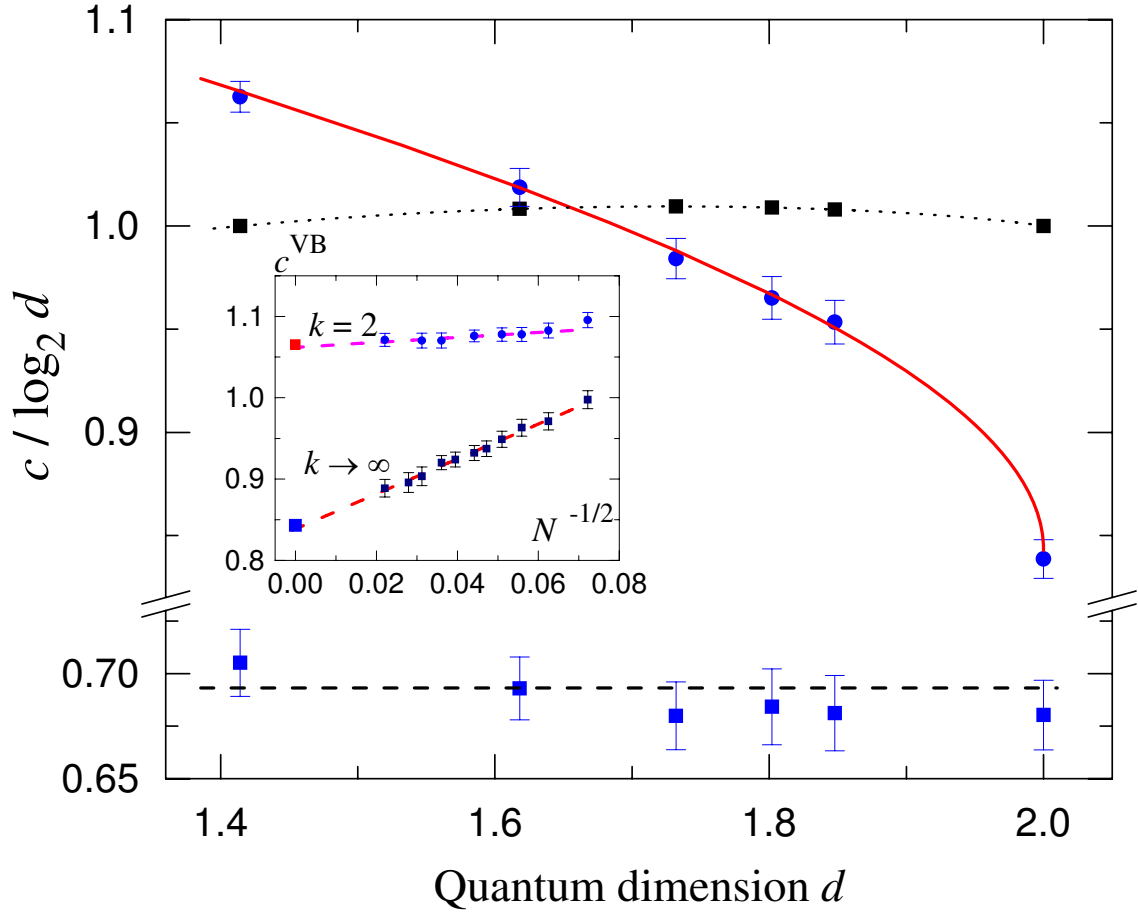


Figure 3.19: d dependence of the valence-bond central charge, c_d^{VB} , for uniform (higher part) and random chains (lower part), along with the true central charges for the conformally invariant uniform models with $d = 2 \cos \frac{\pi}{k+2}$, in units of $\log_2 d$. The solid red line is the exact result in Eq. (3.41), the black squares are the central charges of the uniform chain of interacting non-Abelian anyons for different values of k (the dashed line is a guide to the eye), the green line is the real-space RG result $\tilde{c} / \log_2 d = \ln 2$ for the random models, and the blue circles and triangles are our valence-bond Monte Carlo results for uniform and random models, respectively. The inset shows the finite size extrapolation used to find c^{VB} for the uniform models with $k \rightarrow \infty$ and $k = 2$.

CHAPTER 4

VALENCE-BOND FLUCTUATION

In this chapter a new quantity, which I refer to as the valence-bond fluctuation for the models (1.36), is introduced. It is shown how this new quantity provides a natural language for studying random singlet phases, with some advantages over previous methods. In particular, for random chains, by using this quantity, one can effectively “see” that the valence bonds of a random singlet ground state are locked into a particular valence bond configuration on long-length scales [27]. The length scale which characterizes the valence-bond locking can also be extracted from the valence-bond fluctuations. Another advantage of this quantity is that it can be easily calculated for both uniform and disordered models using valence-bond Monte Carlo, regardless how weak the disorder is. Consequently, the random singlet phase formation in the limit of weak disorder (the uniform model) can be directly probed by analyzing this quantity for disorders of various strengths. In addition, my results for uniform models provide a numerical confirmation for a very recent exact asymptotic result by Jacobsen and Saleur [44].

4.1 Valence bonds in random singlet phases

The ground state of the uniform chain described by (1.36) can be viewed as a strongly fluctuating spin liquid in which valence bonds, which can take any length, strongly resonate on all length scales. While valence bonds in a random singlet ground state can also have any length, they resonate in different ways on different length scales. On long-length scales, they are locked into a particular bond configuration while on short-length scales, they fluctuate strongly, as in the ground state of the uniform chain.

For a more detailed discussion on the fluctuations of the valence bonds in the ground state of either a uniform or a random chain, we define a quantity ξ so that the valence bonds

of the ground state of a chain fluctuate on length scales up to ξ while they are locked on length scales larger than ξ . The fluctuation length scale ξ defined here can be viewed as a crossover from a resonating regime to a locking regime, the former is relevant to the uniform chain while the latter is relevant to random chains. For a random chain, ξ is finite and is a function of the disorder strength u (see Eq. (3.38) and Figure 3.12 for a definition of u). For uniform chains ($u = 0$), because the valence bonds strongly resonate on all length scales, ξ diverges in the limit $N \rightarrow \infty$.

We now come back to the essential features of a random singlet ground state. The existence of valence bonds with any length in a random singlet ground state can be probed directly by the valence-bond entanglement entropy S_L^{VB} and the bond length distribution $P(l)$. In Chapter 3, discussions on these two quantities are given in details. Starting from the random singlet ground state obtained by the real-space RG scheme [10], the block entanglement entropy S_L was shown to scale logarithmically with L [25, 30]. The logarithmic scaling of S_L^{VB} and, as a consequence, the power-law scaling of $P(l)$, were implied from the scaling of S_L and the feature that valence bonds in a random singlet ground state are locked into a particular bond configuration on long-length scales. The divergence of S_L^{VB} and the power law of $P(l)$ directly imply that the valence bonds can have any length [44, 45]. Calculations using valence-bond Monte Carlo both for S_L^{VB} and $P(l)$ are also shown in Chapter 3 and the Ref. [43], giving numerical confirmations for the scalings of S_L^{VB} and $P(l)$, or equivalently, the feature that valence bonds in a random singlet ground state can indeed have any length.

While the scalings of valence-bond entanglement entropy S_L^{VB} and bond length distribution $P(l)$ can provide information on the bond lengths, they provide no information of the bond fluctuations and the fluctuation length scale ξ . In particular, the scalings of S_L^{VB} and $P(l)$ are derived with two assumptions: 1) the logarithmic scaling of S_L , the block entanglement entropy and 2) that the valence bonds of a random singlet ground state are locked into a particular bond configuration beyond the length scale ξ . The first assumption can be traced back to the real-space RG analysis for a given disorder. This analysis adopts the approximation (1.19), which is good in the limit of strong disorder but becomes less effective in the limit of weak disorder. The random singlet ground state, within this approximation, is obtained as a single valence-bond state which exhibits the bonds with arbitrary length [10] but no information of bond fluctuations. The second assumption is basically what we

have to prove and the scalings of S_L^{VB} and $P(l)$ are used as a numerical evidence that this assumption is correct. However, the scalings of S_L^{VB} and $P(l)$ can not be used to provide any information on the fluctuation length scale ξ , which can be expected to be an interesting quantity of a random singlet ground state.

For the reasons, it is my goal to introduce another quantity that minimizes the number of assumptions used. In particular, I will define a new quantity called valence-bond fluctuation whose behavior can be predicted without the first assumption, i.e., it depends solely on the second assumption. This quantity is able to demonstrate clearly that the valence bonds for the uniform chain strongly resonate on all length scales while it shows that the valence bonds they are locked into a particular bond configuration on long-length scales with any disorder strength, especially in the limit of weak disorder. This quantity, therefore, can be used as a new signature of the random singlet phase associated to random chains. The new quantity should also be used for to determine the fluctuation length scale ξ , the interesting quantity which is defined just above. In section 4.2, the valence-bond fluctuation is defined and discussed in details.

4.2 Valence-bond fluctuation

4.2.1 Definition

The valence-bond Monte Carlo, as discussed in the previous Chapters, samples the ground state $|0\rangle$ of either a uniform or a random chain on the valence-bond basis. For each sample state $|\alpha\rangle$, the number of valence bonds crossing one of two ends of a given block A is determined to be $n_L(\alpha)$ (see Figure 3.4 for an illustration). The valence-bond entanglement entropy S_L^{VB} is then defined as the weighted average of $n_L(\alpha)$, given by Eq. (3.20). While the scaling of S_L^{VB} provide no information on the bond fluctuations and the fluctuation length scale ξ , the valence-bond fluctuation σ_L^2 , which is defined as a particular variance of n_L , can provide such information.

For the purpose, the valence-bond fluctuation σ_L^2 of the uniform chain is defined as

$$\sigma_L^2 = \frac{\sum_{\alpha} w(\alpha) n_L^2(\alpha)}{\sum_{\alpha} w(\alpha)} - \left[\frac{\sum_{\alpha} w(\alpha) n_L(\alpha)}{\sum_{\alpha} w(\alpha)} \right]^2, \quad (4.1)$$

or, in an equivalent but more condensed form

$$\sigma_L^2 = \langle n_L^2 \rangle - \langle n_L \rangle^2. \quad (4.2)$$

In this formula, the angular brackets $\langle \dots \rangle$ denote the weighted average (2.10) over the sampling states $|\alpha\rangle$ which is executed during a Monte Carlo simulation. For random models, an additional average over disorders is needed, so the valence-bond fluctuation σ_L^2 is defined as

$$\sigma_L^2 = \overline{\langle n_L^2 \rangle - \langle n_L \rangle^2} \quad (4.3)$$

where the overbar denotes a disorder average. Note that the order of the averages is crucial: first one averages $\langle n_L^2 \rangle$ and $\langle n_L \rangle$, and then compute $\langle n_L^2 \rangle - \langle n_L \rangle^2$ before averaging over disorders for random models.

The valence-bond fluctuation σ_L^2 defined by (4.2) for uniform chains and (4.3) for random chains has some properties which are useful for studying the random singlet phases. In the next section these properties will be discussed, showing a key role of the fluctuation length scale ξ .

4.2.2 Active regions

For a given block of L sites in a chain, σ_L^2 is the variance of n_L , which is the number of valence bonds crossing one of two block ends. We now consider, for example, the left end of the block and the valence bonds crossing this end. Each of these valence bonds has exactly one end inside the block, and this end fluctuates within a length scale of ξ , which is either finite or infinite. Consequently, only the valence bonds ending at a site within a distance of $\sim \xi$ from the left end can fluctuate between inside and outside of the block, thus changing the number of valence bonds crossing the left end. In other words, only the bond fluctuations happening within a distance of $\sim \xi$ from the left end, a region called the *active region*, can change the number of valence bonds crossing the left end, thus contribute to σ_L^2 , the variance of n_L . On the Figure 4.1, an illustration for two active regions of a given block of $L = 7$ sites is shown. The union of two active regions corresponding to the left and right ends of a block is called a *total active region*.

The concept of active region plays a role in a qualitative discussion on σ_L^2 as a function of the block length L of (1.36), either with or without disorders. In particular, the size of

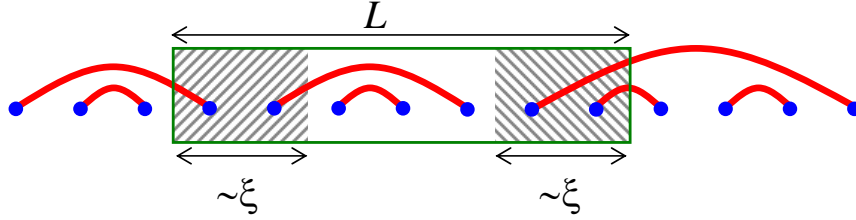


Figure 4.1: A geometry of the definition of valence-bond fluctuation σ_L^2 , which is defined as the variance of n_L , the number of bond crossing one of two ends of the block of length L . Two dashed regions with size of $\sim \xi$ from two ends of the block are called “active regions” in the sense that only the fluctuations of the bonds which have one end in the regions contribute to σ_L^2 . The union of the active regions is called a “total active region” with the size of either equal or smaller than L .

the total active region, by definition, is directly related to the valence-bond fluctuation σ_L^2 . While the asymptotic scaling of σ_L^2 of the uniform chain can be determined exactly by an other method [44], similar things are not available for random chains, so in this case, the concept of active region is somewhat useful.

4.2.3 Valence-bond fluctuation in the uniform model

In the ground state of the uniform chain, valence bonds strongly resonate on all length scales, implying that in the limit $N \rightarrow \infty$, the fluctuation length scale ξ diverges. Therefore, for a block of finite L sites, the total active region size is always equal to L . Any increase of L , consequently, always makes the total active region larger, thus increases σ_L^2 . Therefore, the valence-bond fluctuation σ_L^2 for the uniform chain can be expected, in a *qualitative* way, to grows with the block length L .

In a recent work, Jacobsen and Saleur [44] have shown that one can do more than just a qualitative discussion on the divergence of σ_L^2 as L grows. For the uniform chain, they has shown that the exact asymptotic scaling of the variance of n_L , which is σ_L^2 as defined by (4.2), can be determined exactly as $1 \ll L \ll N$. As discussed in subsection 3.3.1, the averaged number $\langle n_L \rangle$ can be obtained by operating $w \frac{\partial}{\partial w}$ on the correlation function $\langle V_+(0)V_-(L) \rangle$ given in (3.27) [44]. In order to determine valence-bond fluctuation $\sigma_L^2 = \langle n_L^2 \rangle - \langle n_L \rangle^2$, we need to calculate $\langle n_L^2 \rangle$ while $\langle n_L \rangle$ has already been calculated and given in Eq. (3.32). This

quantity, similar to $\langle n_L \rangle$, can be determined by operating $(w \frac{\partial}{\partial w})^2$ on two sides of (3.27). The action on the left hand side simply returns $\langle n_L^2 \rangle$ in the same fashion as Eq. (3.31). On the other hand, the action on the right hand side of (3.27) can be described as

$$\begin{aligned} \left(w \frac{\partial}{\partial w}\right)^2 L^{-2h(w,d)} &= 4w^2 \left(\frac{\partial h(w,d)}{\partial w}\right)^2 L^{-2h(w,d)} (\ln L)^2 \\ &\quad - 2w \left(\frac{\partial h(w,d)}{\partial w} + w \frac{\partial^2 h(w,d)}{\partial w^2}\right) L^{-2h(w,d)} \ln L. \end{aligned} \quad (4.4)$$

Recall that the Eq. (4.4) has to be estimated at $w = \sqrt{Q_b} = \sqrt{2+d}$ at which $h(w,d) = 0$ and therefore $L^{-2h(w,d)} = 1$. When we calculate σ_L^2 which is defined as $\langle n_L^2 \rangle - \langle n_L \rangle^2$, the first term in the right hand side of the Eq. (4.4) cancels exactly the term $\langle n_L \rangle^2$, so the valence-bond fluctuation σ_L^2 is given by

$$\sigma_L^2 = -2w \left(\frac{\partial h(w,d)}{\partial w} + w \frac{\partial^2 h(w,d)}{\partial w^2}\right) \Big|_{w=\sqrt{Q_b}} \ln L. \quad (4.5)$$

Some more basic calculations are needed, and at the final, the valence-bond fluctuation σ_L^2 is found to grow logarithmically with in the regime $1 \ll L \ll N$ as [44]

$$\sigma_L^2 = c_2 \ln L + \mathcal{C} \quad (4.6)$$

where c_2 is a function of d only and is given by

$$c_2 = \frac{4}{\pi} \sqrt{\frac{2+d}{(2-d)^3}} \frac{2 \arccos(d/2) - \sqrt{4-d^2}}{\pi - \arccos(d/2)}. \quad (4.7)$$

Similar to the logarithmic scaling of S_L^{VB} which indicates the presence of valence bonds with any length, the exact asymptotic logarithmic scaling of σ_L^2 given by (4.6) clearly demonstrates that the valence bonds of the ground state of the uniform chain strongly resonate on *all length scales*.

It is an interesting note that σ_L^2 which is defined as (4.2) for the uniform chain can be easily calculated by valence-bond Monte Carlo so it is worth to give a numerical confirmation for the asymptotic scaling (4.6). For the uniform chain, I have simulated the uniform chains of interacting non-Abelian anyons with $d = 2$, $d = \frac{1}{2}(\sqrt{5} + 1)$, and $d = \sqrt{2}$ and then calculated σ_L^2 using Eq. (4.2). Chains used for calculation has the size of $N = 1024$ while the power number n is taken to be $60N$. For each independent simulation, a random non-crossing valence-bond state is generated and used as the initial valence-bond state $|S_0\rangle$. The

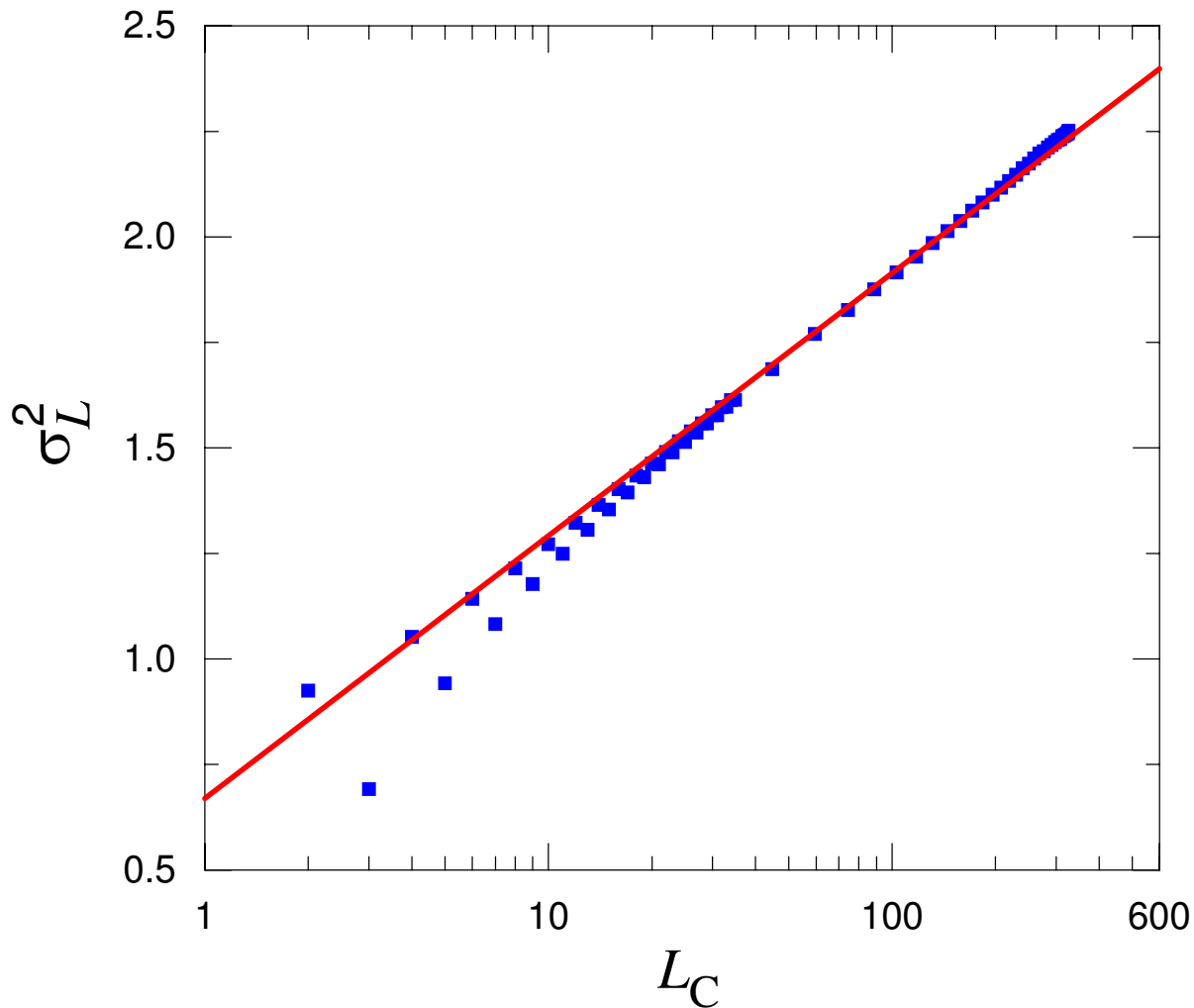


Figure 4.2: Valence-bond fluctuation σ_L^2 for the uniform chain described by Eq. (1.36) with $d = 2$ as function of block conformal length $L_C = N/\pi \sin(\pi L/N)$ for minimizing finite-size effects. The solid line depicts the exact asymptotic scaling (4.6) with the coefficient c_2 determined by (4.7). Parameters for the calculation are $N = 1024$, $n = 60N$. Error bars are smaller than the symbol size.

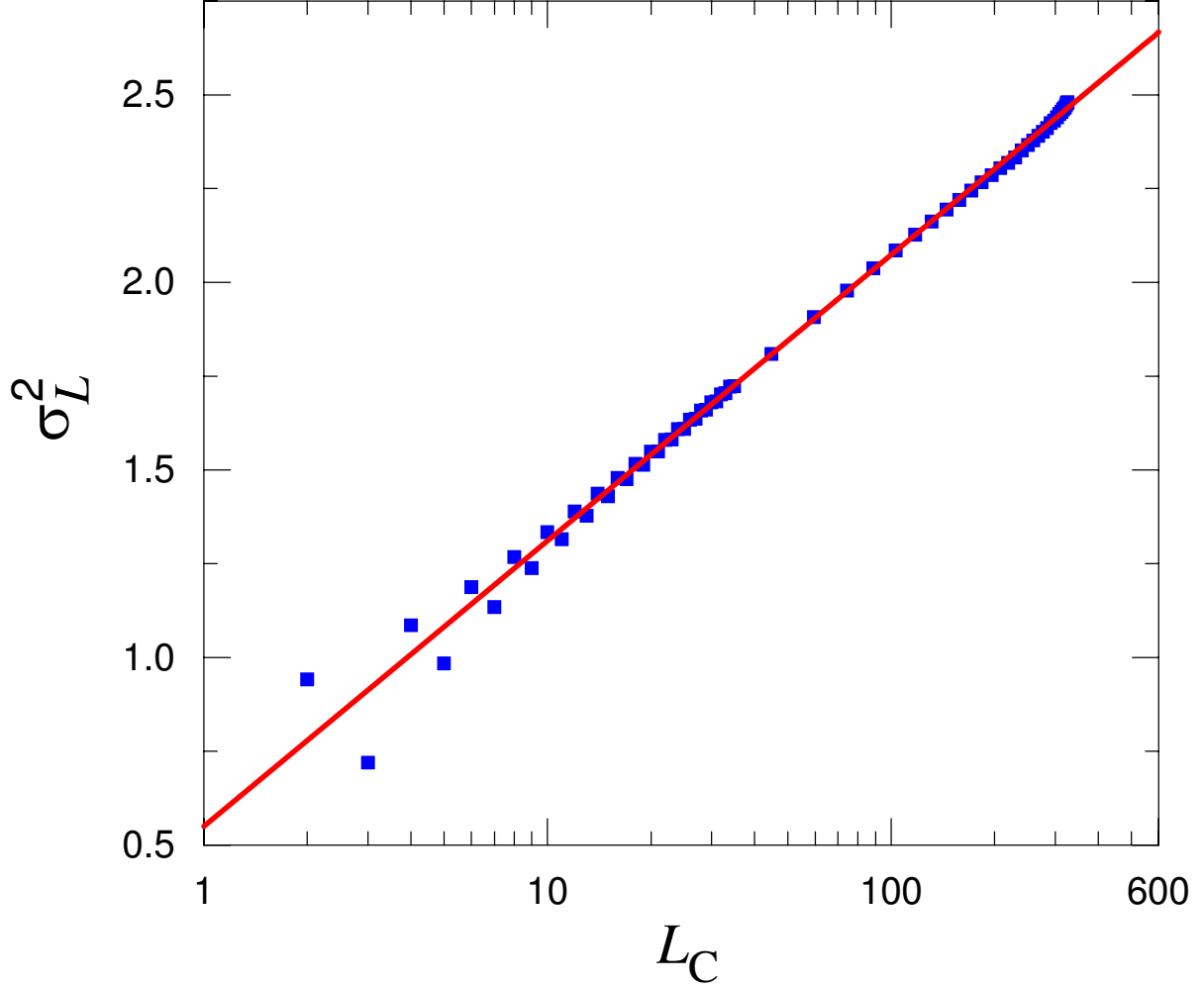


Figure 4.3: Valence-bond fluctuation σ_L^2 for the uniform chain described by Eq. (1.36) with $d = \frac{1}{2}(\sqrt{5} + 1)$ as function of block conformal length $L_C = N/\pi \sin(\pi L/N)$ for minimizing finite-size effects. The solid line depicts the exact asymptotic scaling (4.6) with the coefficient c_2 determined by (4.7). Parameters for the calculation are $N = 1024$, $n = 60N$. Error bars are smaller than the symbol size.

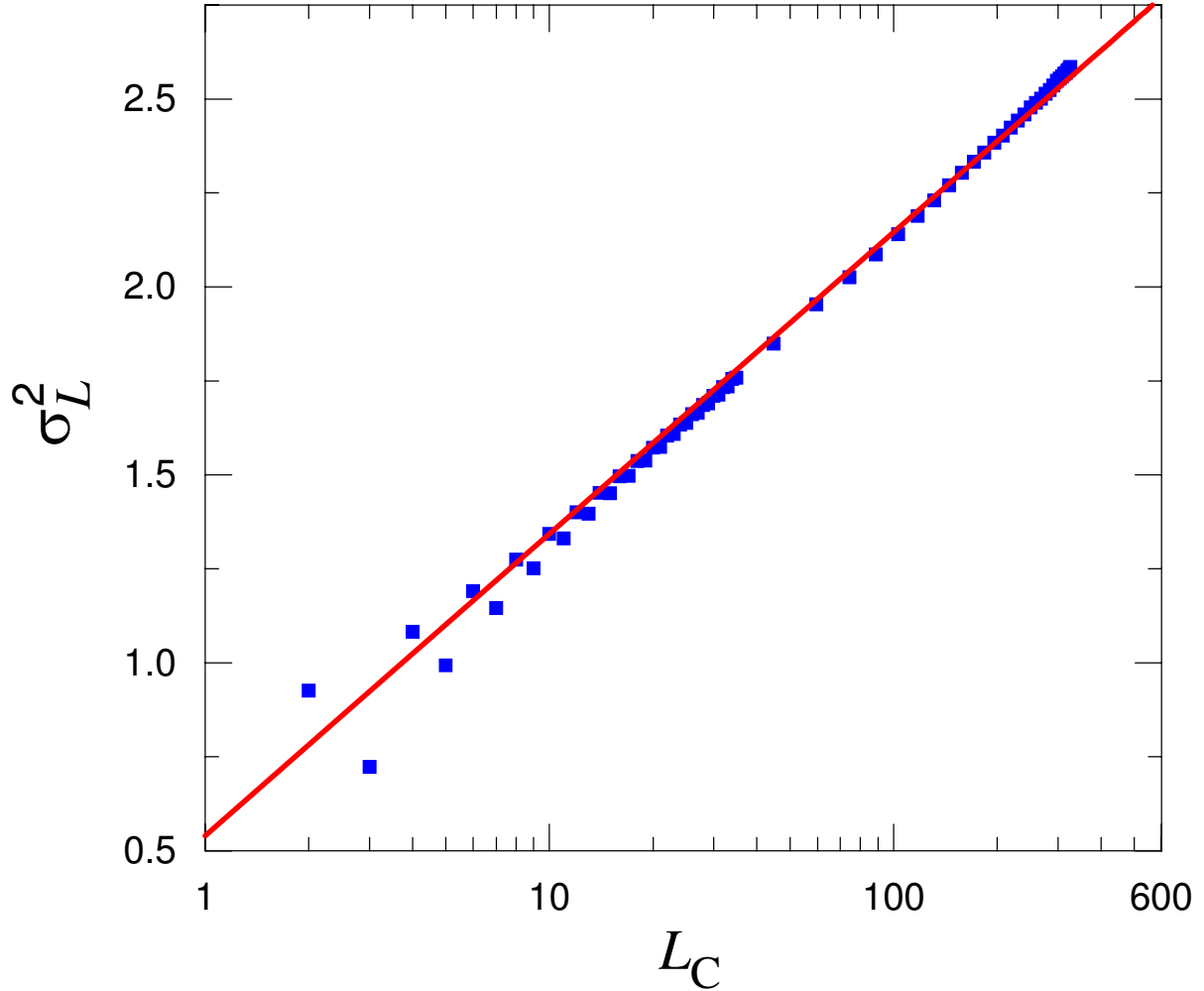


Figure 4.4: Valence-bond fluctuation σ_L^2 for the uniform chain described by Eq. (1.36) with $d = \sqrt{2}$ as function of block conformal length $L_C = N/\pi \sin(\pi L/N)$ for minimizing finite-size effects. The solid line depicts the exact asymptotic scaling (4.6) with the coefficient c_2 determined by (4.7). Parameters for the calculation are $N = 1024$, $n = 60N$. Error bars are smaller than the symbol size.

obtained results, which are averaged over 16 independent simulations are shown on Figures 4.2, 4.3, and 4.4, each for a value of d mentioned above. For minimizing the finite-size effects, σ_L^2 is shown on the Figures 4.2, 4.3, and 4.4 as functions of the block conformal length $L_C = N/\pi \sin(\pi L/N)$. The exact asymptotic scaling (4.6) with the coefficient c_2 determined by Eq. (4.7) are also shown on these figures by red lines for giving comparisons with the calculated results.

Figures 4.2, 4.3, and 4.4 clearly demonstrates an excellent agreement of the calculated valence-bond fluctuation σ_L^2 for the uniform chain for $d = 2$, $d = \frac{1}{2}(\sqrt{5} + 1)$, and $d = \sqrt{2}$ with the exact asymptotic scaling (4.6) recently found. The logarithmic scaling of σ_L^2 shown on these figures can be regarded as the first numerical confirmation for the work by Jacobsen and Saleur [44]. This result also clearly shows that in the spin-liquid ground state of the uniform chain, valence bonds, which can have any length, strongly resonate on all length scales. [43]

4.2.4 Valence-bond fluctuation in random models

For random chains, a qualitative discussion on the valence-bond fluctuation σ_L^2 can also given in the same way as for the uniform chain. While for the uniform chain, the fluctuation length scale ξ diverges, this length scale of a random chain is finite and may be sufficiently small, especially for strong disorders. Therefore, there are two limiting regimes in which we can identify qualitatively the behaviors of σ_L^2 . When $L \ll \xi$, the total active region size is equal L , thus, similar to the uniform chain, an increase of L always results an increase of the total active region size, and then an increase of σ_L^2 . On the other hand, when the block length is large enough, e.g., $L \gg \xi$, an increase of L does *not* result in an increase of the total active region (this case is illustrated on the Figure 4.1). Consequently, the valence-bond fluctuation σ_L^2 *saturates* as the block length L is much larger than the fluctuation length scale ξ , i.e., $L \gg \xi$. The saturation is clearly a *direct* evidence of the feature that valence bonds are locked on long-length scales.

In the limit $N \rightarrow \infty$, the saturation value σ_∞^2 of σ_L^2 (as $L \rightarrow \infty$) and the value of L at which σ_L^2 saturates are naturally expected to depend solely on the disorder strength u . Therefore, by calculating σ_L^2 for large enough chain size N with various disorder strength u , one not only can verify the saturation of σ_L^2 which directly demonstrates the bond locking, but also can extract the fluctuation length scale ξ .

For these purposes, valence-bond fluctuation σ_L^2 for random chains with $d = 2$, $d = \frac{1}{2}(\sqrt{5}+1)$, and $d = \sqrt{2}$ are calculated using valence-bond Monte Carlo. Systems used for these calculations all have the size $N = 1024$ and the power number $n = 60N$. Various disorder strengths are used for each value of d , e.g., $u = 1.0, 0.75, 0.50, 0.25$, and 0.10 , describing various disorder strengths from strong to weak. For each disorder strength, numerical results are averaged over 50 independent random realizations of the disorders. For each disorder, a decimation procedure is performed and then the obtained valence-bond state is used as the initial valence-bond state $|S_0\rangle$ for the valence-bond Monte Carlo simulation. Obtained results for σ_L^2 are shown on Figures 4.5, 4.6, and 4.7 as functions of the block conformal length $L_C = N/\pi \sin(\pi L/N)$, each figure for a value of d as listed above. The σ_L^2 for the uniform chain ($u = 0.00$) is also shown for a comparison.

The Figures 4.5, 4.6, and 4.7 show that for random chains with any disorder strength, σ_L^2 is smaller than that of the corresponding uniform chain, indicating that any disorder suppresses the fluctuations of valence bonds. These figures also show that for any disorder strength, σ_L^2 grows with L as L is small and saturates at a finite value σ_∞^2 when L is large enough. The saturation of a weaker disorder happens at a larger value of L and a higher value σ_∞^2 of σ_L^2 . Tentatively, these figures imply that the fluctuation length scale ξ is smaller for a stronger disorder. More detailed discussions for the dependence of ξ on the disorder strength u can be found in section 4.3.

We now focus on weak disorders, i.e., those with $u = 0.1$ and $u = 0.25$. In random chains with $d = \sqrt{2}$, the valence-bond fluctuation σ_L^2 for both disorder strengths, as seen on Figure 4.7, has not saturated yet, even when $L \simeq N/2$, the largest value it may take. If we move on to random chains with a larger d , e.g., $d = \frac{1}{2}(\sqrt{5} + 1)$, of which results are shown on the Figure 4.6, σ_L^2 for $u = 0.1$ does not saturate while that for $u = 0.25$ almost saturates at $L \simeq N/2$. This implies that for weakly disordered chains with $d = \sqrt{2}$ and $d = \frac{1}{2}(\sqrt{5} + 1)$, a system size $N = 1024$ is not large enough for observing the saturation of σ_L^2 . On the other hand, Figure 4.5 for $d = 2$ shows that the saturation of σ_L^2 can be observed even with $u = 0.1$, the weakest disorder studied in this work. These pictures indicate qualitatively that at the same disorder strength, the fluctuation length scale ξ for random chains with $d < 2$ is larger than ξ for random chains with $d = 2$ (see section 4.3 for more quantitative discussions).

The saturations of σ_L^2 for random chains of various d and different disorder strengths, as shown on Figures 4.5, 4.6, and 4.7, strongly confirm in a quantitative way the qualitative

discussion on the saturation of σ_L^2 . Note that calculations of σ_L^2 are in principle exact, i.e., the approximation (1.19) is not necessary as in the real-space RG scheme [10]. Because the saturation of σ_L^2 is a direct consequence of a finite fluctuation length scale ξ , it can be claimed to be a direct signature of the fact that valence bonds in the ground state of a random chain are locked into a particular valence-bond configuration on long-length scales [43]. This can also be claimed as the first direct numerical signature of the random singlet phases in random chains of non-Abelian anyons, which have been pointed out by a recent real-space RG study by Bonesteel and Yang [30].

4.3 Fluctuation length scales in random singlet phases

4.3.1 Scaling of valence-bond fluctuation

For a random chain with a given disorder strength u , the valence-bond fluctuation σ_L^2 , as shown on the previous sections, can be easily calculated by valence-bond Monte Carlo. While the saturation of σ_L^2 as $L \rightarrow \infty$ can be viewed as a clear and direct signature that valence bonds of a random singlet state are locked on long-length scales (see subsection 4.2.4), the fluctuation length scale ξ can be extracted by analyzing σ_L^2 on the whole range of L , i.e., $0 < L < \infty$.

The fluctuation length scale ξ , by definition, is a crossover length scale which separates the resonating regime with $L \ll \xi$ and the locking regime with $L \gg \xi$. Of these two regimes, the latter is characterized by a constant behavior of σ_L^2 while the former is characterized by the growth of σ_L^2 with L , as discussed qualitatively in the subsection 4.2.4 using the concept of active region. Between these two regimes, there is a crossover regime where $L \sim \xi$. These three regimes can be identified in terms of the dimensionless L/ξ as follow

1. In the resonating regime, i.e., $L/\xi \ll 1$, σ_L^2 grows logarithmically with L/ξ with as:

$$\sigma_L^2 \sim c_2 \ln(L/\xi) \quad (4.8)$$

with c_2 is given by Eq. (4.7).

2. In the locking regime, i.e., $L/\xi \gg 1$, $\sigma_L^2 = \sigma_\infty^2$, which is a constant.
3. In the crossover regime, i.e., $L/\xi \sim 1$, the scaling of σ_L^2 moves from a logarithmically growing function of L to a constant, which is independent of L .

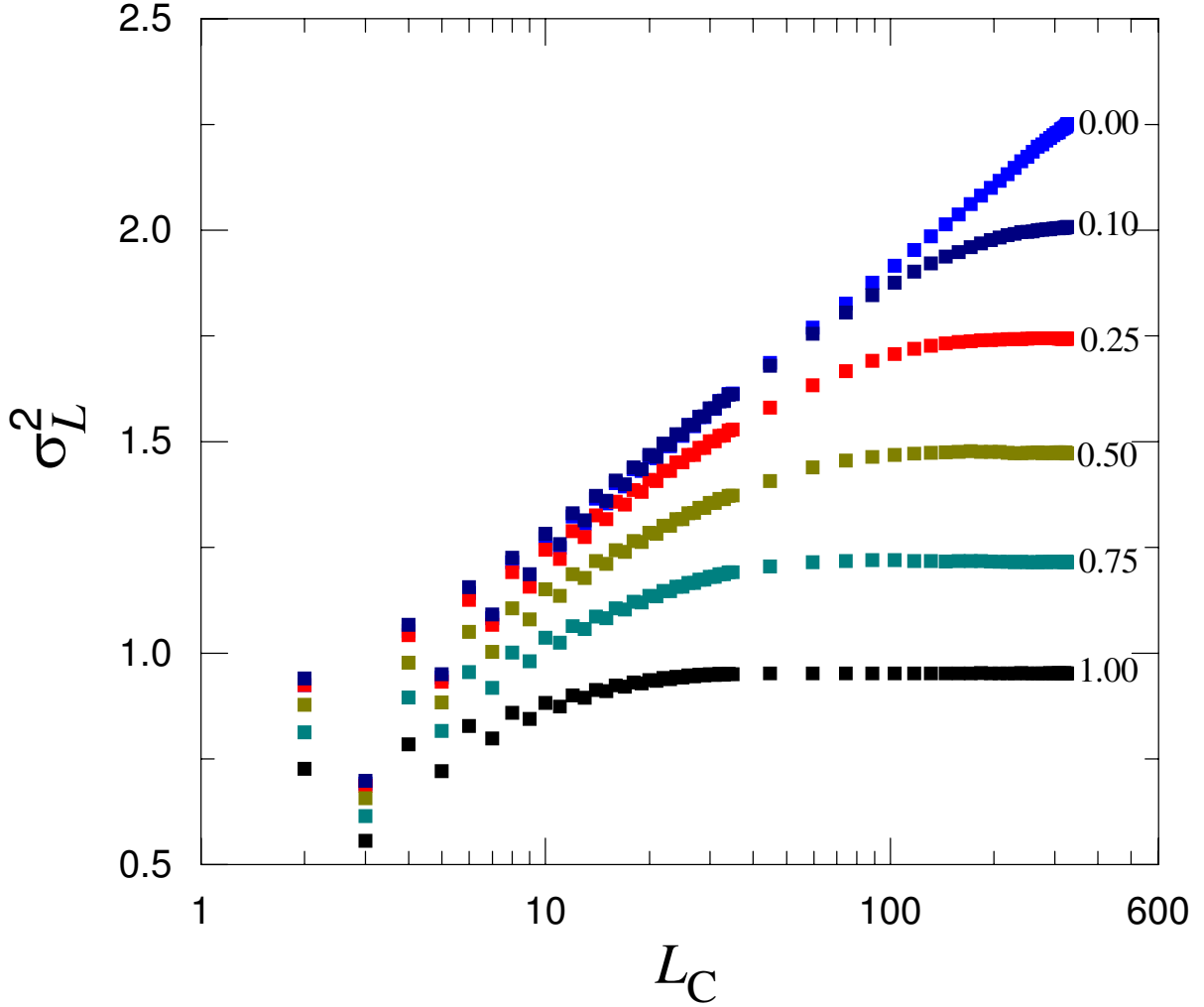


Figure 4.5: Valence-bond fluctuation σ_L^2 for random chains described by Eq. (1.36) with $d = 2$ as functions of block conformal length $L_C = N/\pi \sin(\pi L/N)$ for minimizing finite-size effects. Various values of u , the parameter which specifies the disorder strength are chosen as $u = 1.0, 0.75, 0.5, 0.25, 0.10$. σ_L^2 for the uniform chain ($u = 0.0$) is also shown for a comparison. Parameters for the calculation is $N = 1024$, $n = 60N$. Error bars are smaller than the symbol size.

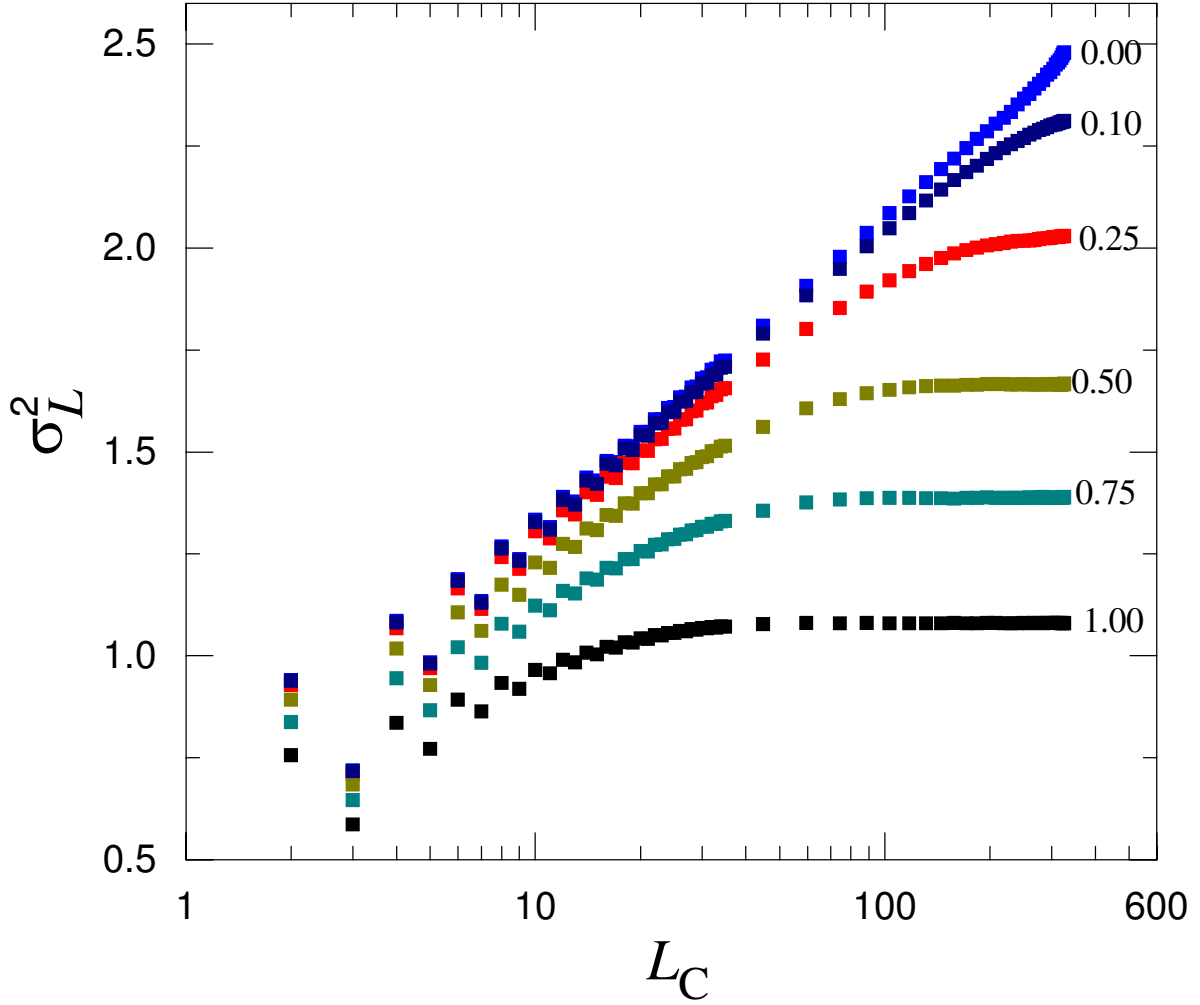


Figure 4.6: Valence-bond fluctuation σ_L^2 random chains described by Eq. (1.36) with $d = \frac{1}{2}(\sqrt{5} + 1)$ as functions of block conformal length $L_C = N/\pi \sin(\pi L/N)$ for minimizing finite-size effects. Various values of u , the parameter which specifies the disorder strength are chosen as $u = 1.0, 0.75, 0.5, 0.25, 0.10$. σ_L^2 for the uniform chain ($u = 0.0$) is also shown for a comparison. Parameters for the calculation is $N = 1024$, $n = 60N$. Error bars are smaller than the symbol size.

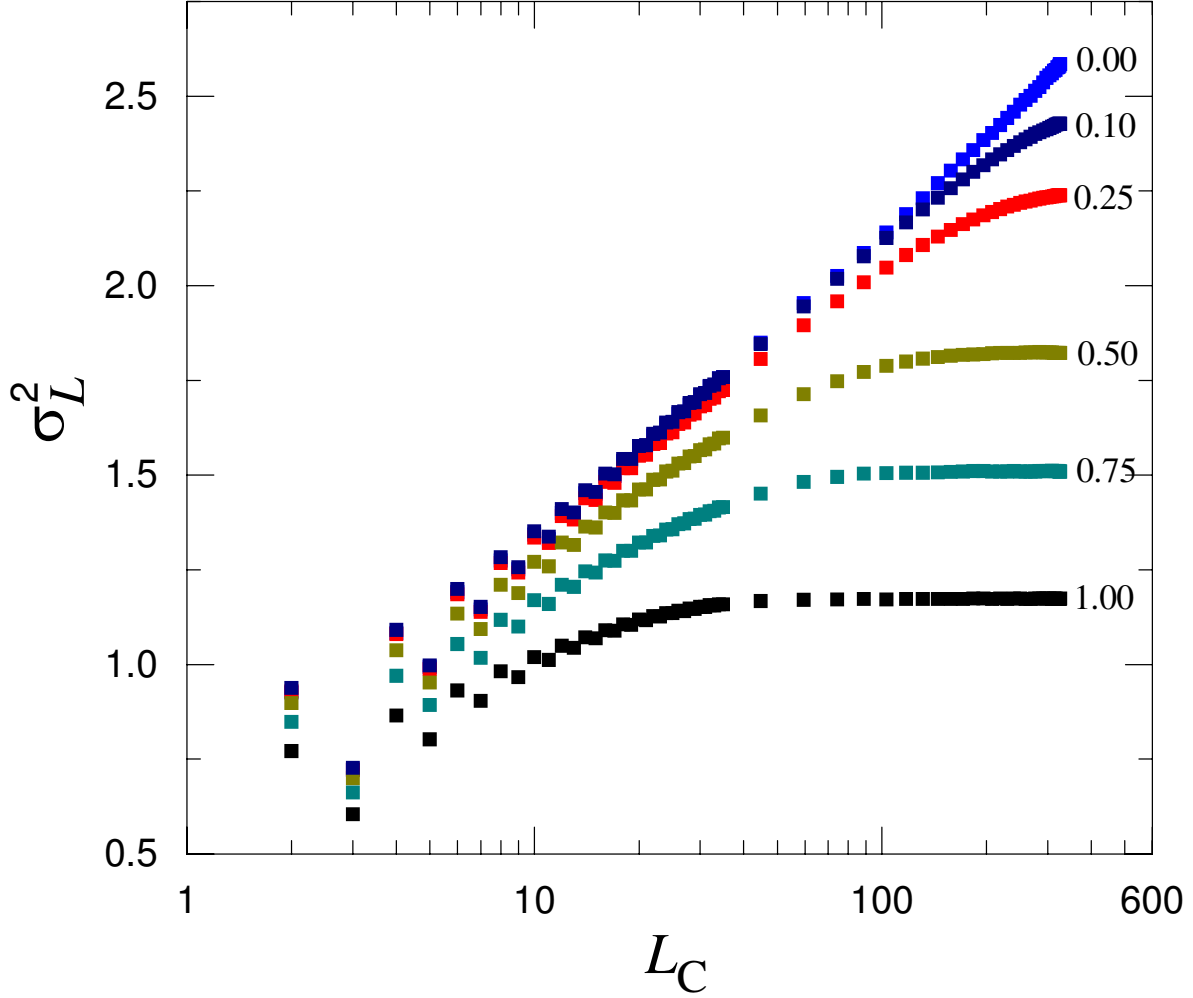


Figure 4.7: Valence-bond fluctuation σ_L^2 random chains described by Eq. (1.36) with $d = \sqrt{2}$ as functions of block conformal length $L_C = N/\pi \sin(\pi L/N)$ for minimizing finite-size effects. Various values of u , the parameter which specifies the disorder strength are chosen as $u = 1.0, 0.75, 0.5, 0.25, 0.10$. σ_L^2 for the uniform chain ($u = 0.0$) is also shown for a comparison. Parameters for the calculation is $N = 1024$, $n = 60N$. Error bars are smaller than the symbol size.

We now look closer to σ_L^2 , which saturates at σ_∞^2 as $L \rightarrow \infty$. The value of σ_∞^2 is finite and depends on the disorder strength $u > 0$. For a given value of u , it is expected that the scaling form of σ_L^2 is given by

$$\sigma_L^2 - \sigma_\infty^2 = \sigma(L/\xi), \quad (4.9)$$

which $\sigma(L/\xi)$ is a function of the dimensionless parameter L/ξ , which grows logarithmically in the same fashion as σ_L^2 of the uniform chain in the resonating regime ($L \ll 1$) and saturates at 0 in the locking regime ($L \gg 1$), as σ_L^2 of a random chain. Note that the effects of disorders are all included in ξ , so $\sigma(L/\xi)$ is independent of u .

Data for valence-bond fluctuation σ_L^2 of random chains with $d = 2$, $d = \frac{1}{2}(\sqrt{5} + 1)$, and $d = \sqrt{2}$ shown on figures 4.5, 4.6, and 4.7, and some more with $u = 0.375$ and $u = 0.625$ are scaled following Eq. (4.9). Because of the even-odd oscillation of σ_L^2 , only data with L odd is kept for doing the scaling. The scaling is done so that the crossover regime is centered at $L/\xi \simeq 1$. Once the proper values of ξ , which depends on u , are obtained, data for all values of u all collapse into a single function $\sigma(L/\xi)$. The scaling plots are shown on figures 4.8, 4.9, and 4.10 for $d = 2$, $d = \frac{1}{2}(\sqrt{5} + 1)$, and $d = \sqrt{2}$, respectively. On these figures, values of ξ for each disorder strength u are also shown.

Figure 4.8 for random chains with $d = 2$ shows a nice scaling plot where σ_L^2 move from the resonating regime with $L/\xi \ll 1$ to the locking regime with $L/\xi \gg 1$. With this value of d , σ_L^2 for all the values of u properly saturates as $L \simeq N/2$ (see figure 4.5) thus they are can all be scaled into an universal function $\sigma(L/\xi)$. For $d = \frac{1}{2}(\sqrt{5} + 1)$, σ_L^2 does *not* saturates for $u = 0.1$ (see figure 4.6) while for $d = \sqrt{2}$, σ_L^2 does *not* saturates for both $u = 0.1$ and $u = 0.25$ (see figure 4.6). Consequently, on the figures 4.9 and 4.10 for the corresponding scaling plots, there are some data points (pointed by arrows) that can not be completely scaled. This implies that one has to simulate random chains with sizes $N > 1024$ to get better scaling plots.

4.3.2 Fluctuation length scales

The fluctuation length scale ξ , which can be obtained by the scaling σ_L^2 , is a crossover between the pure and disordered critical behaviors. For a random chain with finite u , ξ is finite while it diverges when $u \rightarrow 0$. Therefore, it is desirable to study the divergence of ξ in limit of weak disorder and compare it with possible known relevant crossover length

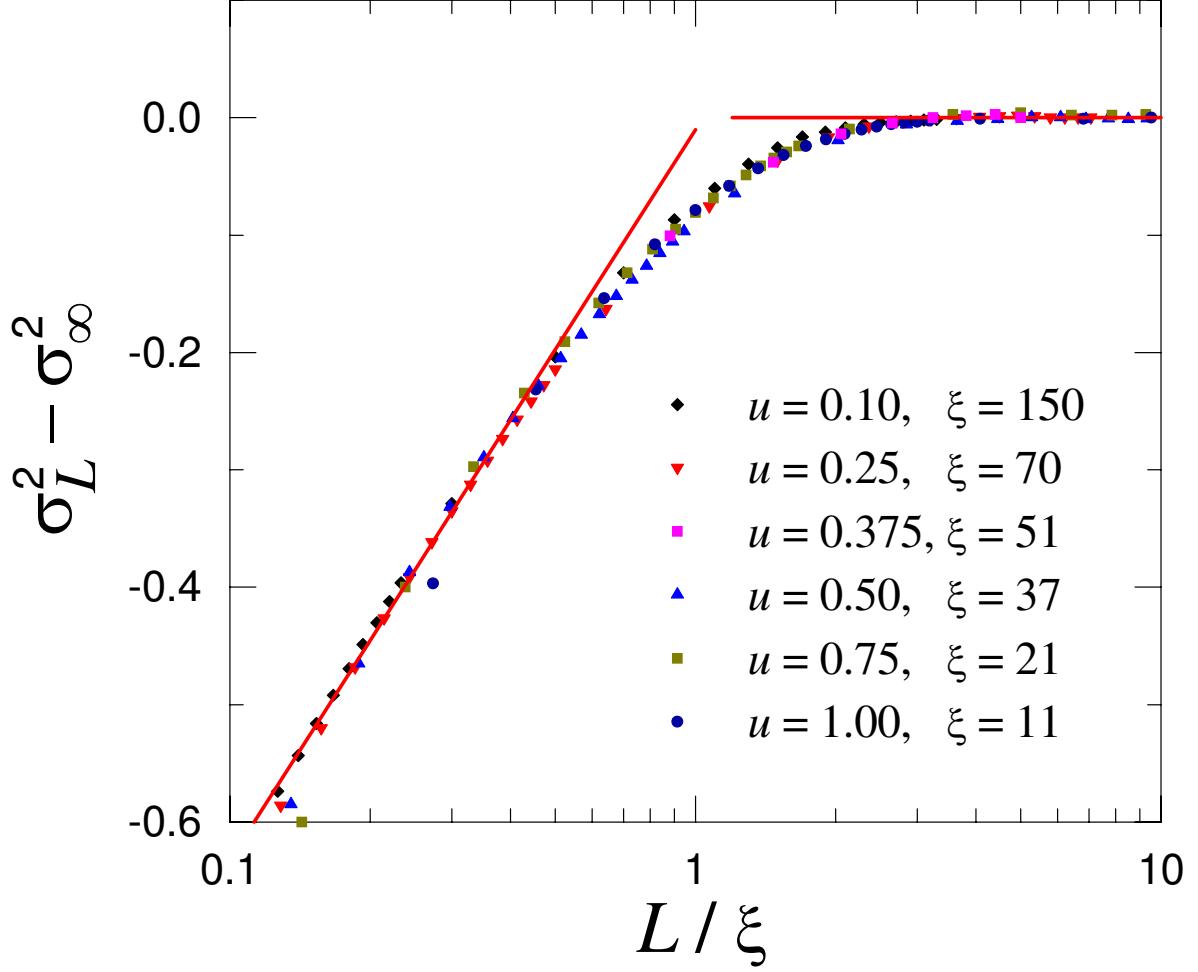
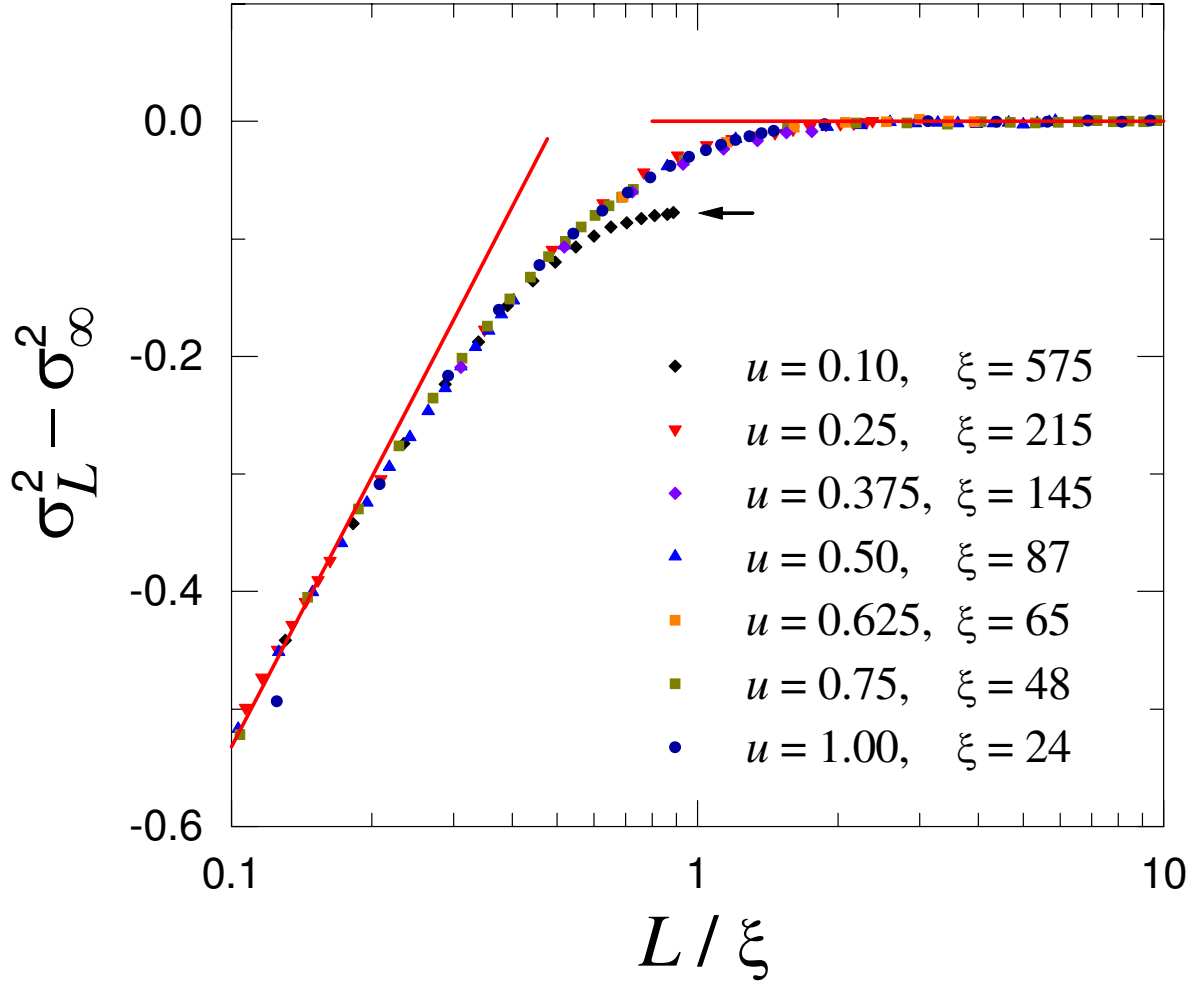


Figure 4.8: Scaling plot according to Eq. (4.9) for the data of σ_L^2 shown on figure 4.5 (random chains with $d = 2$). On the scaling plot, only data with L odd are kept. Corresponding to disorder strength $u = 0.1, 0.25, 0.50, 0.75$, and 1.0 , the fluctuation length scale is found to be $\xi = 140, 70, 37, 21$, and 11 . Two lines illustrate the scaling (4.6) in the resonating regime and the saturation scaling in the locking regime. Explanation for symbols are shown on the figure.



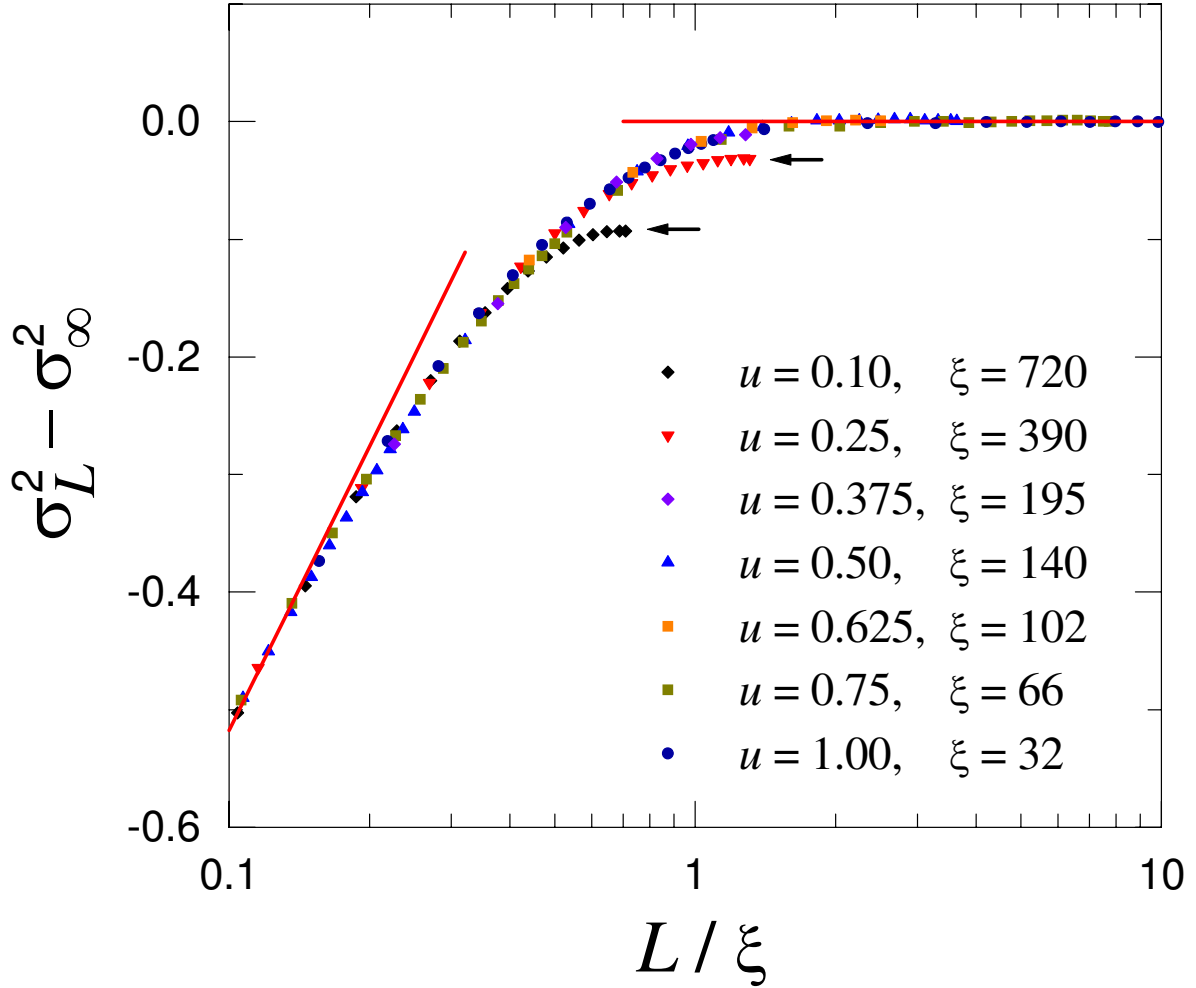


Figure 4.10: Scaling plot according to Eq. (4.9) for the data of σ_L^2 shown on figure 4.7 (random chains with $d = \sqrt{2}$). On the scaling plot, only data with L odd are kept. Corresponding to disorder strength $u = 0.1, 0.25, 0.375, 0.50, 0.625, 0.75$, and 1.0 , the fluctuation length scale is found to be $\xi = 720, 390, 195, 140, 102, 66$, and 32 . Lines illustrate the scaling (4.6) in the resonating regime and the saturation scaling in the locking regime. Explanation for symbols are shown on the figure. The arrows point to the data points which can not be completely scaled because σ_L^2 does not saturates for $u = 0.1$ and $u = 0.25$ (see figure 4.7 for plots of σ_L^2).

scales. The particular crossover length scales to be compared with ξ in this dissertation is the localization length scale ξ^* and the crossover length scale ξ_0 extracted from spin-spin correlation of a spin-1/2 XXX chain [74, 75].

For a random spin-1/2 chain with disorder strength u , the renormalization flow to the infinite-randomness fixed point is controlled by the so-called localization length ξ^* , which can be studied using bosonization technique [9, 76]. In the limit $u \rightarrow 0$, the localization length scale ξ^* diverges as $\xi^* \propto u^{-\gamma}$ with $\gamma = 1$ for a random spin-1/2 XXX chain and $\gamma = 2$ for a random spin-1/2 XX chain. Exact diagonalization calculations for ξ^* using spin stiffness of random chains are in excellent agreement with these bosonization results [74].

The crossover length scale ξ_0 , as reported in the Ref. [74], was determined as the crossover between the behaviors of the spin-spin correlation in pure and disorder regimes. In particular, the authors of Ref. [74] has calculated the correlation function defined as

$$C^\beta \left(\frac{N}{2} \right) = \frac{2}{N} \sum_{i=1}^{N/2} \left\langle S_i^\beta S_{i+(N/2)}^\beta \right\rangle \quad (4.10)$$

where $\langle \dots \rangle$ implies a ground state expectation value. For a spin-1/2 XX chain with $N/2$ even, the correlation function $C^\beta(N/2)$ scales as $N^{-1/2}$ in the pure regime and N^{-2} in the disordered regime [10]. For a spin-1/2 XXX chain, on the other hand, $C^\beta(N/2)$ scales as $\sqrt{\ln(N/2)}N^{-1}$ in the pure regime [77] and N^{-2} in the disordered regime [10]. The correlation function $C^\beta(N/2)$ was then calculated for random XX chains using exact diagonalization and for random XXX chains using a quantum Monte Carlo (stochastic series expansion) method [78]. By studying the scaling form of $C^\beta(N/2)$, the crossover length scale ξ_0 of these models has been extracted from the numerically calculated results [74], showing a good agreement with the scaling of ξ^* determined by bosonization technique.

We now compare the fluctuation length scale ξ , which has been extracted from the scaling of σ_L^2 , as described in the subsection 4.3.1, with ξ_0 and ξ^* . On figure 4.11, the fluctuation length scale ξ for $d = 2$ is shown as functions of u in comparing with the crossover length scale ξ_0 for a spin-1/2 XXX chain. Similarly, on figure 4.12, the fluctuation length scale ξ for $d = \sqrt{2}$ is compared with the crossover length scale ξ_0 for a spin-1/2 XXX chain. It is interesting to note that the fluctuation length scale ξ is in a good agreement with the crossover length scale ξ_0 , especially for the case $d = 2$ (XXX chains).

Figures 4.13 and 4.14 show two attempts of describing the fluctuation length scale ξ for $d = 2$, $d = \frac{1}{2}(\sqrt{5} + 1)$, and $d = \sqrt{2}$ in power laws of disorder strength in a similar way of

those for ξ^* by bosonization. On figure 4.13, ξ is depicted as functions of disorder strength u , while it is shown on figure 4.14 as functions of δ , defined as the variance of the random variable $\ln J_i$, and given in terms of u as

$$\delta = \sqrt{1 - \frac{1 - u^2}{4u^2} \left[\ln \frac{1 + u}{1 - u} \right]^2}. \quad (4.11)$$

In the same way as in the Ref. [74], one can observe on these figures the singular behaviors of ξ for u and $\delta \rightarrow 0$. In particular, the fluctuation length scales ξ for random chains with sufficiently weak disorders are well-fitted to power laws $\xi \propto u^{-\gamma}$ (figure 4.13) and $\xi \propto \delta^{-\gamma}$ (figure 4.14). For $d = 2$, I found $\gamma = 1.0$, which is very close to the exponent 1.16 found in Ref. [74], and is in excellent agreement with the bosonization result $\gamma = 1.0$. On the other hand, for $d = \sqrt{2}$, I found $\gamma = 1.65$, which is smaller than the result by bosonization ($\gamma = 2.0$), and that found for the crossover length scale ξ_0 in Ref. [74] ($\gamma = 1.8$). For random chains of Fibonacci anyons with $d = \frac{1}{2}(\sqrt{5} + 1)$, I also found that the fluctuation length scale ξ diverges as $u^{-\gamma}$ and $\delta^{-\gamma}$ with the exponent $\gamma = 1.4$, which is in between the exponent γ for $d = 2$ and $d = \sqrt{2}$. There is no known result for γ in this model so the result $\gamma = 1.4$ can be regarded as a *new* result of this Dissertation. Because the system size $N = 1024$ is not large enough for the model (1.36) with $k = 3$, a more accurate value of γ can be obtained easily by a scaling analysis with larger system size, e.g., $N > 1024$.

We can now mention something on d -dependence of ξ . Figure 4.13 shows the fluctuation length scales for random chains with various quantum dimension d , i.e., $d = 2$, $d = \frac{1}{2}(\sqrt{5} + 1)$, and $d = \sqrt{2}$. The figure clearly indicates that the fluctuation length scale for a random chain of smaller d is larger, confirming in a quantitative way the qualitative discussion about this issue in the section 4.2.4.

4.4 Concluding remarks

In this Chapter I have presented the *most important new result* of this Dissertation. In particular, I have introduced a new concept, the so-called valence-bond fluctuation σ_L^2 which can be calculated easily using valence-bond Monte Carlo and can be used to quantitatively study random singlet phases in a new way. By calculating and analyzing the valence-bond fluctuation, one can directly observe one of the essential features of random singlet phase: valence bonds are locked into a particular bond configuration on long-length scales while at the same time, they resonate strongly on short-length scales.

The *next new result* of this chapter is based on an advantage of valence-bond fluctuation σ_L^2 is that from this quantity, one can extract the so-called fluctuation length scale ξ , which is a characteristic of a random singlet ground state. In particular, this length scale is the crossover from the resonating regime to the locking regime, the former is relevant to the uniform chain while the latter is relevant to random chains and random singlet phases. From this nature of ξ , it is natural to conclude that ξ is *clearly related* to other crossover length scales, for example, the localization length ξ^* and the crossover length scale ξ_0 [74]. While the fluctuation length scale ξ for $k = 2$ agrees very well with the known crossover length scales, the agreement for $d = \sqrt{2}$ is not very good, which is caused by the fact that $N = 1024$ is not large enough. The fluctuation length scale $\xi \sim u^{-1.4}$ for $d = \frac{1}{2}(\sqrt{5} + 1)$ is *another new result* of this chapter in the sense that this is the first time such crossover length scale is determined for this model.

Finally, the approach to random singlet phase and the fluctuation length scale ξ based on valence-bond fluctuation developed here can be used not only for spin-1/2 (XXX or XX) chains or chains of Fibonacci anyons ($d = \frac{1}{2}(\sqrt{5} + 1)$), but also for the model (1.36) with arbitrary d with no additional modifications on the numerical method. The possible connection of other models, for example higher spin chains, with the model (1.36) with a given value of d , therefore, allows this approach to be used for these models.

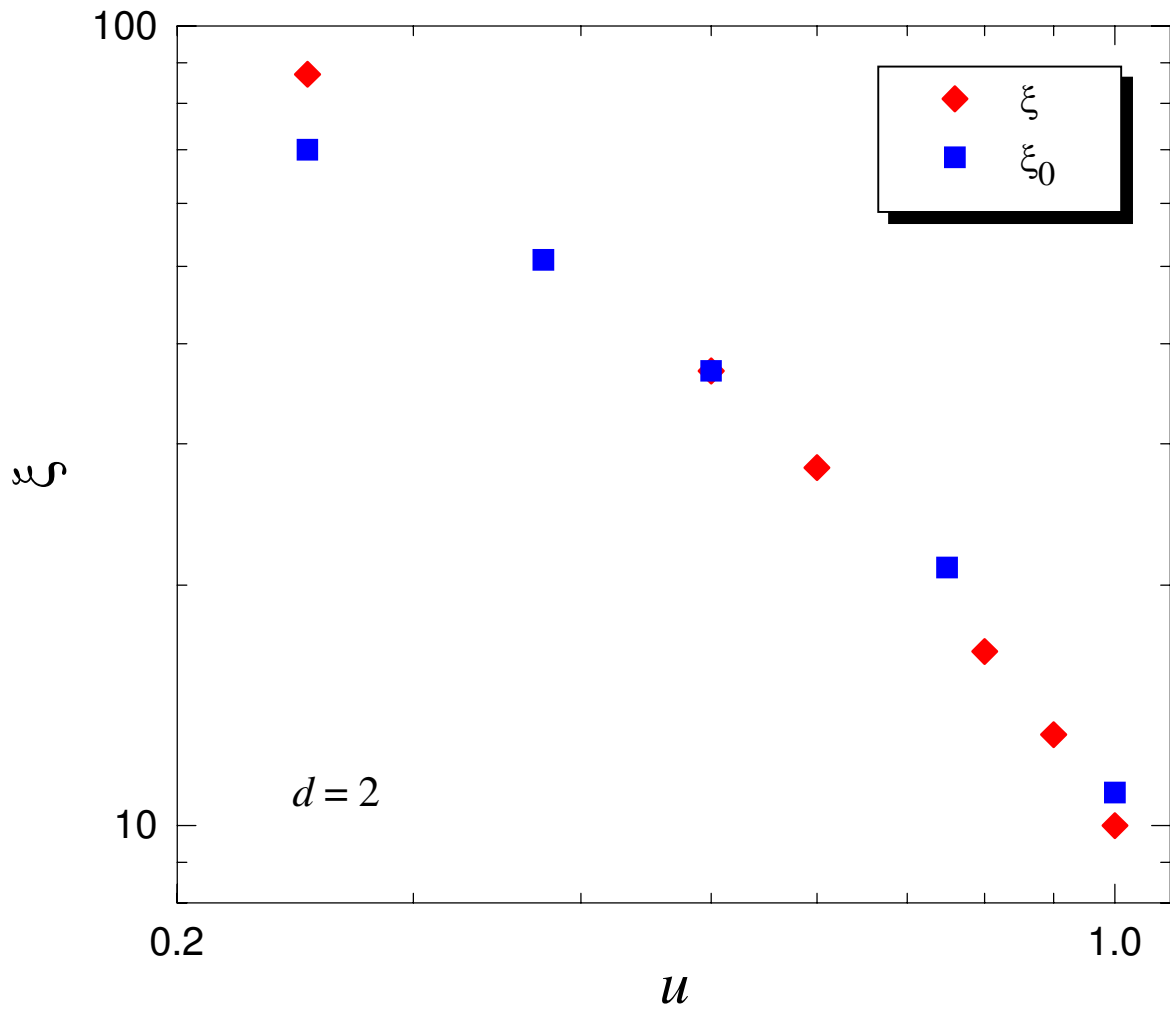


Figure 4.11: Fluctuation length scale ξ for $d = 2$ and crossover length scale ξ_0 for random spin-1/2 XXX chains as functions of u .

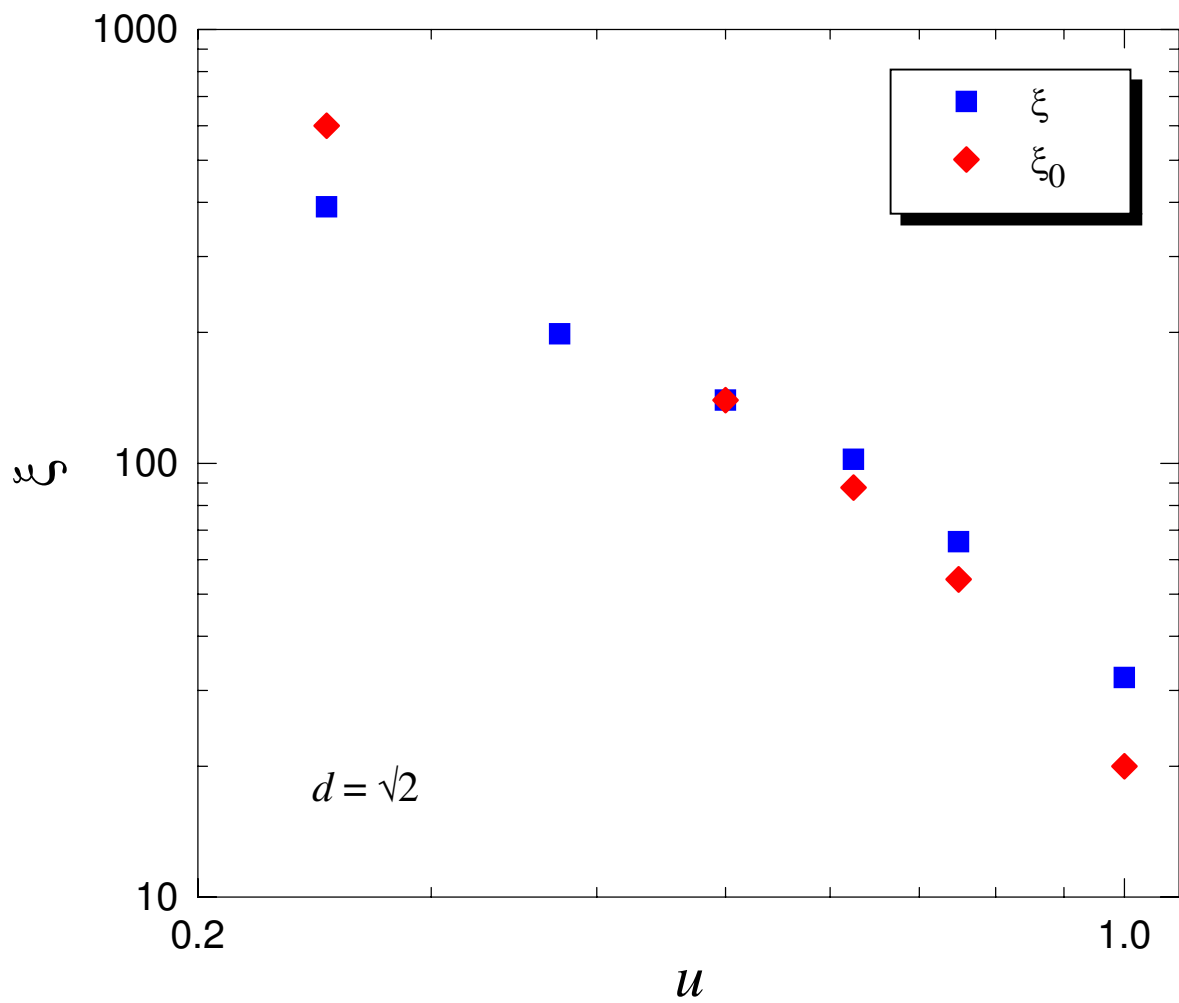


Figure 4.12: Fluctuation length scale ξ for $d = \sqrt{2}$ and crossover length scale ξ_0 for random spin-1/2 XX chains as functions of u

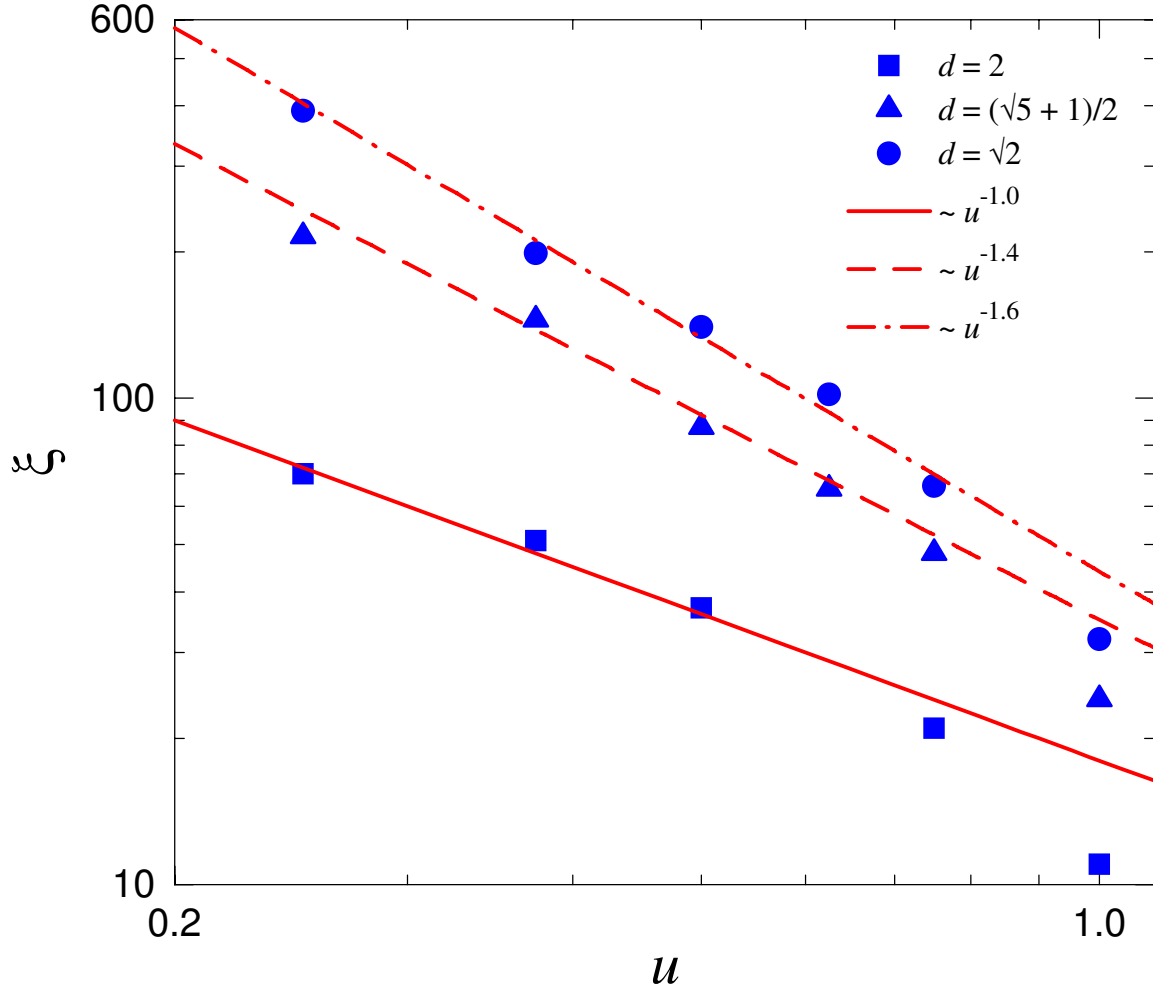


Figure 4.13: Log-log plot of fluctuation length scale ξ as a function of disorder strength u of random chains described by Eq. (1.36) with $d = 2$, $d = \frac{1}{2}(\sqrt{5} + 1)$ and $d = \sqrt{2}$. Three straight lines depict the attempted power laws $u^{-\gamma}$ with $\gamma = 1.0$ for $d = 2$, $\gamma = 1.4$ for $d = \frac{1}{2}(\sqrt{5} + 1)$, and $\gamma = 1.65$ for $d = \sqrt{2}$.

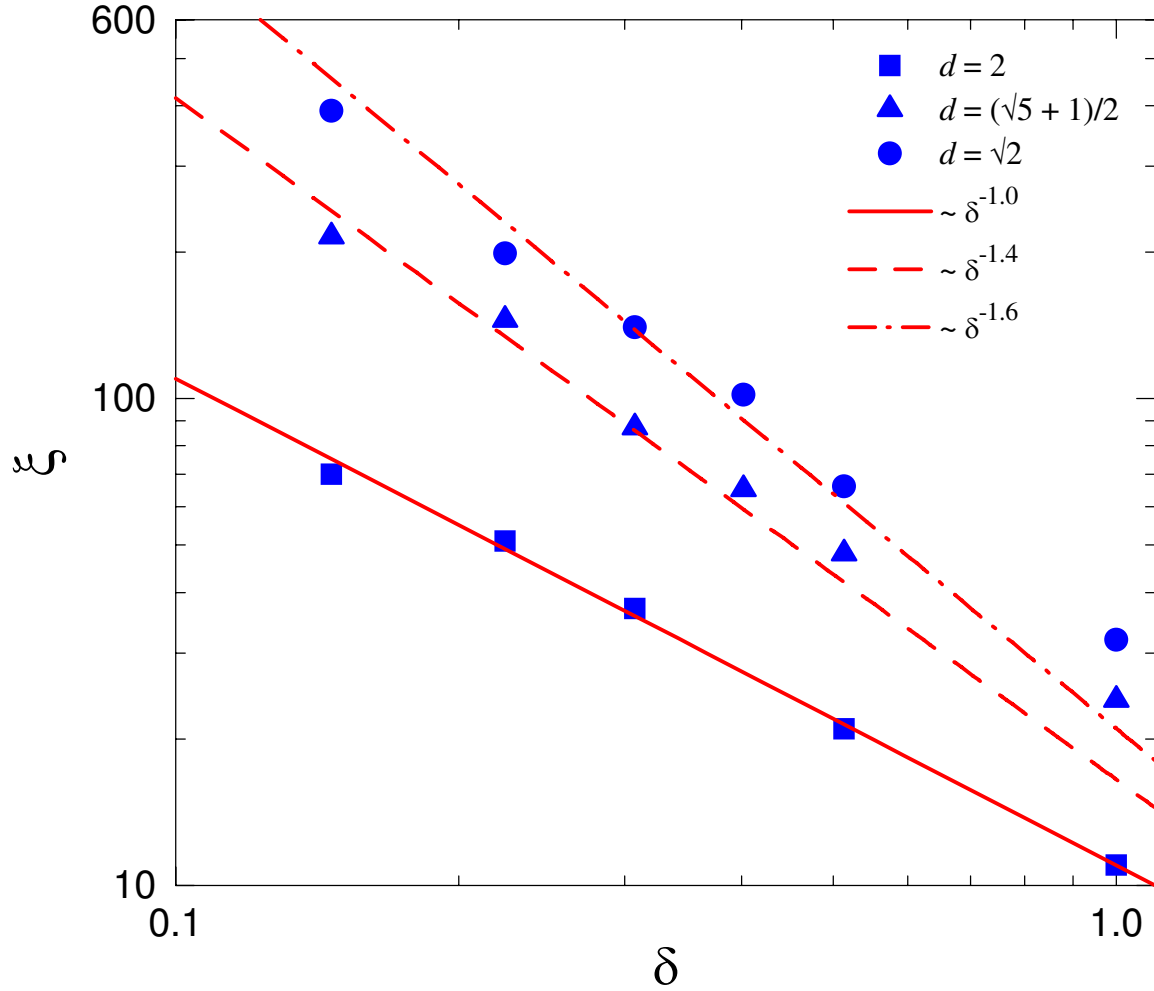


Figure 4.14: Log-log plot of fluctuation length scale ξ as a function of disorder strength δ of random chains described by Eq. (1.36) with $d = 2$, $d = \frac{1}{2}(\sqrt{5} + 1)$ and $d = \sqrt{2}$. Three straight lines depict the attempted power laws $\delta^{-\gamma}$ with $\gamma = 1.0$ for $d = 2$, $\gamma = 1.4$ for $d = \frac{1}{2}(\sqrt{5} + 1)$, and $\gamma = 1.65$ for $d = \sqrt{2}$.

APPENDIX A

PROOFS OF SOME RESULTS

A.1 Spin singlet projection operator

Two spin $-\frac{1}{2}$ particles at sites i and $i + 1$ of the model (1.36) can either be in the singlet state, denoted by $|s_{i,i+1}\rangle$ or one of three triplet states, denoted by $|t_{i,i+1}^{(\mu)}\rangle$ with $\mu = 1, 2$ or 3 . The eigenenergy corresponding to the singlet state is $-\frac{3}{4}$ while that corresponding to any of three triplet states is $\frac{1}{4}$. Therefore, one way to define the singlet projection operator Π_i^0 , acting on spins at site i and $i + 1$, is to start from the eigenenergies of the singlet and triplet states. In this way, Π_i^0 is defined as:

$$\Pi_i^0 = \frac{1}{4} - \vec{S}_i \cdot \vec{S}_{i+1}. \quad (\text{A.1})$$

It can be shown that applying Π_i^0 on $|s_{i,i+1}\rangle$ returns $|s_{i,i+1}\rangle$ while applying Π_i^0 on $|t_{i,i+1}^{(\mu)}\rangle$ returns zero:

$$\begin{aligned} \Pi_i^0 |s_{i,i+1}\rangle &= |s_{i,i+1}\rangle, \\ \Pi_i^0 |t_{i,i+1}^{(\mu)}\rangle &= 0. \end{aligned} \quad (\text{A.2})$$

The above properties of the singlet projection operator Π_i^0 can be easily proved by writing $\vec{S} = \vec{S}_i + \vec{S}_{i+1}$ and then:

$$\vec{S}_i \cdot \vec{S}_{i+1} = \frac{1}{2} \left(\vec{S}^2 - \vec{S}_i^2 - \vec{S}_{i+1}^2 \right), \quad (\text{A.3})$$

therefore

$$\Pi_i^0 = \frac{1}{4} - \frac{1}{2} \left(\vec{S}^2 - \vec{S}_i^2 - \vec{S}_{i+1}^2 \right). \quad (\text{A.4})$$

Now, applying Π_i^0 on the singlet state $|s_{i,i+1}\rangle = \frac{1}{\sqrt{2}} (|\uparrow_i \downarrow_{i+1}\rangle - |\downarrow_i \uparrow_{i+1}\rangle)$ yields:

$$\Pi_i^0 |s_{i,i+1}\rangle = \left[\frac{1}{4} - \frac{1}{2} \left(0 \times 1 - \frac{1}{2} \times \frac{3}{2} - \frac{1}{2} \times \frac{3}{2} \right) \right] |s_{i,i+1}\rangle = |s_{i,i+1}\rangle \quad (\text{A.5})$$

while the same action destroys any of the possible triplet $|t_{i,i+1}^{(\mu)}\rangle$:

$$\Pi_i^0 |t_{i,i+1}^{(\mu)}\rangle = \left[\frac{1}{4} - \frac{1}{2} \left(1 \times 2 - \frac{1}{2} \times \frac{3}{2} - \frac{1}{2} \times \frac{3}{2} \right) \right] |t_{i,i+1}^{(\mu)}\rangle = 0. \quad (\text{A.6})$$

Note that here we use the fact that S_i commutes with S_{i+1} so we can take the eigenstates of \vec{S}^2 , \vec{S}_i^2 , and \vec{S}_{i+1}^2 simultaneously.

In another way, the singlet projection operator defined in Eq. (A.1) can also be defined as:

$$\Pi_i^0 = |s_{i,i+1}\rangle \langle s_{i,i+1}|. \quad (\text{A.7})$$

Because the basis $\{|s_{i,i+1}\rangle, |t_{i,i+1}^{(1)}\rangle, |t_{i,i+1}^{(2)}\rangle, |t_{i,i+1}^{(3)}\rangle\}$ is orthonormal, this definition of Π_i^0 straightforwardly satisfies (A.2).

Two definitions (A.1) and (A.7) can be shown to be equivalent by computing and then comparing the matrix elements of two operators $|s_{i,i+1}\rangle \langle s_{i,i+1}|$ and $\frac{1}{4} - \vec{S}_i \cdot \vec{S}_{i+1}$ on the orthonormal basis $\{|s_{i,i+1}\rangle, |t_{i,i+1}^{(1)}\rangle, |t_{i,i+1}^{(2)}\rangle, |t_{i,i+1}^{(3)}\rangle\}$. In doing this, the expressions in (A.2) are used as well as the fact that the basis $\{|s_{i,i+1}\rangle, |t_{i,i+1}^{(1)}\rangle, |t_{i,i+1}^{(2)}\rangle, |t_{i,i+1}^{(3)}\rangle\}$ is orthonormal. In particular, one finds that for both operators, there is only one non-vanishing element, which is:

$$\langle s_{i,i+1} | s_{i,i+1} \rangle \langle s_{i,i+1} | s_{i,i+1} \rangle = 1, \quad (\text{A.8})$$

and, because of (A.5)

$$\langle s_{i,i+1} | \left(\frac{1}{4} - \vec{S}_i \cdot \vec{S}_{i+1} \right) | s_{i,i+1} \rangle = \langle s_{i,i+1} | s_{i,i+1} \rangle = 1 \quad (\text{A.9})$$

thus proving the equivalence between two definitions (A.1) and (A.7).

A.2 von Neumann entropy

Basic relations

Definition 1 *Given a quantum state which is described by a density matrix ρ , the von Neumann entropy of this state is defined by:*

$$S(\rho) = -\text{Tr}(\rho \log_2 \rho). \quad (\text{A.10})$$

Remark 1 *In general, the density matrix ρ of a particular mixed state can be written as a spectral decomposition*

$$\rho = \sum_i \lambda_i |\varphi_i\rangle \langle \varphi_i| \quad (\text{A.11})$$

with $\sum_i \lambda_i = 1$. The von Neumann entropy $S(\rho)$ defined in (A.10) is then determined by:

$$S(\rho) = - \sum \lambda_i \log_2 \lambda_i. \quad (\text{A.12})$$

Remark 2 *The von Neumann entropy has some interesting and useful properties listed below, which are easy to be proved [65]*

1. *The entropy of a state described by ρ is non-negative. The entropy is zero if and only if ρ describes a pure state.*
2. *Entropy of a tensor product is the sum of the entropies of its components:*

$$S(\rho_1 \otimes \rho_2) = S(\rho_1) + S(\rho_2). \quad (\text{A.13})$$

Proof of the formula (3.11)

This section is intended to give a derivation of the Eq. (3.11) for the von Neumann entanglement entropy of a block A of L sites in a given valence-bond state $|\alpha\rangle$ as shown on the Fig. 3.4. The complement of A is regarded as the subsystem B for the purpose of determining von Neumann entanglement entropy.

Assume that the whole system is described by a state $|\alpha\rangle$, which is, again, the direct product of all the singlet state $|S_i\rangle$. Moreover, the singlet states can be classified into three categories: $|S_i\rangle \in A$ for the singlets having two sites belonging to A , $|S_i\rangle \in B$ for those which have two sites belonging to B , and $|S_i^{(\text{cross})}\rangle$ for the singlets with one site belonging to A and the other belonging to B . The density matrix of the whole system, therefore, can be written as

$$|\alpha\rangle\langle\alpha| = \left(\bigotimes_{|S_i\rangle \in A} |S_i\rangle\langle S_i| \right) \otimes \left(\bigotimes_{|S_i\rangle \in B} |S_i\rangle\langle S_i| \right) \otimes \left(\bigotimes_i |S_i^{(\text{cross})}\rangle\langle S_i^{(\text{cross})}| \right). \quad (\text{A.14})$$

When determining ρ_A , all the degrees of freedom of B are traced out. The second term in (A.14) can be easily shown to return unit:

$$\text{Tr}_B \left(\bigotimes_{|S_i\rangle \in B} |S_i\rangle\langle S_i| \right) = 1 \quad (\text{A.15})$$

thus

$$\rho_A = \text{Tr}_A \left(\bigotimes_i |S_i^{(\text{cross})}\rangle\langle S_i^{(\text{cross})}| \right) \otimes \left(\bigotimes_{|S_i\rangle \in A} |S_i\rangle\langle S_i| \right). \quad (\text{A.16})$$

Now the von Neumann entropy S_A of the reduced density matrix ρ_A can be computed. Because of the first properties mentioned in Remark (2), the contribution of the second factor on the right hand side of Eq. (A.16) is zero, while the second properties in Remark (2) leads to:

$$S_A = \sum_i S_{A_i}^{(\text{cross})}. \quad (\text{A.17})$$

In this formula, $S_{A_i}^{(\text{cross})}$ is defined as the von Neumann entropy of the reduced density matrix

$$\rho_{A_i}^{(\text{cross})} = \text{Tr}_{A_i} \left(|S_i^{(\text{cross})}\rangle \langle S_i^{(\text{cross})}| \right) \quad (\text{A.18})$$

which corresponds to the singlet state $|S_i^{(\text{cross})}\rangle$. Since $S_{A_i}^{(\text{cross})} = S_{\text{bond}}$ are the same for any singlet state $|S_i^{(\text{cross})}\rangle$, the formula (A.17) becomes

$$S_A = n_L S_{\text{bond}}, \quad (\text{A.19})$$

which proves the formula (3.11).

REFERENCES

- [1] A. Auerbach. *Interacting electrons and quantum magnetism*. Springer-Verlag, New York, 1st edition, 1994. [1.1.1](#), [1.1.2](#), [1.2.1](#)
- [2] Lars Onsager. Crystal statistics. i. a two-dimensional model with an order-disorder transition. *Phys. Rev.*, 65(3-4):117, February 1944. [1.1.1](#)
- [3] H. A. Bethe. Eigenwerte und eigenfunktionen der linearen atomkette. *Z. Phys.*, 71(3-4):205, March 1931. [1.1.1](#), [1.1.1](#), [1.3.1](#), [2.3.2](#)
- [4] L. Hulthén. Über das austauschproblem eines kristalles. *Ark. Mat. Astron. Fys. A*, 26:1, 1938. [1.1.1](#), [1.1.1](#), [1.3.1](#), [2.3.1](#), [2.3.2](#)
- [5] E. Fradkin. *Field theories of condensed matter systems*. Addison-Wesley Publishing Company, Redwood City, CA, USA, 1991. [1.1.1](#), [1.1.1](#), [2.3.1](#)
- [6] E. Manousakis. The spin-1/2 heisenberg antiferromagnet on a square lattice and its application to the cuprous oxides. *Rev. Mod. Phys.*, 63(1):1–62, January 1991. [1.1.1](#)
- [7] S. Takagi, H. Deguchi, K. Takeda, M. Mito, and M. Takahashi. Magnetic susceptibility of a spin 1/2 heisenberg antiferromagnetic chain: [3,3'-dimethyl-2,2'-thiazolinocyanine]-tcnq. *J. Phys. Soc. Jpn.*, 65(7):1934–1937, July 1996. [1.1.1](#)
- [8] M. D. Johannes, J. Richter, S.-L. Drechsler, and H. Rosner. $\text{sr}_2\text{cu}(\text{po}_4)_2$: A real material realization of the one-dimensional nearest neighbor heisenberg chain. *Phys. Rev. B*, 74(17):174435, November 2006. [1.1.1](#)
- [9] C. A. Doty and D. S. Fisher. Effects of quenched disorder on spin-1/2 quantum xxz chains. *Phys. Rev. B*, 45(5):2167–2179, February 1992. [1.1.1](#), [1.3.1](#), [4.3.2](#)
- [10] D. S. Fisher. Random antiferromagnetic quantum spin chains. *Phys. Rev. B*, 50(3):3799 – 3821, March 1994. [1.1.1](#), [1.1.1](#), [1.3.1](#), [1.3.2](#), [1.3.2](#), [1.3.2](#), [1.3.2](#), [1.3.2](#), [2.2.4](#), [2.4](#), [4.1](#), [4.2.4](#), [4.3.2](#)
- [11] O. Bratteli. Inductive limits of finite dimensional c^* -algebras. *Trans. Am. Math. Soc.*, 171:195, 1972. [1.1.2](#)
- [12] T. Mansour and S. Severini. Counting paths in bratteli diagrams for $su(2)_k$. *Europhysics Letters*, 86:33001, May 2009. [1.1.2](#), [1.4.2](#)

- [13] P. W. Anderson. The resonating valence bond state in La_2CuO_4 and superconductivity. *Science*, 235(4973):1196–1198, March 1987. [1.2.1](#)
- [14] A. W. Sandvik. Ground state projection of quantum spin systems in the valence-bond basis. *Phys. Rev. Lett.*, 95(20):207203, November 2005. [1.2.1](#), [1.5](#), [2.1](#), [2.2.2](#), [2.3.1](#), [2.3.2](#)
- [15] S. Liang, B. Douçot, and P. W. Anderson. Some new variational resonating-valence-bond-type wave functions for the spin- $\frac{1}{2}$ antiferromagnetic heisenberg model on a square lattice. *Phys. Rev. Lett.*, 61(3):365–368, July 1988. [1.2.1](#), [2.2.4](#)
- [16] L. Pauling. *The nature of the chemical bond*. Cornell University Press, New York, 3rd edition, 1960. [1.2.1](#)
- [17] K. S. D. Beach and A. W. Sandvik. Some formal results for the valence bond basis. *Nucl. Phys. B*, 750(3):142–178, August 2006. [1.2.4](#)
- [18] C. Nayak, S. H. Simon, A. Stern, M. Freedman, and S. Das Sarma. Non-abelian anyons and topological quantum computation. *Rev. Mod. Phys.*, 80(6):1083 – 1159, Semtember 2008. [1.2.5](#), [1.2.5](#), [1.4.1](#), [1.4.2](#), [1.4.2](#)
- [19] J. E. Hirsch and J. V. José. Low-temperature thermodynamic properties of a random heisenberg antiferromagnetic chain ($s = 1/2$). *J. Phys. C: Solid State Phys.*, 13(3):L53, January 1980. [1.3.1](#)
- [20] J. E. Hirsch. Low-temperature thermodynamic properties of a random anisotropic antiferromagnetic chain. *Phys. Rev. B*, 22(11):5355–5365, December 1980. [1.3.1](#)
- [21] S. K. Ma, C. Dasgupta, and C. K. Hu. Random antiferromagnetic chain. *Phys. Rev. Lett.*, 43(19):1434 – 1437, August 1979. [1.3.1](#), [1.3.2](#), [1.3.2](#), [1.3.2](#)
- [22] C. Dasgupta and S. K. Ma. Low-temperature properties of the random heisenberg antiferromagnetic chain. *Phys. Rev. B*, 22(3):1305 – 1319, August 1980. [1.3.1](#), [1.3.2](#), [1.3.2](#), [1.3.2](#), [1.3.2](#)
- [23] T. R. Kirkpatrick and D. Belitz. Long-range order versus random-singlet phases in quantum antiferromagnetic systems with quenched disorder. *Phys. Rev. Lett.*, 76(14):2571–2574, April 1996. [1.3.1](#)
- [24] L. F. Santos. Integrability of a disordered heisenberg spin-1/2 chain. *J. Phys. A: Math. Gen.*, 37(17):4723–4729, April 2004. [1.3.1](#)
- [25] G. Refael and J. E. Moore. Entanglement entropy of random quantum critical points in one dimension. *Phys. Rev. Lett.*, 93(26):260602, December 2004. [1.3.1](#), [1.3.2](#), [1.5](#), [3](#), [3.1.3](#), [3.1.3](#), [3.1.3](#), [3.1.3](#), [3.1.3](#), [3.2.1](#), [3.3.3](#), [4.1](#)
- [26] G. Refael and J. E. Moore. Entanglement entropy of the random $s = 1$ heisenberg chain. *Phys. Rev. B*, 76(02):024419, July 2007. [1.3.1](#)

- [27] Huan Tran and N. E. Bonesteel. *A movie for visualizing a random singlet ground state with finite length scale ξ . It is clearly shown on this movie that the valence bonds are locked into a single valence-bond configuration on length scales greater than ξ while these bonds strongly resonating on length scales less than ξ .* Available online [here](#), 2009. [1.3.3](#), [1.5](#), [4](#)
- [28] J. Preskill. *Lecture notes on Quantum computation, Chapter 9.* California Institute of Technology, available online at <http://www.theory.caltech.edu/people/preskill/ph229/>, 2004. [1.4.1](#), [1.4.2](#), [1.4.2](#)
- [29] A. Feiguin, S. Trebst, A. W. W. Ludwig, M. Troyer, A. Kitaev, Z. Wang, and M. H. Freedman. Interacting anyons in topological quantum liquids: The golden chain. *Phys. Rev. Lett.*, 98(16):160409, April 2008. [1.4.1](#), [1.4.1](#), [1.4.2](#), [1.4.2](#), [1.5](#), [3.1.3](#), [3.3.3](#)
- [30] N. E. Bonesteel and K. Yang. Infinite-randomness fixed points for chains of non-abelian quasiparticles. *Phys. Rev. Lett.*, 99(19):140405, October 2007. [1.4.1](#), [1.4.1](#), [1.4.3](#), [1.4.3](#), [1.5](#), [2.2.2](#), [2.4](#), [3](#), [3.1.2](#), [3.1.2](#), [3.1.2](#), [3.1.3](#), [3.1.3](#), [3.1.3](#), [3.1.3](#), [3.3.2](#), [3.3.3](#), [4.1](#), [4.2.4](#)
- [31] A. Yu. Kitaev. Fault-tolerant quantum computation by anyons. *Ann. Phys.*, 303(1):2 – 30, January 2003. [1.4.1](#)
- [32] A. Stern. Anyons and the quantum hall effect - a pedagogical review. *Ann. Phys.*, 323(1):204 – 249, January 2008. [1.4.1](#), [1.4.2](#)
- [33] D. C. Tsui, H. L. Stormer, and A. C. Gossard. Two-dimensional magnetotransport in the extreme quantum limit. *Phys. Rev. Lett.*, 48(22):1559 – 1562, May 1982. [1.4.1](#)
- [34] R. Willett, J. P. Eisenstein, H. L. Stormer, D. C. Tsui, A. C. Gossard, and J. H. English. Observation of an even-denominator quantum number in the fractional quantum hall effect. *Phys. Rev. Lett.*, 59(15):1776–1779, October 1987. [1.4.1](#), [1.4.2](#)
- [35] G. Moore and N. Read. Nonabelions in the fractional quantum hall effect. *Nucl. Phys. B*, 360(2-3):362, August 1991. [1.4.1](#), [1.4.2](#)
- [36] N. Read and E. Rezayi. Beyond paired quantum hall states: Parafermions and incompressible states in the first excited landau level. *Phys. Rev. B*, 59(12):80848092, March 1999. [1.4.1](#)
- [37] A. Yu. Kitaev. Anyons in an exactly solvable model and beyond. *Ann. Phys.*, 321(1):2–111, January 2006. [1.4.2](#)
- [38] P. P. Martin. *Potts Models and Related Problems in Statistical Mechanics.* World Scientific, Singapore, 1991. [1.4.2](#), [2.3.1](#)
- [39] J. S. Xia, W. Pan, C. L. Vicente, E. D. Adams, N. S. Sullivan, H. L. Stormer, D. C. Tsui, L. N. Pfeiffer, K. W. Baldwin, and K. W. West. Electron correlation in the second landau level: A competition between many nearly degenerate quantum phases. *Phys. Rev. Lett.*, 93(17):176809, October 2004. [1.4.2](#)

- [40] N. Temperley and E. Lieb. Relations between the percolation and colouring problem and other graph-theoretical problems associated with regular planar lattices: some exact results for the percolation problem. *Proc. R. Soc. London A*, 322:251, 1971. [1.4.2](#), [3.3.1](#)
- [41] R. J. Baxter. *Exactly Solved Models in Statistical Mechanics*. Academic Press, San Diego, USA, 1982. [1.4.2](#), [1.4.2](#)
- [42] Huan Tran and N. E. Bonesteel. Monte carlo simulations of interacting anyon chains. *Comput. Math. Sci.*, XX(XX):XXXXXX, April 2010. [1.5](#), [2.1](#), [2.2.2](#), [2.3.1](#), [2.3.1](#), [2.4](#)
- [43] Huan Tran and N. E. Bonesteel. Valence bond entanglement and fluctuations in random singlet phases. *Preprint, submitted to Phys. Rev. Lett.*, 2010. [1.5](#), [2.1](#), [3.2.1](#), [3.3.1](#), [4.1](#), [4.2.3](#), [4.2.4](#)
- [44] J. L. Jacobsen and H. Saleur. Exact valence bond entanglement entropy and probability distribution in the xxx spin chain and the potts model. *Phys. Rev. Lett.*, 100(8):087205, February 2008. [1.5](#), [3.2.1](#), [3.3.1](#), [3.3.1](#), [3.3.1](#), [3.3.1](#), [3.3.1](#), [4](#), [4.1](#), [4.2.2](#), [4.2.3](#), [4.2.3](#), [4.2.3](#)
- [45] F. Alet, S. Capponi, N. Laflorencie, and M. Mambrini. Valence bond entanglement entropy. *Phys. Rev. Lett.*, 99(11):117204, September 2007. [1.5](#), [2.1](#), [2.1](#), [3](#), [3.2.1](#), [3.2.1](#), [3.2.1](#), [3.3.1](#), [3.3.2](#), [4.1](#)
- [46] R. W. Chhajlany, P. Tomczak, and A. Wójcik. Topological estimator of block entanglement for heisenberg antiferromagnets. *Phys. Rev. Lett.*, 99(16):167204, October 2007. [1.5](#), [2.1](#), [3](#), [3.2.1](#), [3.2.1](#)
- [47] I. González A. B. Kallin, M. B. Hastings, and R. G. Melko. Valence bond and von neumann entanglement entropy in heisenberg ladders. *Phys. Rev. Lett.*, 103(11):117203, November 2009. [2.1](#)
- [48] M. B. Hastings, I. González, A. B. Kallin, and R. G. Melko. Measuring renyi entanglement entropy in quantum monte carlo simulations. *Phys. Rev. Lett.*, 104(15):157201, April 2010. [2.1](#)
- [49] N. Metropolis, A. W. Rosenbluth, M. N. Rosenbluth, A. H. Teller, , and E. Teller. Equation of state calculations by fast computing machines. *J. Chem. Phys.*, 21(6):1087, June 1953. [2.2.2](#)
- [50] W. K. Hastings. Monte carlo sampling methods using markov chains and their applications. *Biometrika*, 57(1):97–109, 1970. [2.2.2](#)
- [51] S. Liang. Existence of néel order at $t=0$ in the spin-1/2 antiferromagnetic heisenberg model on a square lattice. *Phys. Rev. B*, 42(10):6555–6560, October 1990. [2.2.4](#)
- [52] C. N. Yang and C. P. Yang. One-dimensional chain of anisotropic spin-spin interactions. i. proof of bethe’s hypothesis for ground state in a finite system. *Phys. Rev.*, 150(1):321–327, October 1966. [2.3.1](#), [2.4](#)

- [53] C. N. Yang and C. P. Yang. One-dimensional chain of anisotropic spin-spin interactions. ii. properties of the ground-state energy per lattice site for an infinite system. *Phys. Rev.*, 150(1):327–339, October 1966. [2.3.1](#), [2.4](#)
- [54] M. Takahashi. Thermodynamical bethe ansatz and condensed matter. In *Conformal Field Theories and Integrable Models*, pages 204–250. Springer, Berlin/Heidelberg, 2007. [2.3.1](#)
- [55] D. Medeiros and G. G. Cabrera. Lanczos calculation for the $s=1/2$ antiferromagnetic heisenberg chain up to $n=28$ spins. *Phys. Rev. B*, 43(4):3703–3705, February 1991. [2.3.1](#), [2.3.1](#)
- [56] N. S. Witte and L. C. L. Hollenberg. Accurate calculation of ground-state energies in an analytic lanczos expansion. *J. Phys.: Condens. Matter.*, 9(9):2031–2042, March 1997. [2.3.1](#), [2.3.1](#)
- [57] T. Barnes and G. J. Daniell. Numerical solution of spin systems and the $s=1/2$ heisenberg antiferromagnet using guided random walks. *Phys. Rev. B*, 37(7):3637–3651, March 1988. [2.3.1](#), [2.3.1](#), [2.3.2](#), [2.3.2](#), [2.2](#)
- [58] M. J. de Oliveira. Ground-state properties of the spin- $1/2$ antiferromagnetic heisenberg chain obtained by use of a monte carlo method. *Phys. Rev. B*, 48(9):6141 – 6143, September 1993. [2.3.1](#), [2.3.1](#), [2.3.2](#), [2.1](#), [2.3.2](#), [2.2](#), [2.3.2](#)
- [59] A. W. Sandvik and K. S. D. Beach. Monte carlo simulations of quantum spin systems in the valence bond basis. In *Computer Simulation Studies in Condensed-Matter Physics XX*, 2007. [2.3.2](#)
- [60] J. B. Parkinson and J. C. Bonner. Spin chains in a field: Crossover from quantum to classical behavior. *Phys. Rev. B*, 32(7):4703–4724, October 1985. [2.3.2](#), [2.1](#), [2.3.2](#), [2.2](#)
- [61] J. Sólyom and T. A. L. Ziman. Ground-state properties of axially anisotropic quantum heisenberg chains. *Phys. Rev. B*, 30(7):3980–3992, 1984. [2.3.2](#), [2.1](#), [2.3.2](#), [2.2](#)
- [62] T. Barnes, J. Riera, and D. A. Tennant. $s = \frac{1}{2}$ alternating chain using multiprecision methods. *Phys. Rev. B*, 59(17):11384–11397, May 1999. [2.4](#)
- [63] T. Papenbrock, T. Barnes, D. J. Dean, M. V. Stoitsov, and M. R. Strayer. Density matrix renormalization group study of critical behavior of the spin $\frac{1}{2}$ alternating heisenberg chain. *Phys. Rev. B*, 68(02):024416, July 2003. [2.4](#)
- [64] A. Einstein, B. Podolsky, and N. Rosen. Can quantum-mechanical description of physical reality be considered complete? *Phys. Rev.*, 47(10):777–780, May 1935. [3.1.1](#)
- [65] M. A. Nielsen and I. L. Chuang. *Quantum computation and quantum information*. Cambridge University Press, Cambridge, UK, 2000. [3.1.1](#), [2](#)
- [66] G. Vidal, J. I. Latorre, E. Rico, and A. Kitaev. Entanglement in quantum critical phenomena. *Phys. Rev. Lett.*, 90(22):227902, 2003. [3.1.3](#), [3.1.3](#), [3.1.3](#), [3.3.1](#)

- [67] V. E. Korepin. Universality of entropy scaling in one dimensional gapless models. *Phys. Rev. Lett.*, 92(9):096402, March 2004. [3.1.3](#), [3.1.3](#)
- [68] C. Holzhey, F. Larsen, and F. Wilczek. Geometric and renormalized entropy in conformal field theory. *Nucl. Phys. B*, 424(3):443–467, August 1994. [3.1.3](#)
- [69] I. Affleck, N. Laflorencie, and E. S. Sørensen. Entanglement entropy in quantum impurity systems and systems with boundaries. *J. Phys. A: Math. Theor.*, 42:504009, December 2009. [3.1.3](#)
- [70] N. Laflorencie. Scaling of entanglement entropy in the random singlet phase. *Phys. Rev. B*, 72(14):140408, October 2005. [3.1.3](#)
- [71] R. Santachiara. Increasing of entanglement entropy from pure to random quantum critical chains. *J. Stat. Mech.*, page L06002, 2006. [3.1.3](#)
- [72] J. A. Hoyos, A. P. Vieira, N. Laflorencie, and E. Miranda. Correlation amplitude and entanglement entropy in random spin chains. *Phys. Rev. B*, 74(17):174425, November 2007. [3.2.2](#)
- [73] D. S. Fisher. Random transverse field ising spin chains. *Phys. Rev. Lett.*, 69(3):534–537, July 1992. [3.3.2](#)
- [74] N. Laflorencie, H. Rieger, A. W. Sandvik, and P. Henelius. Crossover effects in the random-exchange spin- $\frac{1}{2}$ antiferromagnetic chain. *Phys. Rev. B*, 70(05):054430, August 2004. [4.3.2](#), [4.3.2](#), [4.3.2](#), [4.4](#)
- [75] N. Laflorencie and H. Rieger. Scaling of the spin stiffness in random spin- $\frac{1}{2}$ chains—crossover from pure-metallic behaviour to random singlet-localized regime. *Eur. Phys. Journal B*, 40(2):201–207, August 2004. [4.3.2](#)
- [76] T. Giamarchi and H. J. Schulz. Anderson localization and interactions in one-dimensional metals. *Phys. Rev. B*, 37(1):325–340, January 1988. [4.3.2](#)
- [77] I. Affleck, D. Gepner, H. J. Schulz, and T. Ziman. Critical behaviour of spin-s heisenberg antiferromagnetic chains: analytic and numerical results. *J. Phys. A: Math. Gen.*, 22(5):511–529, March 1989. [4.3.2](#)
- [78] A. W. Sandvik. Stochastic series expansion method with operator-loop update. *Phys. Rev. B*, 59(22):14157–14160, June 1999. [4.3.2](#)

BIOGRAPHICAL SKETCH

Personal information

- Full name: “Trần Doãn Huân” in Vietnamese, or “Huan Doan Tran” in Western name order and Latin alphabet

Education

Florida State University	Tallahassee, FL, USA
PhD in Physics	<i>2010</i>

Hanoi University of Technology	Hanoi, Vietnam
BSc in Physics	<i>2000</i>

Working experience

- **Research Assistant and Teaching Assistant**, Department of Physics and National High Magnetic Field Laboratory, Florida State University, Tallahassee, FL 32306, USA: August 2003 – June 2010
- **Assistant Lecturer**, Institute of Engineering Physics, Hanoi University of Technology, Hanoi, Vietnam: September 2000 – July 2003

Research projects

- **Florida State University**: “Valence-Bond Monte Carlo Study of Random Singlet Phases”
- **Hanoi University of Technology**: “Electronic and Transport Properties of Low-Dimensional Semiconductor Quantum Structures”

Publications

Submitted papers

1. Huan Tran and N. E. Bonesteel, “Valence-bond entanglement and Fluctuations in random singlet phases”, Preprint: [arXiv:0909.0038](https://arxiv.org/abs/0909.0038), submitted to Physical Review Letters (2009)

Papers in preparation

2. Huan Tran and N. E. Bonesteel, “Fluctuation length scales in random singlet phases”

Published papers

3. Huan Tran and N. E. Bonesteel, “Monte Carlo simulations of interacting anyon chains”, in press, [Computational Materials Science](#), (2010)
4. Tran Doan Huan and Nguyen Phuc Hai, “Diffusion thermopower of a p -type Si/Si_{1-x}Ge_x heterostructure at zero magnetic field”, [physica status solidi \(b\)](#) **244**, 2100 (2007)
5. Doan Nhat Quang, Vu Ngoc Tuoc, Tran Doan Huan and Pham Nam Phong, “Low-temperature mobility of holes in Si/SiGe p-channel heterostructures”, [Physical Review B](#) **70**, 195336 (2004)
6. Doan Nhat Quang, Vu Ngoc Tuoc, and Tran Doan Huan, “Roughness-induced piezoelectric scattering in lattice-mismatched semiconductor quantum wells”, [Physical Review B](#) **68**, 195316 (2003)
7. Doan Nhat Quang, Vu Ngoc Tuoc, Nguyen Huyen Tung, and Tran Doan Huan, “Strain fluctuations in a real [001]-oriented zinc-blende structure surface quantum well”, [Physical Review B](#) **68**, 153306 (2003)
8. Doan Nhat Quang, Vu Ngoc Tuoc, Nguyen Huyen Tung, and Tran Doan Huan, “Random piezoelectric field in real [001]-oriented strain-relaxed semiconductor heterostructures”, [Physical Review Letters](#) **89**, 077601 (2002)
9. Doan Nhat Quang, Nguyen Huyen Tung, and Tran Doan Huan, “Effect of impurity correlation in modulation-doped quantum wires”, [Physical Review B](#) **64**, 125324 (2001)

Talks/presentations

1. “Fluctuation length scales in random singlet phases”, *2010 APS March Meeting*, Portland, Oregon, USA, March 18, 2010.
2. “Valence-bond Monte Carlo study of random singlet phases”, *5th Conference of the Asian Consortium on Computational Materials Science (ACCMS-5)*, Hanoi, Vietnam, September 10, 2009.
3. “Valence-bond Monte Carlo study of random-singlet phase formation”, *2009 APS March Meeting*, Pittsburgh, Pennsylvania, USA, March 17, 2009.
4. “Valence-bond Monte Carlo for chains of non-Abelian quasiparticles”, *2008 APS March Meeting*, New Orleans, Louisiana, USA, March 13, 2008.
5. “Valence bond entanglement entropy of the random chain of non-Abelian quasiparticles”, poster at the mini workshop of the *Advanced School on Quantum Monte Carlo Methods in Physics and Chemistry*, ICTP, Trieste, Italy, February 02, 2008.
6. “Monte Carlo study of entanglement scaling in random $S=1/2$ Heisenberg chains”, *2007 APS March Meeting*, Denver, Colorado, USA, March 05, 2007.